ABSTRACT

New Insight into the Coordination and Reactivity of Hetero-Substituted Maltol and Method Development for Complex Mixture Analysis of Asphaltene

Michael T. Spiegel, Ph.D.

Mentor: Patrick J. Farmer, Ph.D.

The metal complexes of maltol and its hetero-substitutions have a wide variety of bioinorganic applications. However, the latest addition to this family of molecules, 3-hydroxy-2-methyl-4H-pyran-4-selenone (selenomaltol), had not previously had its metal complexes characterized. To remedy this, transition metal complexes were made using Fe(III), Ni(II), Cu(II) and Zn(II) to characterize the homoleptic-complexes of selenomaltol and compare them to previously published maltol-like ligands. The selenomaltol complexes were found to be similar to thiomaltol complexes. In addition, new insights were gained into the redox chemistry of the thiomaltol and selenomaltol ligands, and the complexes of selenomaltol and thiomaltol were found to be more aromatic than the free ligand.

The increased aromaticity of the complexes over the ligands was thought to be due to the complexes stabilizing the pyrylium resonance structure of hetero-substituted maltols. To explore if the free ligand exhibited this resonance, NMR spectroscopy and reactivity studies were performed. Polar solvents seemed to favor the pyrylium

resonance, and significantly impacted the nucleophilicity of the hetero-substituted maltol ligands. This reactivity study led to the generation of the two new ligands 3-hydroxy-2-methyl-4-(methylsulfanyl)pyrylium and 3-hydroxy-2-methyl-4-(methylselanyl)pyrylium. This new ligand class is of interest as it contains a stable pyrylium species, which can be used to generate a new family of ligands for use in bioinorganic chemistry.

The second project explored was on the development of a new method for investigating asphaltenes, the heaviest and most problematic fraction of crude oil, by NMR spectroscopy and mass spectrometry. To study asphaltenes by mass spectrometry, we reacted a sample of asphaltene with elemental bromine (Br_2). This was done to selectively substitute the aromatic protons on asphaltenes to probe their structure. The subsequent high-resolution mass spectra were visualized by Kendrick Mass Defect (KMD) plots. These reactivity studies showed fewer aromatic protons available to react than predicted by current models of asphaltene. To more accurately characterize the number of aromatic protons present, a new method for performing ^1H NMR spectroscopy was developed, which removed paramagnetic materials from the sample.

New Insight into the Coordination and Reactivity of Hetero-Substituted Maltol and Method Development for Complex Mixture Analysis of Asphaltene

by

Michael T. Spiegel, B.S.

A Dissertation

Approved by the Department of Chemistry and Biochemistry

_____

Patrick J. Farmer, Ph.D., Chairperson

Submitted to the Graduate Faculty of
Baylor University in Partial Fulfillment of the
Requirements for the Degree
of

Doctor of Philosophy

Approved by the Dissertation Committee

_____

Patrick J. Farmer, Ph.D., Chairperson

_____

Touradj Solouki, Ph.D.

_____

Kevin Klausmeyer, Ph.D.

_____

Caleb D. Martin, Ph.D.

_____

Ramon Lavado, Ph.D.

Accepted by the Graduate School

December 2019

_____

J. Larry Lyon, Ph.D., Dean

Page bearing signatures is kept on file in the Graduate School.

TABLE OF CONTENTS

LIST OF FIGURES

LIST OF SCHEMES

LIST OF TABLES

ACKNOWLEDGMENTS

First and foremost, I would like to acknowledge Dr. Patrick J. Farmer. His mentorship and commitment to the highest possible standards drove me to constantly improve. Thank you.

To my committee, I would like to thank Dr. Touradj Solouki for sparking my joy in mass spectrometry, and their analytical expertise; Dr. Klausmeyer for his advice and crystallographic examination and elucidation; Dr. Martin for their support in my oral examinations and research; Dr. Lavado, for their environmental expertise and availability for my dissertation defense.

I would also like to acknowledge the Department of Chemistry at Baylor University for providing me with an opportunity to better myself with excellent facilities and the people who upkeep those facilities. Many thanks go to those who work in the chemistry office, who help bring the department together. To my lab mates in the Farmer group, Murugaeson (Ravi) Kumar, Carrie Poe, Adrian Zapata, Ottis Scrivner, Lasien Rymbai, thank you for your companionship and support though the many ups and downs throughout my time here at Baylor. In addition, I would like to acknowledge my fantastic undergraduate students Maaz Syeed, Amanda Hoogerbrugge, Shamus Truska, Feven Iyassu, William Chan, Anish Sasmal, Ryan Wong and David Hunter for their work with me on my various projects here at Baylor.

Last, and certainly not least, my friends and family. I cannot express with mere words my gratitude for your constant support and love.

ATTRIBUTIONS

Publication 1

Amanda Hoogerbrugge – Helped in generating and purifying ligands and metal complexed presented, such as thiomaltol and selenomaltol.

Shamus Truksa – Helped in generating and purifying ligands and metal complexed presented, such as thiomaltol and selenomaltol.

Andrew G. Smith – Responsible for NICS calculations.

Kevil L. Shuford – Advisor to Andrew G. Smith, lent expertise on computation chemistry.

Kevin K. Klausmeyer – Ran the X-ray crystallography instrument and solved the crystal structures for this publication (and those shown in CHAPTER 3).

Patrick J. Farmer – Advisor on this project, helped direct where the research went.

Michael T. Spiegel – Primary graduate student on this project, came up with and executed the synthesis of the ligands and complexes. Responsible for the characterization of the ligand and complexes by NMR/EPR spectroscopy, mass spectrometry, and UV-Vis. In addition, was also responsible for crystal growth.

Publication 2

Ian G. M. Anthony – Prepared asphaltene samples and helped run mass spectrometry analysis. Helped with literature searches and the editing of the manuscript.

Matthew R. Brantley – Helped with literature searches, setting up the mass spectrometer, and the editing of the manuscript.

Alton Hassel - Helped with literature searches and the editing of the manuscript.

Patrick J. Farmer – Advisor of Michael T. Spiegel, lent expertise on NMR spectra characterization and column purification.

Touradj Solouki – Advised on the mass spectrometry and ideas present in the manuscript.

Michael T. Spiegel - Primary graduate student on this project, responsible for the bromination reactivity, ICP and Orbitrap MS analysis, NMR and EPR spectra generation and analysis, and prediction of new asphaltene structure.

Chapter Five

Bradley S. Pierce – Computational analysis of EPR radicals

Michael T. Spiegel – Primary graduate student on this project, came up with and executed the synthesis of the ligands and complexes. Responsible for the characterization of the ligand and complexes by NMR/EPR spectroscopy, and mass spectrometry.

DEDICATION

To my grandfather Herbert Spiegel, without his love and example I would not be the person, mentor or chemist that I am today.

CHAPTER ONE

An Introduction to Maltol and Asphaltene Chemistry

Maltol (3-hydroxy-2-methyl-4-pyrone, Scheme 1.1) is an FDA approved food additive with the odor of cotton candy and is commonly used as a flavor enhancer. It is also a bidentate metal chelator that is widely used in bioinorganic chemistry because of its high bioavailability and low toxicity.[1] Hetero-substitutions of maltol, such as those shown in Figure 1.1, have been developed and used for a variety of bioinorganic applications.

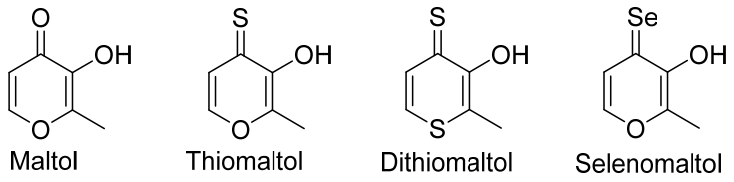

Figure 1.1 Structures of maltol, thiomaltol, dithiomaltol and selenomaltol

The Orvig lab was responsible for much of the early examples of maltols use in bioinorganic chemistry, where vanadium maltol complexes were used to enhance insulin sensitivity in the treatment of diabetes.[2] Since then, maltol has been used in the treatment of anemia[3], and its ring N-substituted product named deferiprone has been used in the treatment of iron overload.[4-5] Maltol itself has been shown to prevent enzymatic browning of food, and several of its derivatives have been found to inhibit tyrosinase, a Cu-oxygenase, purportedly by complexing with the metal ion active site.[6]

Thiomaltol (3-hydroxy-2-methyl-4H-pyran-4-thione) was first synthesized by the Viktor Hahns lab in 1969.[7] The synthesis was later streamlined and used as a potential lead chelator by Cohen group[8] and as a potential antifungal agent by Franz.[9] The Farmer lab is currently investigating thio- and dithiomaltol for use in melanoma treatment.[10-11] Each of these applications take advantage of hetero-substituted maltols as metal chelators.

Dithiomaltol (3-hydroxy-2-methyl-4H-thiopyran-4-thione) was first characterized by the Farmer lab[12] and had its coordination and oxidation chemistry studied. The coordination chemistry of dithiomaltol was similar to that of thiomaltol. While studying the ligand oxidation of dithiomaltol, the expected oxidation of the sulfur did not occur. Instead, an unusual C-H activation of the methyl group was observed when the ligand was coordinated to a metal. This unusual reactivity was attributed to the aromaticity of the thiopyrylium resonance structure of the ligand, similar to the pyrylium structure seen in Scheme 1.1.[13]

The most recent ketone derivative of maltol made is selenomaltol (3-hydroxy-2-methyl-4H-pyran-4-selenone), which was first characterized by the Tejchman group in 2008.[14] However, despite the wide range of uses and studies for previously studied hetero-substituted maltols, the metal complexes of selenomaltol had not been studied. This may be due to the difficult original synthesis, as their selenating agent, P_2Se_5, is made *in situ* and required a lengthy purification. The second chapter of this dissertation focuses on a simpler synthesis of selenomaltol using commercially available starting materials, and the characterization of new selenomaltol coordination compounds. We then

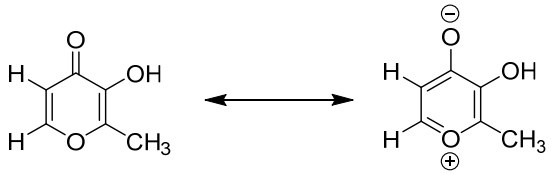

Scheme 1.1 Maltol and its zwitterionic pyrylium resonance form.

explore the increased aromaticity of the ligand when coordinated to a metal ion, and the ligand-based redox chemistry of these new complexes.

Maltol and other pyrone heterocycles have been suggested to have aromatic pyrylium resonance forms, as illustrated in Figure 1.1, which may affect the ligands reactivity. The pyrylium form of maltol has been studied computationally by Zborowski, who used various aromaticity calculations such as Nuclear Independent Chemical Shifts (NICS) and Harmonic Oscillator Model of Aromaticity (HOMA) to predict how predominant the aromatic pyrylium resonance structure was in gas phase calculations. Zborowski concluded that the pyrylium resonance form of maltol is not very significant in the neutral form of maltol, but it is significant in the protonated form of maltol.[15]

The reactivity of the pyrylium form of maltol has been utilized by Pernak in the generation of ionic liquids.[16] The pyrylium state of maltol has also been used by the various groups as an intermediate in the synthesis of 5+2 additions to the pyrone ring system.[17-20] However, no isolable pyrylium forms of any hetero-substituted analogs have been reported.

The third chapter focuses on the solvent dependence of pyrylium resonance forms in maltol and its hetero-substitutions and is characterized by NMR spectroscopy and reactivity studies. In addition, we utilize the enhanced pyrylium resonance forms of these derivatives to generate a new family of ligands. We expect these new ligands to be used

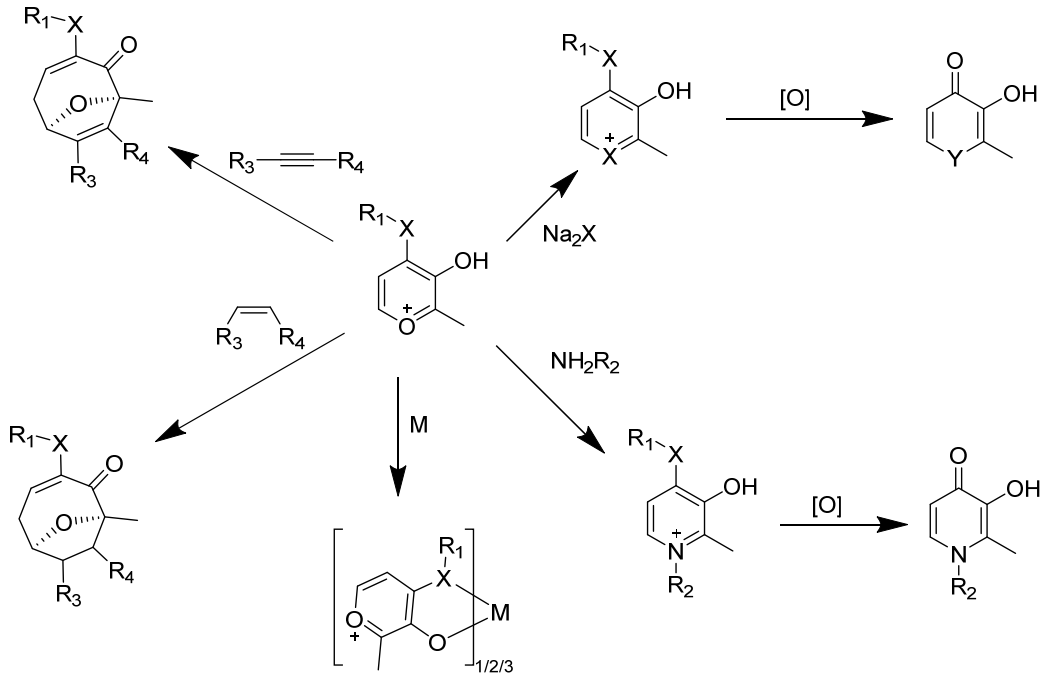

Figure 1.2 Suggested reactions for ketone substituted hetero-substituted maltols.

as starting material, taking advantage of the pyrylium functionality to generate a variety of new ligand functionalities for use in bioinorganic chemistry, as shown in Figure 1.2.

Complex Mixture Analysis of Crude Oil and Asphaltene

Asphaltenes are a broad class of hydrocarbons, characterized as the *n*-heptane insoluble, toluene soluble fraction of crude oil.[21] They consist of the heaviest components of crude oil, and consist of highly substituted polyaromatic rings.[22] Previous studies show that these rings stack and aggregate, forming insoluble deposits that are difficult to remove during the processing and transportation of crude oil.[23] The tendency for asphaltenes to aggregate out of solution has given rise to research into the general structure of asphaltenes, to better predict the behavior of these molecules.

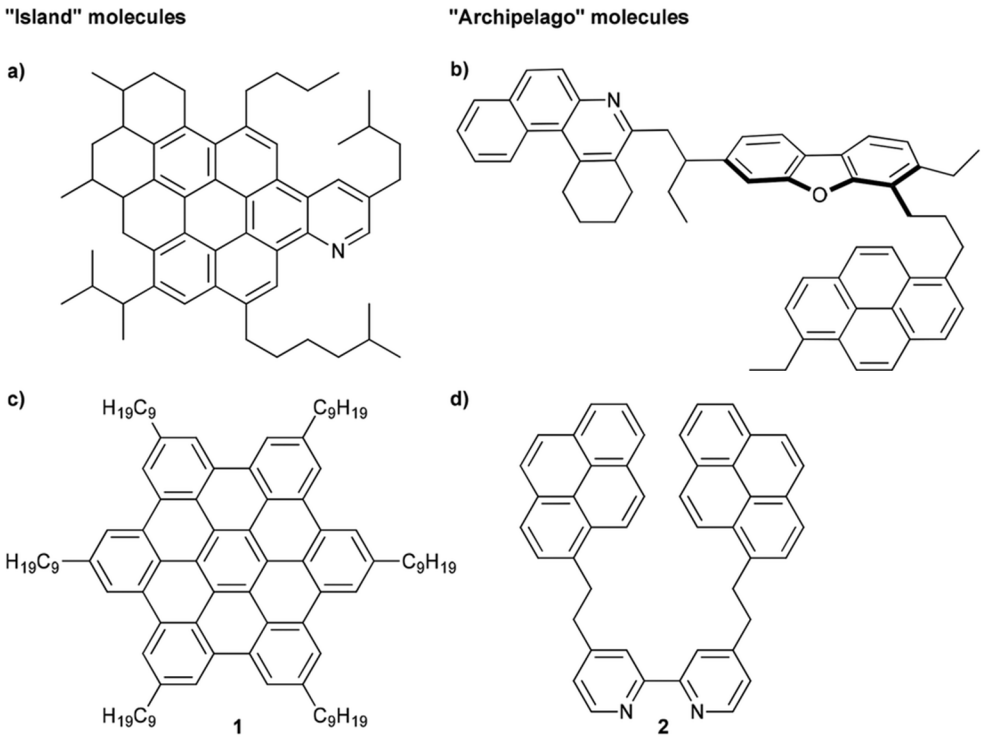

Figure 1.3 Structures of asphaltene from an "island" model and an "archipelago" model.[24]

There are two general structures of asphaltenes that are accepted, the most commonly shown is the "island" model, as shown on the left in Figure 1.3. The Island model consists of one large central aromatic core with various aliphatic carbons attached. The alternative "archipelago" model is made up of multiple aromatic cores attached by alkyl bridges. The island model of asphaltenes is based on work from Yen and co-workers, who used X-ray diffraction to model asphaltene structures.[25] Since the early 2000s however, asphaltene analysis by fluorescence depolarization,[26] tandem MS/MS,[27] and molecular imaging[28] has been used to demonstrate that the island structure is also significantly present in asphaltenes. Last, the molecular weight of asphaltene is generally accepted to be between 250 and 1250 g•mol^{-}, with an average of 750 g•mol^{-}.[29] These values are from time resolved fluorescence depolarization[30] and mass spectrometry studies.[31]

Much of the current research on asphaltene attempts to understand their structure to better predict their reactivity. However, there have been relatively few attempts to utilize reactivity to probe the structure of asphaltenes. In the fourth chapter, we explore the reactions of asphaltenes, as well as crude oil and the *n*-heptane fractions of crude oil, with elemental bromine. Bromine was chosen because of its well understood reactivity with hydrocarbons, and its large mass defect. The latter attribute allowing for simple identification of and visualization of asphaltenes reactivity using Kendrick mass defect (KMD) plots to better elucidate the structure of asphaltene.

Kendrick mass is a redefinition of the unified atomic mass unit, or Dalton (u), from ^{12}C (12.0000…) to any other mass, herein we use CH_2 (14.0000…).[32] Kendrick mass defect is the difference between the nominal/integer mass, and the observed mass. This difference comes from some elements being more mass deficient, such as bromine, which has a nominal mass of 79 or 81 (depending on the isotope) but has an observed mass of 78.918336 and 80.91629. Elements can also be mass proficient, for example hydrogen (^1H) has a nominal mass of 1, but an exact mas of 1.007825. To better understand how Kendrick mass and the mass deficiency of a molecule can be used together as an example KMD plot is shown in Figure 1.4.

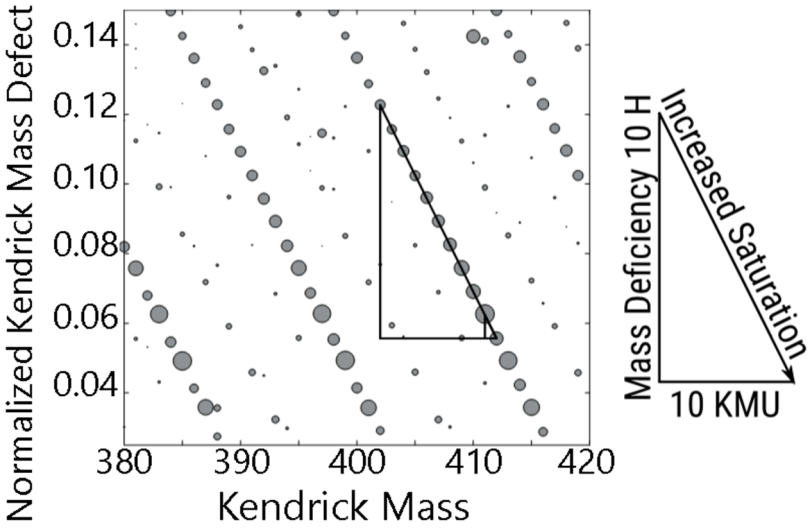

Figure 1.4 An example of a standard KMD plot between 380 and 420 kmu. The Y axis is a measure of a molecules "mass defect", the higher on the plot the more mass deficient the analyte is. The size of a point correlates to signal intensity.

These plots are a 2-dimensional way of showing mass spectra, with the X axis representing the "Kendrick mass" of a molecule and the Y axis being the molecules difference between its nominal (integer) Kendrick mass and its observed mass (its mass defect). Each point represents one of the molecules present in the solution, and the size of the point is respective to the signal intensity. The lines that move up diagonally, as shown by the triangle imposed on the plot, show the change for a loss of hydrogen. As the molecules in solution lose protons, which are mass proficient, the mass deficiency of the molecule goes up, and the mass goes down. Therefore, the trends shown move up and to the left. While still complicated, it is much easier to interpret data from a KMD plot than it would be from any raw data.

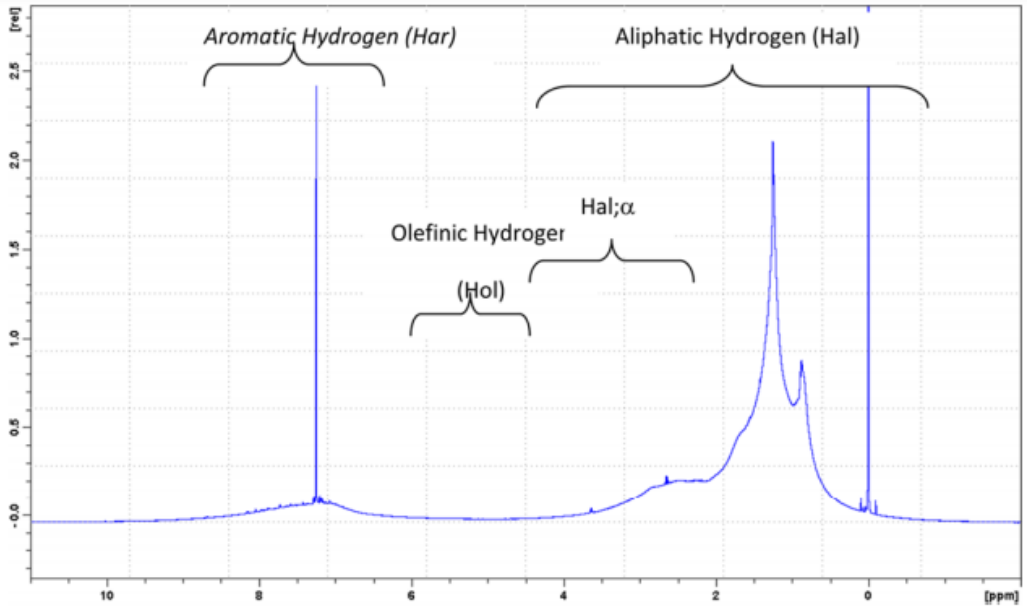

Figure 1.5 A typical asphaltene ^{1}H spectrum with crude peak assignments of an asphaltene mixture from Ratawi-Burgan and Lower-Fars crude oil.[33]

Last, to support the findings of the Br_2 reactivity experiments, ^{1}H NMR spectroscopy was attempted to identify the relative abundance of the functional groups present. Unfortunately, as seen in Figure 1.5, previous studies of asphaltene NMR spectroscopy display extensive line-broadening.[33] Thus the resolution in these spectra is much too low to differentiate functional groups.

The poor quality of NMR spectra of asphaltenes has previously been attributed to their tendency to aggregate in solution, which inhibits their rotation within the spectrometer and cause the observed signal broadening.[34] However, paramagnetic species such certain transition metal ions or organic radicals also cause broadening in the NMR spectra by shortening the signal relaxation time. These metal ions (such as Fe, V and Ni) and organic radicals are known to be in both crude oil and asphaltene.[35-37] Therefore, the removal of these known paramagnetic compounds would drastically improve the resolution of asphaltene NMR spectra. The fourth chapter describes one method to

characterize the presence of such paramagnetic metal ions, and how to remove them from asphaltene mixtures. The resulting NMR spectra have significantly improved resolution, which allows for speciation of various chemical moieties within the asphaltene fractions. The data also correlates with the previous reactivity study conducted on asphaltene. We believe this methodology is widely applicable to introduce NMR spectroscopy and simple asphaltene reactivity as a method for studying the structure of asphaltene.

Chapter five contains a variety of additional experiments that are tangential to chapters 2 and 3. The synthesis and characterization of oxidized hetero-substituted maltols are described. Oxidized thiomaltol, 3-hydroxy-2-methylpyrylium-4-yl)sulfenate) (Htmao-O), was then explored as a potential ligand and reacted with Cu^{2+} and Zn^{2+}, however the metal complexes observed lost the oxygen attached to the sulfur in Htma-O and formed the metal thiomaltol coordination product. In addition, other alkyl substituted thiomaltol synthesis were attempted, and 4-(butylthio)-3-hydroxy-2-methylpyrylium was formed and partially characterized. The oxidized product of selenomaltol described in chapter two was expanded upon, with the generation and EPR spectroscopy of the cation radical described. Last, disulfiram was reacted with Ag to form a new sulfur oxide donor, with less toxic counterions than those found in similar species.[40-42]

References

1. Woodhead Publishing Series in Food Science, Technology and Nutrition. In *Flavour Development, Analysis and Perception in Food and Beverages*, Parker, J. K.; Elmore, J. S.; Methven, L., Eds. Woodhead Publishing: 2015; pp xiii-xxv.

2. Thompson, K. H.; Barta, C. A.; Orvig, C., Metal complexes of maltol and close analogues in medicinal inorganic chemistry. *Chemical Society Reviews* **2006,** *35* (6), 545-556.

3. Melchior, M.; Thompson, K. H.; Jong, J. M.; Rettig, S. J.; Shuter, E.; Yuen, V. G.; Zhou, Y.; McNeill, J. H.; Orvig, C., Vanadium Complexes as Insulin Mimetic Agents: Coordination Chemistry and in Vivo Studies of Oxovanadium(IV) and Dioxovanadate(V) Complexes Formed from Naturally Occurring Chelating Oxazolinate, Thiazolinate, or Picolinate Units. *Inorganic Chemistry* **1999,** *38* (10), 2288-2293.

4. Kontoghiorghe, C. N.; Kolnagou, A.; Kontoghiorghes, G. J., Phytochelators Intended for Clinical Use in Iron Overload, Other Diseases of Iron Imbalance and Free Radical Pathology. *Molecules* **2015,** *20* (11), 20841-20872.

5. HIDER, R. C.; ZHOU, T., The Design of Orally Active Iron Chelators. *Annals of the New York Academy of Sciences* **2005,** *1054* (1), 141-154.

6. Liu, Z. D.; Hider, R. C., Design of clinically useful iron(III)-selective chelators. *Medicinal Research Reviews* **2002,** *22* (1), 26-64.

7. Kahn, V., Multiple Effects of Maltol and Kojic Acid on Enzymatic Browning. In *Enzymatic Browning and Its Prevention*, American Chemical Society: 1995; Vol. 600, pp 277-294.

8. Blazevic, K. B. K., 4-Pyrones and 4-pyridones. IV. 4-Thiopyrones. *Bulletin Scientifique, Section A: Sciences Naturelles, Techniques et Medicales (Zagreb)* **1969,** *14* (1-2), 1-2.

9. Lewis, J. A.; Puerta, D. T.; Cohen, S. M., Metal Complexes of the trans-Influencing Ligand Thiomaltol. *Inorganic Chemistry* **2003,** *42* (23), 7455-7459.

10. Lewis, J. A.; Cohen, S. M., Addressing Lead Toxicity: Complexation of Lead(II) with Thiopyrone and Hydroxypyridinethione O,S Mixed Chelators. *Inorganic Chemistry* **2004,** *43* (21), 6534-6536.

11. Helsel, M. E.; White, E. J.; Razvi, S. Z. A.; Alies, B.; Franz, K. J., Chemical and functional properties of metal chelators that mobilize copper to elicit fungal killing of Cryptococcus neoformans. *Metallomics* **2017,** *9* (1), 69-81.

12. Brayton, D. F., Targeting melanoma via metal based drugs: Dithiocarbamates, disulfiram copper specificity, and thiomaltol ligands. **2006**.

13. Farmer, P.; Cu-based drugs in combination therapy for melanoma. *Abstracts of Papers, 245th ACS National Meeting* **2013**, INOR-1149.

14. Brayton, D.; Jacobsen, F. E.; Cohen, S. M.; Farmer, P. J., A novel heterocyclic atom exchange reaction with Lawesson's reagent: a one-pot synthesis of dithiomaltol. *Chemical Communications* **2006,** (2), 206-208.

15. Backlund, M.; Ziller, J.; Farmer, P. J., Unexpected C−H Activation of Ru(II)−Dithiomaltol Complexes upon Oxidation. *Inorganic Chemistry* **2008,** *47* (7), 2864-2870.

16. Tejchman, W.; Zborowski, K.; Lasocha, W.; Proniewicz, L. M., Selenomaltol-synthesis, spectroscopy and theoretical calculations. *Heterocycles* **2008,** *75* (8), 1931-1942.

17. Zborowski, K. K.; Solà, M.; Poater, J.; Proniewicz, L. M., Theoretical studies on aromaticity of selected hydroxypyrones. Part 3#. Chelatoaromaticity phenomenon in metalcomplexes of hydroxypyrones. *Journal of Physical Organic Chemistry* **2011,** *24* (6), 499-506.

18. Pernak, J.; Świerczyńska, A.; Kot, M.; Walkiewicz, F.; Maciejewski, H., Pyrylium sulfonate based ionic liquids. *Tetrahedron Letters* **2011,** *52* (33), 4342-4345.

19. Rumbo, A.; Castedo, L.; Mourino, A.; Mascarenas, J. L., Temporary tethering strategies for [5 + 2] pyrone-alkene cycloadditions. *The Journal of Organic Chemistry* **1993,** *58* (21), 5585-5586.

20. Ramón Rodríguez, J.; Rumbo, A.; Castedo, L.; Mascareñas, J. L., Straightforward Construction of Fused 6,7,5-Tricarbocyclic Systems by Tandem [5 + 2]/[4 + 2] Cycloadditions. *The Journal of Organic Chemistry* **1999,** *64* (3), 966-970.

21. Ylijoki, K. E. O.; Stryker, J. M., [5 + 2] Cycloaddition Reactions in Organic and Natural Product Synthesis. *Chemical Reviews* **2013,** *113* (3), 2244-2266.

22. Mei, G.; Yuan, H.; Gu, Y.; Chen, W.; Chung, L. W.; Li, C.-c., Dearomative Indole [5+2] Cycloaddition Reactions: Stereoselective Synthesis of Highly Functionalized Cyclohepta[b]indoles. *Angewandte Chemie Int. Ed.* **2014,** *126* (41), 11231-11235.

23. Artok, L.; Su, Y.; Hirose, Y.; Hosokawa, M.; Murata, S.; Nomura, M., Structure and Reactivity of Petroleum-Derived Asphaltene. *Energy & Fuels* **1999,** *13* (2), 287-296.

24. Mullins, O. C.; Sabbah, H.; Eyssautier, J.; Pomerantz, A. E.; Barré, L.; Andrews, A. B.; Ruiz-Morales, Y.; Mostowfi, F.; McFarlane, R.; Goual, L.; Lepkowicz, R.; Cooper, T.; Orbulescu, J.; Leblanc, R. M.; Edwards, J.; Zare, R. N., Advances in Asphaltene Science and the Yen–Mullins Model. *Energy & Fuels* **2012,** *26* (7), 3986-4003.

25. Chaisoontornyotin, W.; Haji-Akbari, N.; Fogler, H. S.; Hoepfner, M. P., Combined Asphaltene Aggregation and Deposition Investigation. *Energy & Fuels* **2016,** *30* (3), 1979-1986.

26. Schulze, M.; Lechner, M. P.; Stryker, J. M.; Tykwinski, R. R., Aggregation of asphaltene model compounds using a porphyrin tethered to a carboxylic acid. *Organic & Biomolecular Chemistry* **2015,** *13* (25), 6984-6991.

27. Yen, T. F.; Erdman, J. G.; Pollack, S. S., Investigation of the Structure of Petroleum Asphaltenes by X-Ray Diffraction. *Analytical Chemistry* **1961,** *33* (11), 1587-1594.

28. Buenrostro-Gonzalez, E.; Groenzin, H.; Lira-Galeana, C.; Mullins, O. C., The Overriding Chemical Principles that Define Asphaltenes. *Energy & Fuels* **2001,** *15* (4), 972-978.

29. Tang, W.; Hurt, M. R.; Sheng, H.; Riedeman, J. S.; Borton, D. J.; Slater, P.; Kenttämaa, H. I., Structural Comparison of Asphaltenes of Different Origins Using Multi-stage Tandem Mass Spectrometry. *Energy & Fuels* **2015,** *29* (3), 1309-1314.

30. Schuler, B.; Meyer, G.; Peña, D.; Mullins, O. C.; Gross, L., Unraveling the Molecular Structures of Asphaltenes by Atomic Force Microscopy. *Journal of the American Chemical Society* **2015,** *137* (31), 9870-9876.

31. Chacón-Patiño, M. L.; Rowland, S. M.; Rodgers, R. P., Advances in Asphaltene Petroleomics. Part 1: Asphaltenes Are Composed of Abundant Island and Archipelago Structural Motifs. *Energy & Fuels* **2017,** *31* (12), 13509-13518.

32. Groenzin, H.; Mullins, O. C., Asphaltene Molecular Size and Structure. *The Journal of Physical Chemistry A* **1999,** *103* (50), 11237-11245.

33. Pomerantz, A. E.; Hammond, M. R.; Morrow, A. L.; Mullins, O. C.; Zare, R. N., Asphaltene Molecular-Mass Distribution Determined by Two-Step Laser Mass Spectrometry. *Energy & Fuels* **2009,** *23* (3), 1162-1168.

34. Kendrick, E., A Mass Scale Based on CH2 = 14.0000 for High Resolution Mass Spectrometry of Organic Compounds. *Analytical Chemistry* **1963,** *35* (13), 2146-2154.

35. AlHumaidan, F. S.; Hauser, A.; Rana, M. S.; Lababidi, H. M. S., NMR Characterization of Asphaltene Derived from Residual Oils and Their Thermal Decomposition. *Energy & Fuels* **2017,** *31* (4), 3812-3820.

36. Lisitza, N. V.; Freed, D. E.; Sen, P. N.; Song, Y.-Q., Study of Asphaltene Nanoaggregation by Nuclear Magnetic Resonance (NMR). *Energy & Fuels* **2009,** *23* (3), 1189-1193.

37. Di Mauro, E.; Guedes, C. L. B.; Nascimento, O. R., Multifrequency (X-band to W-band) CW EPR of the organic free radical in petroleum asphaltene. *Applied Magnetic Resonance* **2005,** *29* (4), 569.

38. Kurian, V.; Gupta, R., Distribution of Vanadium, Nickel, and Other Trace Metals in Soot and Char from Asphaltene Pyrolysis and Gasification. *Energy & Fuels* **2016,** *30* (3), 1605-1615.

39. Nelson, J.; Yamanaka, M.; Lopez-Linares, F.; Poirier, L.; Rogel, E., Characterization of Dissolved Metals and Metallic Nanoparticles in Asphaltene Solutions by Single-Particle Inductively Coupled Plasma Mass Spectrometry. *Energy & Fuels* **2017**, *31* (11), 11971-11976.

40. Chen, I.; Das, T. P., Molecular Orbital Theory of Sulfur and Selenium Radicals. *The Journal of Chemical Physics* **1966**, *45* (10), 3526-3535.

41. Cen, D.; Brayton, D.; Shahandeh, B.; Meyskens, F. L.; Farmer, P. J., Disulfiram Facilitates Intracellular Cu Uptake and Induces Apoptosis in Human Melanoma Cells. *Journal of Medicinal Chemistry* **2004**, *47* (27), 6914-6920.

42. Ainscough, E. W.; Brodie, A. M., Sulphur-ligand–metal complexes. Part 7. The interaction of some diphosphine dichalcogenides and tetra-alkylthiuram disulphides with halogens and some first-row transition-metal salts. Journal of the Chemical Society, *Dalton Transactions* **1977**, *6* (6), 565-570.

CHAPTER TWO

Synthesis of First Row Transition Metal Selenomaltol Complexes

This chapter is published as: "Spiegel, M. T.; Hoogerbrugge, A.; Truksa, S.; Smith, A. G.; Shuford, K. L.; Klausmeyer, K. K.; Farmer, P. J., "Synthesis of first row transition metal selenomaltol complexes," *Dalton Transactions* **2018**, 47 (27), 9030-9037."

Introduction

Maltol, 3-hydroxy-2-methyl-4-pyrone (Hma), is a natural product commonly used as a food additive and useful bidentate metal chelator.[1] Maltol complexes have been investigated for use in areas such as cell-labelling,[2] dental care,[3] radiopharmaceuticals,[4] insulin mimetics,[5–7] and enzymatic browning prevention.[8] Over the past two decades, hetero-substituted maltols and their metal complexes have been studied for applications like antimicrobials,[9,10] metalloprotein inhibition,[10–12] anti-melanoma properties[13] and chelation therapy.[14] Previously our group has reported on the synthesis of the ligands 3-hydroxy-2-methyl-4-thione (thiomaltol or Htma) and 3-hydroxy-2-methyl-4-thiopyran-4-thione (dithiomaltol or Httma) and their metal complexes.[13,15,16] A new addition to this family of chelates is selenomaltol, 3-hydroxy-2-methyl-4-selenone (Hsma), first reported in 2008.[17] Despite the wide range of interest in the metal complexes of maltol and its hetero-substitutions, no metal complexes of selenomaltol have been reported. However, the ligand and its aromaticity has been studied by the Tejchman group, who suggested that the chelato-aromatic effect would occur in metal complexes of selenomaltol.[18,19] We have developed a rapid, high-yield microwave synthesis of selenomaltol, which was used to generate the first homoleptic first row transition metal complexes of selenomaltol.

These new complexes have been characterized by X-ray crystallography, electronic absorption, NMR spectroscopy, EPR spectroscopy and cyclic voltammetry. To assess the compounds aromaticity after metal chelation computations of Nuclear Independent Chemical Shifts (NICS) were also done. These mixed O,Se chelating ligands are expected to find utility in a variety of bioinorganic applications such as heavy metal waste remediation.[19]

Results and Discussion

Improved synthesis of Hsma

The previously reported synthesis of selenomaltol was via reaction of maltol with P_4Se_{10} generated in situ from elemental Se and red phosphorus;[17] the reaction took twelve hours to complete and required recrystallization in xylenes. Here we report a modified synthesis, in which maltol is treated directly with Woollins reagent, Scheme 1, and heated to 100 °C in a microwave reactor for thirty minutes. Extraction with hexanes and evaporation yields pure selenomaltol, (Hsma) as a red powder in 60% yield. Subsequently, crystals were grown from hexanes to confirm the structure by X-ray crystallography.

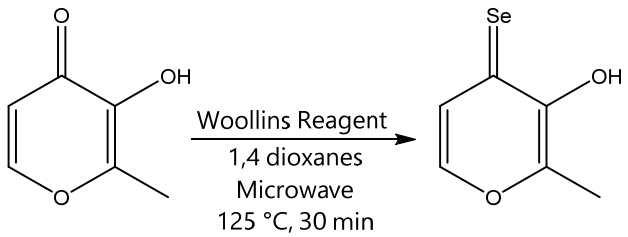

Scheme 2.1. Modified synthesis of selenomaltol from maltol

Synthesis and structures of metal complexes

Hsma was then reacted with a series of late first row transition metal ions to generate homoleptic complexes, Scheme 2. In a typical synthesis, a slight excess of Hsma in EtOH was added dropwise to an aqueous solution of the desired metal ion, resulting in precipitation. The precipitate was washed with water and hexane and dried via vacuum overnight to give the products $Zn(sma)_2$ (**1**), $Cu(sma)_2$ (**2**), $Ni(sma)_2$ (**3**) and $Fe(sma)_3$ (**4**).

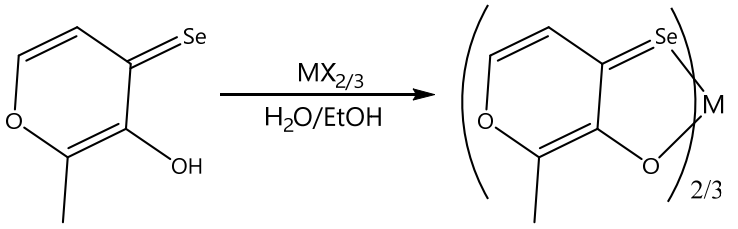

Scheme 2.2. Synthesis of metal complexes

Single crystals of each complex were obtained by vapor diffusion of diethyl ether into CH_2Cl_2, and their structures were determined via X-ray crystallography, and are shown in Figure 2.1. The Zn(II) complex **1** has a distorted 4-coordinate tetrahedral geometry. Bond lengths are 1.97 and 2.43 Å for the Zn–O and Zn–Se bonds with a O1–Zn–O3 angle of 120.0° and Se1–Zn–Se2 angle of 125.6°, almost identical to the analogous thiomaltol complex.[20] The Cu(II) complex **2** is 4-coordinate with a *trans* square planar geometry, analogous to the previously published $Cu(tma)_2$ complex.[22] The bond lengths are 1.91 and 2.40 Å for the Cu–O and Cu–Se bonds, respectively. The O1–Cu–Se1 bond angle within the ligand is 88.74°.

The Ni(II) complex **3** is also a four coordinate, square planar geometry, but in a *cis* configuration. The average Ni–O and Ni–Se bond distances are 1.88 and 2.28 Å, respectively. There is a slight distortion in the square planar conformation due to its *cis* geometry, with the Se1–Ni–Se2 bond angle 93.86° and the O1–Ni–O3 angle 85.81°. This distortion is slightly more pronounced than the analogous thiomaltol and maltol Ni complexes.[21]

The Fe(III) complex **4** has an octahedral fac geometry analogous to the previously reported $Fe(tma)_3$.[21] The average Fe–O and Fe–Se bond lengths are 1.99 and 2.61 Å, respectively. The twist angle of the complex of 47.91° is slightly less than that reported twist angles for both the Fe maltol and thiomaltol complexes (48.2 and 50.43, respectively).[21]

EPR characterizations

The oxidation states of complexes **2** and **4** were investigated by electron paramagnetic resonance (EPR) spectroscopy, which allows comparisons of ligand field strength and electronic structural variations in transition metal ion complexes. As shown in Figure 2.2, the EPR spectrum of complex **2** displays the axial absorbance expected for a d^9 square planar Cu(II) species. The analogous $Cu(tma)_2$ EPR spectrum shows $g \parallel$ = 2.15 and $g\perp$ = 2.07, implying that Hsma is the weaker field ligand (Appendix A). The spectrum of complex **4** is characteristic of a d^5 S = 3/2 system similar to the previously published $Fe(tma)_3$ complex, which also has an octahedral *fac* geometry.[22]

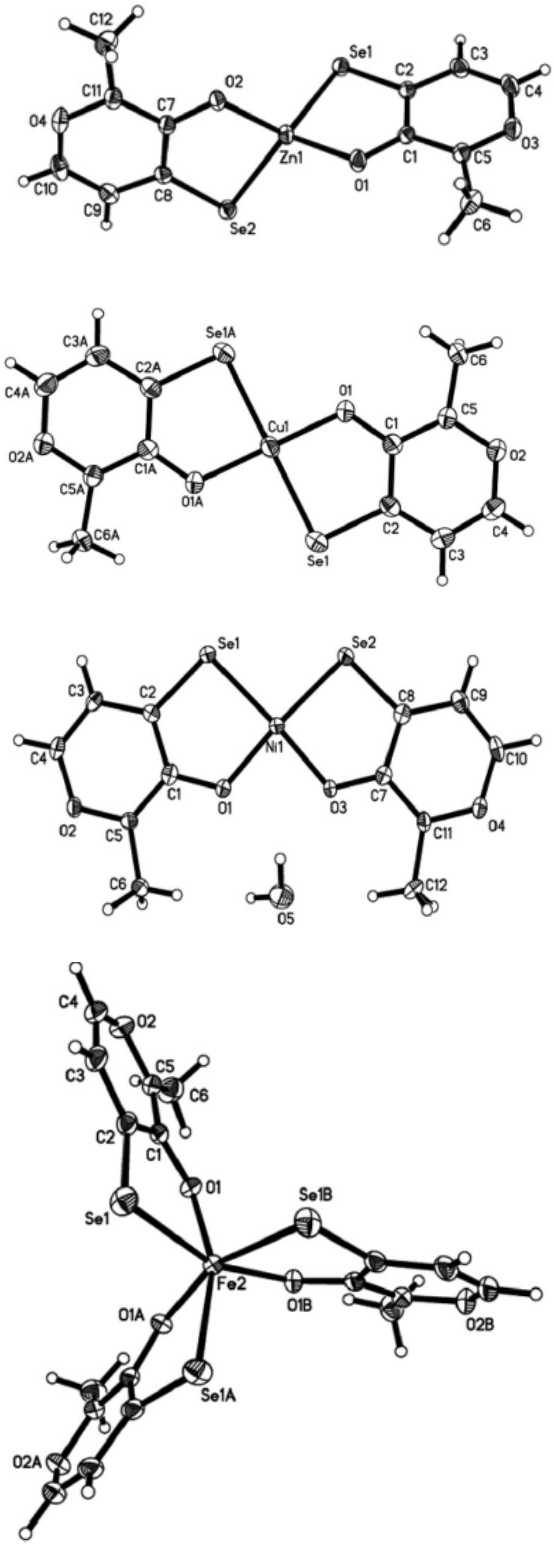

Figure 2.1. Crystal Structures of $Zn(sma)_2$ (**1**), $Cu(sma)_2$ (**2**), $Ni(sma)_2$ (**3**) and $Fe(sma)_3$ (**4**) from top to bottom.

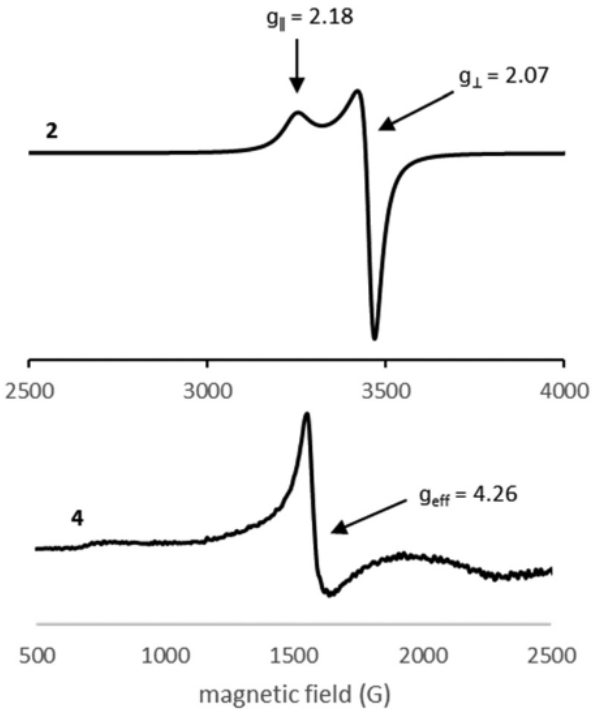

Figure 2.2. EPR spectra of crystalline powder sample of **2** taken at room temperature (top), and a frozen solution of **4** in toluene at 77 K (bottom).

Absorption spectra

Electronic absorption spectra for Hsma and its metal complexes are shown in Figure 2.3. Selenomaltol itself has absorbance bands at 287 and 399 nm, the latter resulting in selenomaltol's bright red color. $Zn(sma)_2$ and $Cu(sma)_2$, complexes **1** and **2**, do not share the same low energy transitions (>500 nm) of $Ni(sma)_2$ and $Fe(sma)_3$, complexes **3** and **4**. These low energy transitions are attributed to ligand/metal charge transfer. In general, the absorption bands for these species are ca. 50 nm lower in energy than those of the analogous thiomaltol complexes,[20,21] consistent with selenomaltolato being a slightly weaker field donor than thiomaltolato.

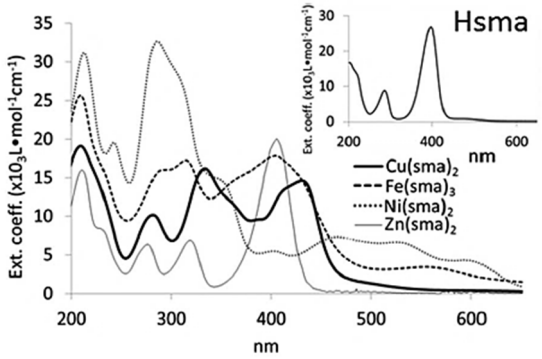

Figure 2.3. Comparison of normalized absorption spectra of $Zn(sma)_2$ (**1**, line), $Cu(sma)_2$ (**2**, bold), $Ni(sma)_2$ (**3**, dotted), and $Fe(sma)_3$ (**4**, dashed) using the calculated molar extinction coefficient (L mol^{-1} cm^{-1}) in CH_2Cl_2. Inset: The absorbance of Hsma over the same range.

Cyclic voltammetry

Redox properties of Hsma, **1**, **2**, **3** and **4** were assessed by voltammetry in anhydrous, anaerobic CH_2Cl_2 with 100 mM TBAHFP as an electrolyte. As seen in Figure 2.4, Hsma undergoes irreversible oxidation ca. 0.8 V. All complexes **1–4** have similar oxidations at close to the same potentials, which suggests that all are attributable to the oxidation of ligand.

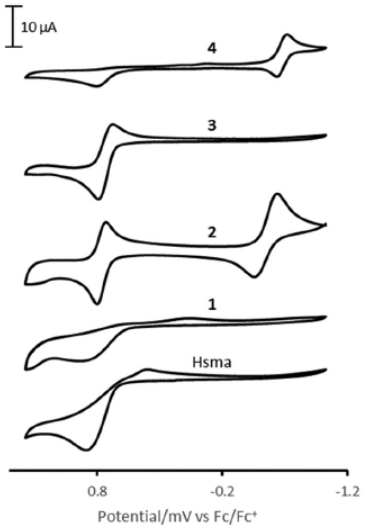

Figure 2.4. Cyclic voltammograms of Hsma and complexes **1-4** in anhydrous CH_2Cl_2 with 0.1 M $TBAPF_6$ as the supporting electrolyte with Pt disc electrode, scan rate 100 mV s^{-1}.

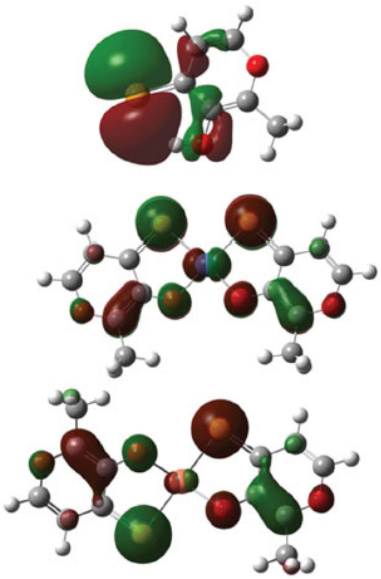

Figure 2.5. HOMO occupancies of Hsma (top) and $Ni(sma)_2$, (**3**, middle), and SOMO occupancy of $Cu(sma)_2$, (**2**, bottom).

Indeed, DFT calculations of free Hsma and diamagnetic complexes **1** and **3** suggest that the Se lone pair are dominant in the HOMO of these complexes, Figure 2.5. Significantly, both the Cu(II) and Ni(II) complexes, **2** and **3**, show chemically reversible oxidations at 0.76 V (E_p = 69 mV, i_{pa}/I_{pc} of 0.735) and 0.74 V with (E_p = 86 mV, i_{pa}/I_{pc} of 0.748), respectively. The free ligand and the Zn(II) and Fe(III) complexes **1** and **4** display irreversible oxidations at very similar potentials, which suggests that all have significant Se character as above. For complexes **2** and **3**, these oxidations are much more reversible than those reported previously for the analogous thiomaltol complexes (Appendix A), which may suggest significant M–Se delocalization.

Additionally, the Cu(II) and Fe(III) complexes **2** and **4** undergo observable reductions. Complex **2** undergoes a quasi-reversible reduction at −0.51 V (Δ Ep = 105 mV, ipa/Ipc 0.569) which we attribute to Cu(II/I) couple; the large peak separation is characteristic of the expected reorganization from square planar Cu(II) to tetrahedral

Cu(I).[23,24] Complex **4** undergoes a reversible reduction at −0.68 V (Δ Ep = 59 mV, ipa/Ipc 0.542), which we attribute to the Fe(III/II) couple; this reduction potential is somewhat more positive than those reported for Fe thiomaltol and maltol complexes.[21] Thus the softer selenone chelate stabilizes the reduced state relative to thione or ketone chelates.

NMR spectral characterizations

In previous studies of thio- and dithiomaltol complexes, the downfield shifts of the vinylic protons in ^{1}H NMR spectra were interpreted as increased aromaticity of the heterocycle, and found to be enhanced by chelation to metal ions.[15,16] The apparent increase in aromaticity was attributed to the stability of the aromatic resonance structure when the ligand was bound to a metal, Scheme 2.3, which was also suggested to engender unique redox and photochemistry.

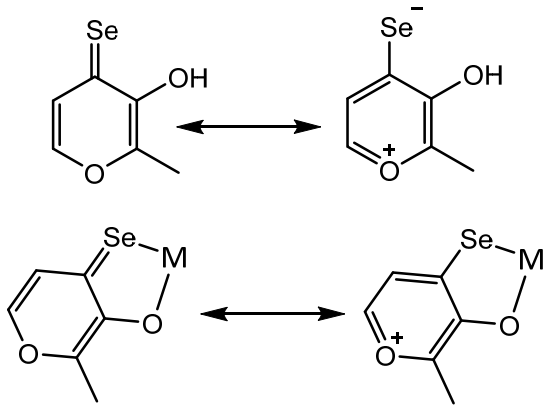

Scheme 2.3. Resonance structures related to aromaticity.

In selenomaltol, we believe the aromatic resonance form is stabilized due to the poor π bond between selenium and carbon.[25] These changes should cause a shift in the NMR spectra and bond lengths of these complexes. As seen in Figure 2.6, Hsma appears to be slightly more aromatic than thiomaltol.[13–15,20,21] However, spectra of complexes **1**

and **3** exhibit opposite shifts of the vinylic protons in comparison to the free ligand, with **1** shifting downfield and **3** upfield, as seen in Figure 2.6. These effects are also observed for the analogous thiomaltol complexes.[20,21] But a contrary trend is seen in the ^{13}C NMR spectra of Hsma and complexes **3** and **1**, Figure 2.7. Specifically, the unique selenone peak moves from 186 ppm for Hsma to 172 and 175 ppm respectively for complexes **1** and **3**, consistent with greater shielding from the aromatic tautomer. Because of the discrepancy between the ^{13}C and ^{1}H NMR spectra, ^{77}Se NMR spectroscopy was performed to directly probe the increase in electron density on the selenium, Figure 2.8. The ^{77}Se peak of the free ligand is considerably shifted more upfield than one would expect of a selenone (~700 ppm vs. 2000 ppm), closer to that of a selenoamide (Figure 2.9).[26] When complexed, the ^{77}Se peak is shifted farther upfield, suggesting more electron- density on the selenium, as in the zwitterionic aromatic resonance structure shown in Scheme 2.3.

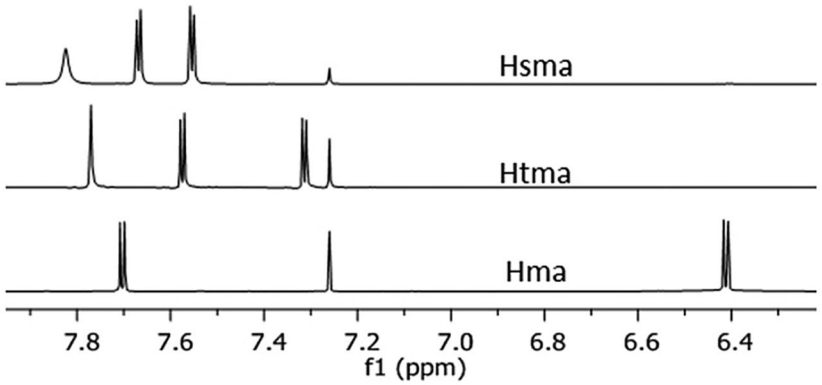

Figure 2.6. ^{1}H NMR spectrum in CD_3Cl of the aromatic region of Hsma, Htma, and Hma from top to bottom.

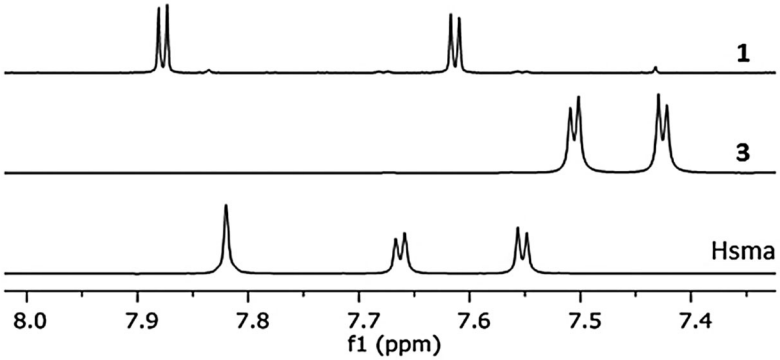

Figure 2.7. ^{1}H NMR spectrum in CD_3Cl in the aromatic region of complex **1, 3** and Hsma.

The greater ^{77}Se peak shift in complex **1** vs. complex **3** is likely due to the Zn(II) ion being a better electron donor than the Ni(II) ion. Thus, there is good agreement between the ^{77}Se and ^{13}C NMR spectroscopic analysis, which counters that of the ^{1}H NMR spectra, regarding the resonance structures of metal complexed ligands.

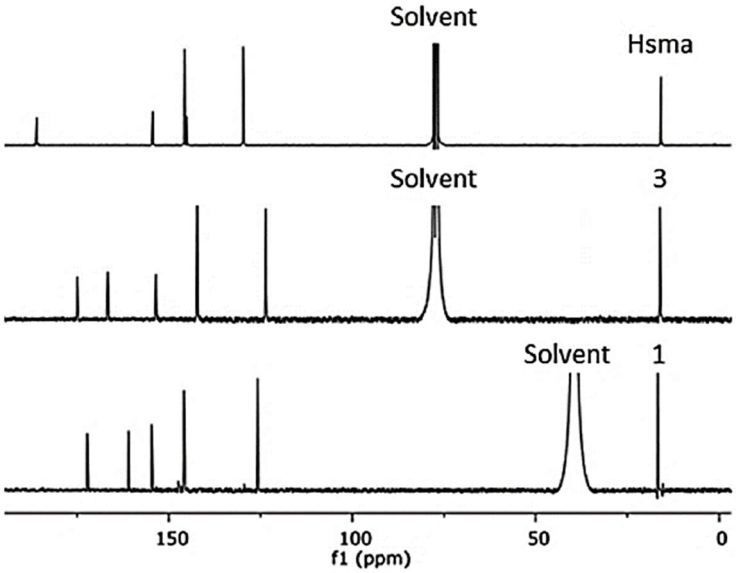

Figure 2.8. ^{13}C NMR spectrum of Hsma and complex **3** and **1**.

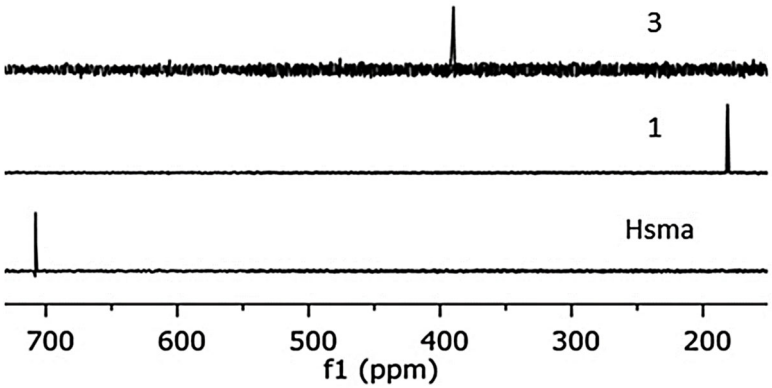

Figure 2.9. ^{77}Se NMR spectrum in CD_3Cl of complex **1**, **3** and Hsma.

Other measures of aromaticity

To further characterize the pseudo-aromaticity of the zwitterionic resonance form and its enhancement when complexed to a metal ion, several other approaches were investigated. Crystallographic data relating to alteration of double and single bonds within a heterocyclic ring can be used to distinguish delocalization and aromaticity.[27] Bond distances for C–Se and various C–C bonds within the ring system are shown in Table 2.1. As previously mentioned, the C–Se bond distances in Table 2.1 are longer than that expected for a C=Se double bond, especially when complexed to a metal ion.[17,28]

Table 2.1. Select bond distances of Hsma and complexes **1-4**

	C2-Se1 Å	C1-C2 Å	C2-C3 Å	C3=C4 Å	C1=C5 Å
Hsma	1.827(2)	1.421(3)	1.420(3)	1.344(3)	1.358(3)
$Zn(sma)_2$ (**1**)	1.866(2)	1.425(3)	1.414(3)	1.348(3)	1.392(3)
$Cu(sma)_2$ (**2**)	1.854(2)	1.416(3)	1.411(3)	1.348(3)	1.386(4)
$Ni(sma)_2$ (**3**)	1.869(4)	1.408(5)	1.400(5)	1.354(5)	1.389(5)
$Fe(sma)_3$ (**4**)	1.855(3)	1.426(4)	1.407(4)	1.344(5)	1.386(4)

The ring C=C double bonds are longer and the single bonds shorter when complexed, suggesting enhanced aromaticity in the complexed heterocycles, however the difference is not enough to be statistically relevant. A similar examination of the M–Se

Table 2.2. Predicted and observed M-Se bond lengths

Complex	M-Se^{0},[a] Å	M-Se^{2-},[a] Å	Observed, Å
$Fe(sma)_3$ (**4**)	1.945	2.765	2.6114(6)
$Ni(sma)_2$ (**3**)	1.790	2.610	2.2799(6)
$Cu(sma)_2$ (**2**)	1.870	2.690	2.4002(2)
$Zn(sma)_2$ (**1**)	1.900	2.720	2.4246(3)

[a]Sum of ionic radii for metal ion and Se^{0} and Se^{2-}.[29,30]

bonds also implies the dominance of the zwitterionic resonance state shown in Scheme 2.3. Table 2.2 compares the predicted ion bond lengths for metal-selenium bonds with the Se in the neutral and anionic form.

As seen, the observed bond lengths are best matched by its reduced ionic radius, as would be seen for the zwitterion. Also note that the Fe(III) complex **4** displays the longest M–Se and M–O bonds, likely due to its high spin state. A computational measure of aromaticity is by nuclear independent chemical shift (NICS) analysis, based on the predicted magnetic shielding due to the aromatic ring current. The magnetic shielding can be calculated in the center of the ring, which is determined by the non-weighted mean of the heavy atom coordinates (NICS(0)iso) or at 1 Å above it (NICS $(1)_{zz}$). Strongly negative NICS values are indicative of high aromaticity.[31,32] Both NICS(0)iso and NICS(1)zz analysis were performed on free ligands Hsma, Htma, and Hma as well as on the Zn(II), Ni(II) and Fe(III) thio- and selenomaltolato complexes, Table 3.

Table 2.3. Nuclear independent chemical shifts (NICS)

Complex	$NICS(0)_{iso}$	$-NICS(1)_{zz}$
Hsma/Htma/Hma	-1.85/-1.65/-1.50	-8.96/-9.00/-5.77
$Zn(sma)_2/(tma)_2$	-3.41/-3.53	-12.95/-13.09
$Cu(sma)_2/(tma)_2$	-2.57/-3.42	-10.37/-12.27
$Ni(sma)_2/(tma)_2$	-4.22/-4.67	-14.12/-14.44
$Fe(sma)_3/(tma)_3$	-3.87/-4.04	-15.91/-16.43

Of the free ligands, selenomaltol has a greatest degree of aromaticity for the NICS(0)iso measurement, but thiomaltol has the greatest aromaticity in the NICS(1)zz assessment. Likewise, the Ni(II) complexes have the greatest degree of aromaticity by NICS(0)iso, while the Fe(III) complexes the most aromatic by NICS(1)zz assessments. Overall, there is a significant increase in aromaticity for the metal complexes when compared to the free ligands, for both the thio- and selenomaltolato species.

Conclusions

A new high-yield synthesis of selenomaltol is described. The crystal structures of the homoleptic Zn(II), Cu(II), Ni(II) and Fe(III) complexes have been determined, which are the first reported for this unique chelator. The complexes exhibit analogous coordination geometries to previously reported thiomaltol complexes. Electrochemical properties found an unexpected reversible oxidation in the Ni and Cu species attributed to the ligand, which are subjects of ongoing research. Additionally, selenomaltol is being assessed as a heavy metal chelator for potential medical applications.

Experimental

Materials. Maltol, $Fe(NO_3)_3 \cdot 9\ H_2O$, $Zn(C_2H_3O_2)_2$, and $Ni(C_2H_3O_2)_2 \cdot 4\ H_2O$ were purchased from Alfa Aesar and used as received. All solvents used, Woollins reagent,

Lawessons reagent and Tetrabutylammonium Hexafluorophosphate ($TBAPF_6$) were purchased from Sigma-Aldrich. The thiomaltol ligand was prepared in a similar fashion to selenomaltol and its metal complexes were prepared using methods similar to previously published complexes (Appendix A).[15,22]

Physical measurements

Electronic absorption spectra were recorded with an Agilent 8453 diode array spectrophotometer. Microwave syntheses were carried out in a Discover SP microwave system. Mass spectra were obtained on a Thermo Electron Linear Trap Quadrupole Orbitrap Discovery mass spectrometer. NMR spectra were recorded on a 600 MHz Bruker NMR spectrometer.

EPR spectral characterizations were recorded from solid polycrystalline samples of **2** and $Cu(tma)_2$ and complex **4** at 77 K with an EMXplus EPR spectrometer. Conditions for **2**: microwave frequency 9.86 GHz, microwave power 2.00 mW, modulation amplitude 4.00G, time constant 0.01 ms, sweep width 2000 G, sweep time 20.0 ms. Conditions for **4**: microwave frequency 9.47 GHz, microwave power 2.00 mW, modulation amplitude 4.00 G, time constant 0.01 ms, sweep width 6000 G, sweep time 20.0 ms.

Cyclic voltammetry experiments were performed using a CHI-760B potentiostat in dry-degassed CH_2Cl_2 with 0.1 M tetrabutylammonium hexafluorophosphate ($TBAPF_6$) as the supporting electrolyte. The cells consisted of a platinum working electrode (3.0 mm dia.), AgCl/Ag reference, and a coiled Pt auxiliary electrode. Measured potentials were corrected using a ferrocene standard, with Fe/Fe^+ couples set to 229 mV vs. NHE. Crystallographic data was collected on crystals with dimensions 0.198 × 0.184 × 0.125

mm^3 for $Fe(sma)_3$, 0.136 × 0.089 × 0.020 mm^3 for $Ni(sma)_2$, 0.242 × 0.113 × 0.083 mm^3 for $Cu(sma)_2$ and 0.404 × 0.141 × 0.101 mm^3 for $Zn(sma)_2$. Data was collected at 110 K on a Bruker D8 quest using Mo-K α radiation (λ = 0.71073 Å) radiation. The data was processed using the Bruker AXS SHELXTL software, version 6.10. Crystallographic parameters for structural determinations of selenomaltol, $Fe(sma)_3$, $Ni(sma)_2$, $Cu(sma)_2$ and $Zn(sma)_2$ are given in the Appendix A.

Computational details

All calculations were done at the B3LYP/6-311+G(d,p) computational level using Gaussian09.[31] For the NICS calculations, the GIAO method was used to calculate the magnetic shielding tensor of a ghost atom. Due to the systems being symmetrical, the NICS values for only one of the rings are shown. Firstly, the ring is aligned along the x and y-axes, so the face of the ring is in the z-direction. Next, a ghost atom is placed in the center of the ring either within the same plane (NICS(0)iso) or 1.0 Å above the ring (NICS(1)zz). A property of ghost atoms is that they will not interact with other atoms, so the NICS(0)iso and NICS(1)zz can be measured simultaneously. The NICS(0)iso represents the negative of isotropic shielding tensor, while the NICS(1)zz represents the negative of the tensor in the zz direction. All NICS values are in ppm.

Synthesis of selenomaltol

Selenomaltol was prepared by dissolving 0.4192 grams (3.324 mmol) of maltol in 15 mL of anhydrous 1,4-dioxane in a 35 mL microwave reaction vessel. Woollins reagent (0.5650 g, 1.062 mmol) was added to the vessel, and the mixture heated in the microwave for 30 minutes at 125 °C. Water was added to the resulting black mixture. Extraction with

hexane produced a dark red organic phase, which yielded pure selenomaltol after hexane was removed via rotavap. The resulting red powder was washed with cold water and stored as a solid. The compound was crystallized via slow evaporation of hexanes top produce samples suitable for X-ray diffraction. Yield 0.3771 grams (60%). ESI MS: m/z (pos.) 190.9604 (M + H) (calculated: 190.9611). ^{1}H NMR (600 MHz,$CDCl_3$): δ 7.68 (d, ^{1}H), 7.55 (d, ^{1}H), 2.30 (s, ^{3}H), δ 7.83 (s, ^{1}H).^{13}C NMR (600 MHz, $CDCl_3$): δ 186, 154, 146, 145, 130, 16.

*Synthesis of $Zn(sma)_2$ **(1)***

A sample of Hsma (0.0610 g, 0.3194 mmol) was dissolved in 2 mL of ethanol to form a bright red solution. $Zn(C_2H_3O_2)_2$ (0.0293 g, 0.1597 mmol) was then dissolved in 3 mL of deionized water and stirred under nitrogen. The selenomaltol mixture was added drop wise to the zinc solution, immediately forming a yellow precipitate. The solution was centrifuged, and the pellet washed with hexane twice to remove any excess selenomaltol. The flask was placed under vacuum to dry overnight and yielded 0.0467 g (79%) of an orange solid. The compound was crystallized in CH_2Cl_2 by vapor diffusion with hexane to produce samples suitable for X-ray diffraction. ^{1}H NMR (600 MHz, $CDCl_3$): δ 7.87 (d, 1H), 7.62(d, 1H), 2.56 (s, 3H). ^{13}C NMR (600 MHz, $(CD_3)_2SO$): δ 172, 161, 155, 146, 126, 17. ESI MS: m/z (pos.) 442.8263(M + H) (calculated: 442.8279).

*Synthesis of $Cu(sma)_2$ **(2)***

A sample of Hsma (0.0627 g, 0.3316 mmol) was dissolved in 2 mL of ethanol. $Cu(OAc)_2$ (0.0300 g, 0.1652 mmol) was then dissolved in 3 mL of deionized water and

stirred under nitrogen. The selenomaltol mixture was added drop wise to the copper solution, immediately forming a brown precipitate. An additional 10 mL of water was added to further facilitate precipitation. The resulting mixture was filtered and washed with 5 mL of hexanes twice and an additional 5 mL of deionized water. The solid was placed under vacuum to dry overnight and yielded 0.0511 g (70%) of a reddish-brown solid. The compound was crystallized in CH_2Cl_2 by vapor diffusion with diethyl ether to produce samples suitable for X-ray diffraction. ESI-MS: m/z (pos.) 441.8281 (M + H) (calculated: 441.8284).

*Synthesis of Ni(sma)$_2$ (**3**)*

A sample of Hsma (0.0565 g, 0.2974 mmol) was dissolved in 2 mL of ethanol. $Ni(C_2H_3O_2)_2 \cdot 4\ H_2O$ (0.0367 g, 0.1477 mmol) was dissolved in 3 mL of deionized water and stirred under nitrogen. The selenomaltol mixture was added drop wise to the nickel solution, forming a dark purple precipitate. An additional 10 mL of water was added to further facilitate precipitation. The resulting mixture was filtered and washed with 5 mL of hexanes twice and an additional 5 mL of deionized water. The solid was placed under vacuum to dry overnight and yielded 0.0486 g (79%) of a black solid. The compound was crystallized in CH_2Cl_2 by vapor diffusion with diethyl ether to produce samples suitable for X-ray diffraction. ^{1}H NMR (600 MHz, $CDCl_3$): δ 7.50 (d, ^{1}H), 7.42 (d, ^{1}H), 2.45 (s, 3H). ^{13}C NMR(600 MHz, $CDCl_3$): δ 175, 167, 154, 142, 124, 16. ESI-MS: m/z(pos.) 436.8341 (M + H) (calculated: 436.8341).

*Synthesis of Fe(sma)$_3$ (**4**)*

A sample of Hsma (0.0631 g, 0.3338 mmol) was dissolved in 2 mL of ethanol. $Fe(NO_3)_3 \cdot 9\ H_2O$ (0.0433 g, 0.1073 mmol) was dissolved in 3 mL of deionized water and stirred under nitrogen. The selenomaltol mixture was added drop wise to the iron solution, immediately forming a black precipitate. An additional 10 mL of water was added to further facilitate precipitation. The resulting mixture was filtered and washed with 5 mL of hexanes twice and an additional 5 mL of deionized water. The solid was placed under vacuum to dry overnight and yielded 0.0561 g (84%) of a black solid. The compound was crystallized in CH_2Cl_2 by vapor diffusion with hexane to produce samples suitable for X-ray diffraction. ESI MS: m/z (pos.) 433.8255 (M +-sma) (calculated: 433.8259). Anal. calc'd for $H_{15}C_{18}Se_3O_6Fe$: C, 34.87; H, 2.44. Found: C, 34.95; H, 2.47.

References

1. K. H. Thompson, C. A. Barta and C. Orvig, *Chem. Soc. Rev*., **2006**, 35, 545–556.
2. B. L. Ellis, A. K. Duhme, R. C. Hider, M. B. Hossain, S. Rizvi and D. van der Helm, *J. Med. Chem*., **1996**, 39, 3659–3670.
3. M. C. Barret, M. F. Mahon, K. C. Molloy, J. W. Steed and P. Wright, *Inorg. Chem*., **2001**, 40, 4384–4388.
4. H. Luo, S. J. Rettig and C. Orvig, *Inorg. Chem*., **1993**, 32, 4491–4497.
5. S. J. Lord, N. A. Epstein, R. L. Paddock, C. M. Vogels, T. L. Hennigar, M. J. Zaworotko, N. J. Taylor, W. R. Driedzic, T. L. Broderick and S. A. Westcott, *Can. J. Chem*., **1999**, 77, 1249–1261.
6. M. Melchior, K. H. Thompson, J. M. Jong, S. J. Rettig, E. Shuter, V. G. Yuen, Y. Zhou, J. H. McNeill and C. Orvig, *Inorg. Chem*., **1999**, 38, 2288–2293.
7. B. D. Liboiron, K. H. Thompson, G. R. Hanson, E. Lam, N. Aebischer and C. Orvig, *J. Am. Chem. Soc*., **2005**, 127, 5104–5115.

8. V. Kahn, in Enzymatic Browning and Its Prevention, *American Chemical Society*, **1995**, ch. 22, vol. 600, pp. 277–294.

9. M. E. Helsel, E. J. White, S. Z. A. Razvi, B. Alies and K. J. Franz, *Metallomics*, **2017**, 9, 69–81.

10. S. R. Schlesinger, B. Bruner, P. J. Farmer and S.-K. Kim, *J. Enzyme Inhib. Med. Chem.*, **2013**, 28, 137–142.

11. D. P. Martin, P. G. Blachly, A. R. Marts, T. M. Woodruff, C. A. F. de Oliveira, J. A. McCammon, D. L. Tierney and S. M. Cohen, *J. Am. Chem. Soc*., **2014**, 136, 5400–5406.

12. J. A. Jacobsen, J. L. Fullagar, M. T. Miller and S. M. Cohen, *J. Med. Chem*., **2011**, 54, 591–602.

13. D. Brayton, F. E. Jacobsen, S. M. Cohen and P. J. Farmer, *Chem. Commun*., **2006**, 206–208.

14. J. A. Lewis and S. M. Cohen, *Inorg. Chem*., **2004**, 43, 6534–6536.

15. M. Backlund, J. Ziller and P. J. Farmer, *Inorg. Chem*., **2008**, 47, 2864–2870.

16. B. Bruner, M. B. Walker, M. M. Ghimire, D. Zhang, M. Selke, K. K. Klausmeyer, M. A. Omary and P. J. Farmer, *Dalton Trans*., **2014**, 43, 11548–11556.

17. W. Tejchman, K. Zborowski, W. Lasocha and L. M. Proniewicz, *Heterocycles*, **2008**, 75, 1931–1942.

18. W. Tejchman, E. Żesławska, K. Zborowski, W. Nitek and M. Żylewski, *ARKIVOC*, **2015**, 216–230.

19. W. Tejchman, L. M. Proniewicz and K. K. Zborowski, *J. Phys. Org. Chem*., **2015**, 28, 536–541.

20. J. A. Lewis, B. L. Tran, D. T. Puerta, E. M. Rumberger, D. N. Hendrickson and S. M. Cohen, *Dalton Trans*., **2005**, 2588–2596.

21. J. A. Lewis, D. T. Puerta and S. M. Cohen, *Inorg. Chem*., **2003**, 42, 7455–7459.

22. E. Orlowska, A. Roller, M. Pignitter, F. Jirsa, R. Krachler, W. Kandioller and B. K. Keppler, *Sci. Total Environ*., **2017**, 577, 94–104.

23. A. M. Bond and R. L. Martin, *Coord. Chem. Rev*., **1984**, 54, 23–98.

24. J. P. Barbier, A. El Biyyadh, C. Kappenstein, N. D. Mabiala and R. P. Hugel, *Inorg. Chem*., **1985**, 24, 3615–3620.

25. H. J. Reich and R. J. Hondal, *ACS Chem. Biol*., **2016**, 11, 821–841.

26. E. R. Cullen, F. S. Guziec, C. J. Murphy, T. C. Wong and K. K. Andersen, J. Am. *Chem. Soc.*, **1981**, 103, 7055–7057.

27. T. M. Krygowski, H. Szatylowicz, O. A. Stasyuk, J. Dominikowska and M. Palusiak, *Chem. Rev*., **2014**, 114, 6383–6422.

28. T. W. Keal and D. J. Tozer, *Mol. Phys*., **2005**, 103, 1007–1011.

29. R. D. Shannon, Acta Crystallogr., Sect. A: Cryst. Phys., Diffr.,*Theor. Gen. Crystallogr*., **1976**, 32, 751–767.

30. J. C. Slater, *J. Chem. Phys.*, **1964**, 41, 3199–3204.

31. M. J. Frisch, G. W. Trucks, H. B. Schlegel, G. E. Scuseria, M. A. Robb, J. R. Cheeseman, G. Scalmani, V. Barone, B. Mennucci, G. A. Petersson, H. Nakatsuji, M. Caricato, X. Li, H. P. Hratchian, A. F. Izmaylov, J. Bloino, G. Zheng, J. L. Sonnenberg, M. Hada, M. Ehara, K. Toyota, R. Fukuda, J. Hasegawa, M. Ishida, T. Nakajima, Y. Honda, O. Kitao, H. Nakai, T. Vreven, J. A. Montgomery, Jr., J. E. Peralta, F. Ogliaro, M. Bearpark, J. J. Heyd, E. Brothers, K. N. Kudin, V. N. Staroverov, R. Kobayashi, J. Normand, K. Raghavachari, A. Rendell, J. C. Burant, S. S. Iyengar, J. Tomasi, M. Cossi, N. Rega, J. M. Millam, M. Klene, J. E. Knox, J. B. Cross, V. Bakken, C. Adamo, J. Jaramillo, R. Gomperts, R. E. Stratmann, O. Yazyev, A. J. Austin, R. Cammi, C. Pomelli, J. W. Ochterski, R. L. Martin, K. Morokuma, V. G. Zakrzewski, G. A. Voth, P. Salvador, J. J. Dannenberg, S. Dapprich, A. D. Daniels, Ö. Farkas, J. B. Foresman, J. V. Ortiz, J. Cioslowski and D. J. Fox, Gaussian 09, Gaussian, Inc., Wallingford CT, **2009**.

32. Z. Chen, C. S. Wannere, C. Corminboeuf, R. Puchta and P. v. R. Schleyer, *Chem. Rev*., **2005**, 105, 3842–3888.

CHAPTER THREE

Solvent-Dependent Enchantment of Pyrylium Resonance forms of Thio- and Selenomaltol

Introduction

Maltol, 3-hydroxy-2-methyl-4-pyrone or Hma, and its derivatives shown in Scheme 3.1 has been used in a variety of bioinorganic applications such as insulin mimetics,[1] antimicrobials,[2] and other medicinal areas.[3-6] In many applications maltol is thought to exist as its neutral resonance structure.

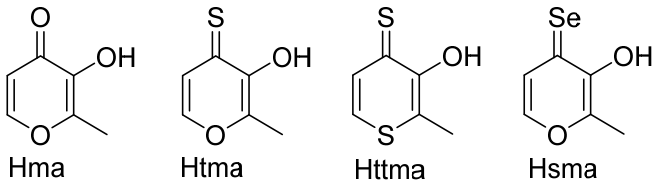

Scheme 3.1

However, these compounds may adopt a more delocalized aromatic resonance structure, resembling the pyrylium resonance shown in Scheme 3.2. These structures have been briefly studied before as intermediates in [5+2] cycloadditions[7-8] and nucleophilic–ring opening–ring closure reactions.[9] In addition, they have also been accessed by powerful acids, which allowed for the synthesis of new ionic liquids.[10] Last, the pyrylium structure has been briefly studied computationally.[11-13] However, each of these studies were conducted on maltol. There have been few examples of how the reactivity of the hetero-substitutions of maltol is affected by the pyrylium resonance structure.

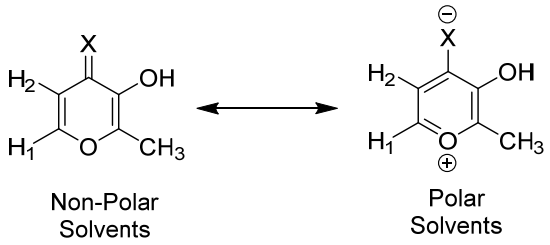

Scheme 3.2

There are two examples where, when chelated to a metal, the ligands 3-hydroxy-2-methyl-4-selenone (selenomaltol or Hsma) and 3-hydroxy-2-methyl-4-pyrone (dithiomaltol or Httma) seemed to display more of this aromatic resonance structure shown in Scheme 3.2.[14-16] In the Httma complexes, an unusual C-H bond activation was observed during the oxidation of the complex. This led to the formation of an aldehyde on the methyl group, instead of the expected oxidation of the sulfur. This odd oxidation was attributed to the aromatic resonance form of the ligand, with a thiopyrylium-like reactive intermediate.[17] In a more recent publication we saw similar evidence of an enhanced pyrylium resonance form when selenomaltol (3-hydroxy-2-methyl-selenone or Hsma) was chelated to various metal ions.[14] In both of these cases, the cation of the chelated metals seemed to stabilize the aromatic resonance form of Httma and Hsma. Herein, we evaluate if polar solvents can have a similar effect on maltol and its hetero-substitutions.

Solvents of increasing polarity were used to take to characterize the solvents effect on Hma, Htma, and Hsma, ^{1}H and ^{77}Se NMR spectra where applicable. In addition, maltol and its hetero-substitutions had their nucleophilicity tested by reacting them with methyl iodide in polar and non-polar solvents. The reaction only occurred in acetonitrile and resulted in the generation of two new pyrylium salts: 3-hydroxy-2-methyl-4-

(methylthio)pyrylium [(mtp)I] and 3-hydroxy-2-methyl-4-(methylselanyl)pyrylium [(msp)I]. These new products were characterized by X-ray crystallography, NMR spectroscopy and mass spectrometry. We suggest the increased understanding behind the pyrylium forms of maltol will allow facile access to the pyrylium states and may lead to similar reactivity in other heterocyclic systems.

Results and Discussion

Solvent Dependence

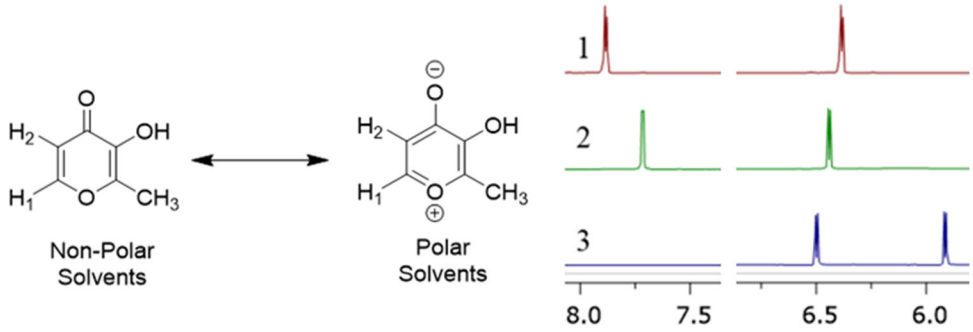

Figure 3.1. Proton NMR spectra of the vinylic protons, H_1 (left peak) & H_2 (right peak), in (1) 50/50 mixture CD_3CN/D_2O (2) $CDCl_3$ (3) C_6D_6.

The vinylic protons were monitored to evaluate which resonance form of maltol was favored, using benzene (dielectric constant of 2.27), chloroform (4.81) and an acetonitrile water mixture (58.1)[18] as the solvents for NMR spectroscopy. Figure 3.1. As the solvents shift from the non-polar benzene solvent, to the slightly polar chloroform and polar acetonitrile/water mixture the vinylic protons are shifted downfield. This downfield shift is consistent with the more pyrylium like resonance structure. The full list of vinylic proton peaks are shown in Table 2.1.

Table 3.1. Vinylic protons of Hma, Htma and Hsma.

Solvent	Hma	Htma	Hsma
Benzene	6.50/5.91	6.78/6.17	7.14/6.26
Chloroform	7.71/6.44	7.57/7.32	7.67/7.56
Acetonitrile/Water*	7.89/6.49	7.80/7.30	7.80/7.68

* 50/50 mixture of D_2O and CD_3CN
** The first number is H_1 and the second is H_2 as depicted on Scheme 1

As with the maltol example, there is a large downfield shift in the Hsma and Htma NMR spectra when the solvent polarity is increased. To better probe the effect the solvent has on the predominant resonance structure, ^{77}Se NMR spectroscopy was used. This is because the selenoketone would exhibit a large shift upfield as more electron density is localized on it, as it adopts the aromatic pyrylium resonance structure. A shift of ~150 ppm can be seen in Figure 3.2 as the solvent is changed from benzene to acetonitrile/water, which also suggests that the aromatic resonance structure is stabilized.

Reactivity

The increased electron density on the Se in the ^{77}Se NMR spectra suggests selenomaltol, and perhaps thiomaltol and maltol, are more nucleophilic in polar solvents. To test if the solvent-dependent changes in charge on the hetero-substituent might lead to a difference in reactivity, the three molecules (Hma, Htma and Hsma) were reacted with methyl iodide (CH_3I) in hexane and acetonitrile.

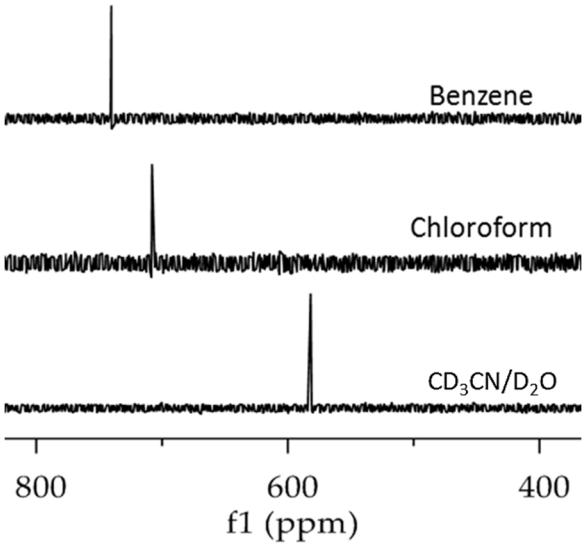

Figure 3.2. ^{77}Se NMR spectrum of selenomaltol in various solvents.

After 30 minutes at 65 °C both selenomaltol and thiomaltol react in acetonitrile, as shown in Scheme 3.3, generating stable pyrylium salts. No reactions were observed in hexane, which we attribute to the molecules adopting the neutral resonance structures in non-polar solvents. Under these conditions, maltol does not react in either solvent, which is likely due to oxygen being a less nucleophilic in comparison to sulfur and selenium.

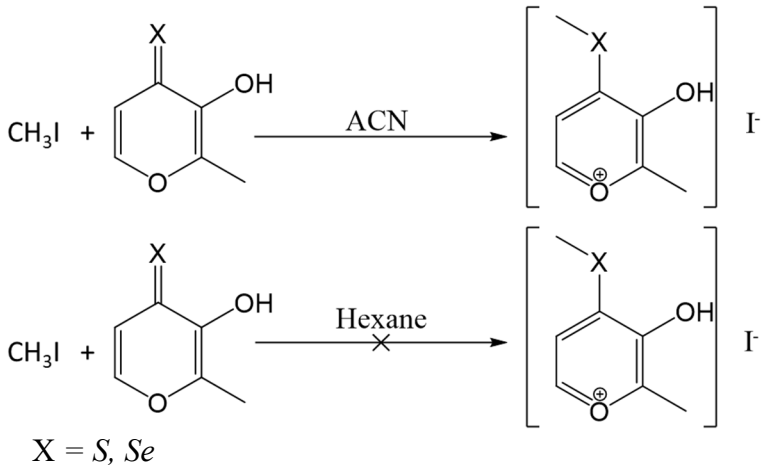

Scheme 3.3

The new derivatives, 3-hydroxy-2-methyl-4-(methylthio)pyrylium [(mtp)I] and 3-hydroxy-2-methyl-4-(methylselanyl)pyrylium [(msp)I] are air and moisture stable; both

were dried in air and washed with hexanes. The site of methylation is confirmed by the crystal structure, shown in Figure 3.3.

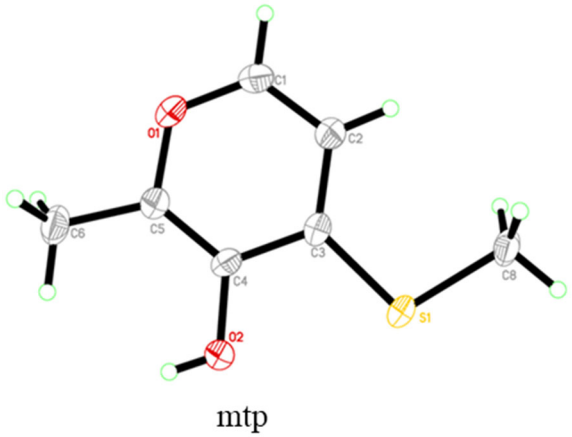

mtp

Figure 3.3. Crystal structure of (mtp)I. The structure for (msp)I is similar and can be found in the Appendix B.

A slight increase in ring bond-equivalence, a measure of aromaticity, is seen for both (msp)I and (mtp)I, compared with parent hetero-maltol in Table 3.2, as may be expected for a pyrylium salt. The individual bonds in the six-membered ring adopt more uniform bond distances, especially those adjacent to the hetero-substitution, however these are not statistically relevant from the free ligand (greater than 3 estimated standard deviations). A large elongation of the X=C bond (where X is Se or S) is also seen, closer to that of the expected single bond (C-S 1.81 Å, C-Se 1.98 Å). When compared to previously reported Zn, Cu, Ni and Fe complexes, (msp)I and (mtp)I are almost identical to that of the respective metal complexes, indicating similar pyrylium-like resonance forms. Additional crystallographic information is available in Appendix B.

Table 3.2. Bond length study of Htma and Hsma in comparison to (mtp)I and (msp)I

Compound	C3=X	C3-C4	C2-C3	C4=C5	C1=C2	C5-O	C1-O
Htma	1.677(1)	1.430(2)	1.426(2)	1.363(2)	1.345(2)	1.360(2)	1.345(2)
(mtp)I	1.720(4)	1.418(5)	1.406(5)	1.366(5)	1.353(5)	1.355(4)	1.341(5)
Hsma	1.827(19)	1.421(3)	1.420(3)	1.344(3)	1.358(3)	1.340(3)	1.355(2)
(msp)I	1.871(3)	1.415(4)	1.398(4)	1.355(4)	1.370(4)	1.337(4)	1.345(3)

*atom labeling is consistent with those labeled in Figure 3.3.

Experimental

Materials

Maltol was purchased from Alfa Aesar and used as received. All solvents used, Woollins reagent, Lawessons reagent and methyl iodide were purchased from Sigma-Aldrich. Thiomaltol and selenomaltol were prepared using previously published methods.

Physical measurements

Electronic absorption spectra were recorded with an Agilent 8453 diode array spectrophotometer. Microwave syntheses were carried out in a discover SP microwave system. Mass spectra were obtained on a Thermo Electron Linear Trap Quadrupole Orbitrap Discovery mass spectrometer. NMR spectra were recorded on a 600 MHz NMR spectrometer.

Crystallographic data was collected on crystals with the dimensions 0.216 x 0.078 x 0.051 mm^3 for msp-I and 0.331 x 0.072 x 0.045 mm^3 for (mtp)I. Data was collected at 110 K on a Bruker D8 quest using Mo–K (λ = 0.71073 Å) radiation. The data was processed using the Bruker AXS SHELXTL software, version 6.10. Crystallographic parameters for structural determinations of (mtp)I and (msp)I are given in the Appendix B. Crystals were grown using vapor diffusion with ether into methanol.

Synthesis 3-hydroxy-2-methyl-4-(methylselanyl)pyrylium Iodide [(msp)I]

Methylated selenomaltol ($C_7H_9O_2Se$) was prepared by dissolving 0.305 g (1.614 mmol) of selenomaltol with 1.01 mL (3.12 mmol) of CH_3I in acetonitrile. The reaction was done at 60 °C for 30 minutes heated via microwave. The subsequent evaporation of the solvent by rotovap and washing with hexane yielded 0.320 g (60%) of the dark red product methyl-selenomaltol. ESI MS: m/z (pos.) 204.9730 (M+) (calculated: 204.9768). In methanol-d_4 ^{1}H NMR (600 MHz, $CDCl_3$): δ 8.74 (d, 1H), 8.06 (d, 1H), 8.06 (d, 1H), 7.92 (s, 1H), δ 2.75 (s, 3H), δ 2.71 (s, 3H). ^{77}Se (600 MHz, $CDCl_3$): δ 342. Crystals were grown in chloroform with hexane diffusing into solution.

Synthesis of 3-hydroxy-2-methyl-4-(methylthio)pyrylium Iodide [(mtp)I]

Methylated thiomaltol ($C_7H_9O_2Se$) was prepared in a similar fashion to (msp)I. A sample of 0.506 g (3.563 mmol) of thiomaltol was reacted with 2.22 mL (6.86 mmol) of CH_3I in acetonitrile. Subsequent evaporation of the solvent and washing with hexane yielded 0.506 grams (50 %) of the dark red product methyl-thiomaltol. ESI MS: m/z (pos.) 157.0317 (M +) (calculated: 157.0323). In acetonitrile-d_3 ^{1}H NMR (600 MHz, $CDCl_3$): δ 8.66 (d, 1H), 7.75 (d, 1H), 2.84 (s, 3H), δ 2.74 (s, 3H).

Conclusions

Reactivity studies and NMR spectroscopy of maltol and similar hetero-substituted species show different resonance structures depending on the polarity of the solvent used to dissolve the molecule. The greater nucleophilicity of thiomaltol and selenomaltol in MeCN shown in the aforementioned reactivity studies led to the generation of new stable pyrylium compound (mtp)I and (msp)I, which are moisture and air stable. We expect

these new stable pyrylium species will find use in the bioinorganic and synthetic community, and perhaps similar reactivity and resonance stabilization may be found in other analogous ring systems such as flavanols.

References

1. Melchior, M.; Thompson, K. H.; Jong, J. M.; Rettig, S. J.; Shuter, E.; Yuen, V. G.; Zhou, Y.; McNeill, J. H.; Orvig, C., Vanadium Complexes as Insulin Mimetic Agents: Coordination Chemistry and in Vivo Studies of Oxovanadium(IV) and Dioxovanadate(V) Complexes Formed from Naturally Occurring Chelating Oxazolinate, Thiazolinate, or Picolinate Units. *Inorganic Chemistry* **1999**, 38 (10), 2288-2293.

2. Morris, J. A.; Khettry, A.; Seitz, E. W., Antimicrobial activity of aroma chemicals and essential oils. *Journal of the American Oil Chemists' Society* **1979**, 56 (5), 595-603.

3. Ma, Y.; Luo, W.; Quinn, P. J.; Liu, Z.; Hider, R. C., Design, Synthesis, Physicochemical Properties, and Evaluation of Novel Iron Chelators with Fluorescent Sensors. *Journal of Medicinal Chemistry* **2004**, 47 (25), 6349-6362.

4. Thompson, K. H.; Barta, C. A.; Orvig, C., Metal complexes of maltol and close analogues in medicinal inorganic chemistry. *Chemical Society Reviews* **2006**, 35 (6), 545-556.

5. Helsel, M. E.; White, E. J.; Razvi, S. Z. A.; Alies, B.; Franz, K. J., Chemical and functional properties of metal chelators that mobilize copper to elicit fungal killing of Cryptococcus neoformans. *Metallomics* **2017**, 9 (1), 69-81.

6. Lewis, J. A.; Cohen, S. M., Addressing Lead Toxicity: Complexation of Lead(II) with Thiopyrone and Hydroxypyridinethione O,S Mixed Chelators. *Inorganic Chemistry* **2004**, 43 (21), 6534-6536.

7. Mascareñas, J. L.; Pérez, I.; Rumbo, A.; Castedo, L., A New [5+2] Annulation Method for the Synthesis of 8-Oxabicyclo[3.2.1]octanes from Pyrones. *Synlett* **1997**, 1 (01), 81-82.

8. Ylijoki, K. E. O.; Stryker, J. M., [5 + 2] Cycloaddition Reactions in Organic and Natural Product Synthesis. *Chemical Reviews* **2013**, 113 (3), 2244-2266.

9. Balaban, A. T., CHAPTER 3 - Monocyclic Hetarenes with π-Electron Aromatic Sextet. In *Advances in Heterocyclic Chemistry*, Katritzky, A. R., Ed. Academic Press: **2010**; Vol. 99, pp 61-105.

10. Platzer, S.; Sap, O.; Leyma, R.; Wallner, G.; Jirsa, F.; Kandioller, W.; Krachler, R.; Keppler, B. K., Extraction of natural radionuclides from aqueous solutions by novel maltolate-based task-specific ionic liquids. *J Radioanal Nucl Chem* **2015**, 303 (3), 2483-2488.

11. Zborowski, K.; Grybos, R.; Proniewicz, L. M., Theoretical studies on the aromaticity of selected hydroxypyrones and their cations and anions. Part 1—Aromaticity of heterocyclic pyran rings. *Journal of Physical Organic Chemistry* **2005**, 18 (3), 250-254.
12. Tejchman, W.; Zborowski, K.; Lasocha, W.; Proniewicz, L. M., Selenomaltol-synthesis, spectroscopy and theoretical calculations. *Heterocycles* **2008**, 75 (8), 1931-1942.

13. Zborowski, K. K.; Solà, M.; Poater, J.; Proniewicz, L. M., Theoretical studies on aromaticity of selected hydroxypyrones. Part 3#. Chelatoaromaticity phenomenon in metalcomplexes of hydroxypyrones. *Journal of Physical Organic Chemistry* **2011**, 24 (6), 499-506.

14. Spiegel, M. T.; Hoogerbrugge, A.; Truksa, S.; Smith, A. G.; Shuford, K. L.; Klausmeyer, K. K.; Farmer, P. J., Synthesis of first row transition metal selenomaltol complexes. *Dalton Transactions* **2018**, 47 (27), 9030-9037.

15. Brayton, D.; Jacobsen, F. E.; Cohen, S. M.; Farmer, P. J., A novel heterocyclic atom exchange reaction with Lawesson's reagent: a one-pot synthesis of dithiomaltol. *Chemical Communications* **2006**, (2), 206-208.

16. Backlund, M.; Ziller, J.; Farmer, P. J., Unexpected C−H Activation of Ru(II)−Dithiomaltol Complexes upon Oxidation. *Inorganic Chemistry* **2008**, 47 (7), 2864-2870.

17. Bruner, B.; Walker, M. B.; Ghimire, M. M.; Zhang, D.; Selke, M.; Klausmeyer, K. K.; Omary, M. A.; Farmer, P. J., Ligand-based photooxidations of dithiomaltolato complexes of Ru(ii) and Zn(ii): photolytic CH activation and evidence of singlet oxygen generation and quenching. *Dalton Transactions* **2014**, 43 (30), 11548-11556.

18. Gagliardi, L. G.; Castells, C. B.; Ràfols, C.; Rosés, M.; Bosch, E., Static Dielectric Constants of Acetonitrile/Water Mixtures at Different Temperatures and Debye−Hückel A and a0B Parameters for Activity Coefficients. *Journal of Chemical & Engineering Data* **2007**, 52 (3), 1103-1107.

CHAPTER FOUR

Reactivities of Aromatic Protons in Crude Oil Fractions toward Br_2 Tagging for Structural Characterization by Nuclear Magnetic Resonance and Electron Paramagnetic Resonance Spectroscopy and Mass Spectrometry

This chapter published as: "Michael T. Spiegel, Ian G. M. Anthony, Matthew R. Brantley, Alton Hassell, Patrick J. Farmer, and Touradj Solouki. *Energy & Fuels* **2018** 32 (10), 10549-10555"

Introduction

Crude oil is a complex mixture of hydrocarbons with a variety of functional group variations, including various hetero-substituents, such as oxygen, sulfur, and metals.[1] The heptane-insoluble, toluene-soluble fraction of crude oil is known as the asphaltene fraction, which contains the heaviest components of crude oil, generally with the highest boiling points.[2,3]Asphaltenes contain highly substituted, polyaromatic rings that stack and aggregate, forming sediments that are typically removed during the processing of crude oil to increase the ease of handling of the remaining oil fractions.[4–6] Because of the complexity of asphaltene samples, it is difficult to efficiently prevent premature aggregation. Therefore, a better understanding of the chemical structures present in asphaltene samples could help minimize their adverse effects on industrial processes.[1-7]

Although significant contributions have been made to elucidate structures of asphaltenes to predict their reactivities, there has been comparatively little work done to use the reactivities of asphaltenes to characterize their reactivities.[8,9] For instance, analyte tagging with mass deficient reagents can be used for functional group identification.[10] Elemental bromine (Br_2) is a particularly useful mass deficient tag for probing the

reactivities of asphaltenes because the reactivity of Br_2 with hydrocarbons is well-known.[11] Moreover, Br_2 is well-suited for mass spectrometry (MS) analysis of crude oil fractions because it is an easy to introduce reactant (i.e., it is a liquid that is miscible with both toluene and n-heptane solutions), provides a distinct isotopic pattern (i.e., two peaks, at roughly 51% and 49% relative abundances with an ~2 m/z separation), and introduces a mass deficit (i.e., the lower mass isotope of bromine is 78.9183 amu instead of the nominal 79 amu, a difference of -0.0817 amu).

As shown in Scheme 4.1, there are three main pathways that Br_2 can react with organic molecules: (1) addition to an unconjugated double bond, (2) free radical bromination, (3) and electrophilic aromatic substitution (EAS).[11–15]Asphaltenes lack unconjugated double bonds, and hence, bromine addition reactions should not occur.[2] Free radical bromination requires ultraviolet (UV) light to generate free radicals and, thus, can be avoided via an opaque container. Therefore, EAS is expected to be the primary reaction resulting from the addition of Br_2 to asphaltenes under dark conditions.

Kendrick mass defect (KMD, or difference from the nominal mass) analysis is a data visualization technique in MS for "mass-deficiency-based" compound or hydrocarbon classification that is useful for analysis of complex samples, including crude oil fractions.[16–19]Although highly useful for observing differences between the mass spectra of complex samples, KMD has not been widely used to probe chemical reactivities of crude oils via mass deficient derivatization agents. "Labeling" via Br_2 electrophilic aromatic substitution predictably alters analytes in both the mass and mass deficiency dimensions and can move signals of reactive molecules from the congested regions of Kendrick plots.[17] Moreover, the distinctive isotopic pattern of Br_2 makes KMD

plots especially useful for visualizing the extent of a molecule's reactivity toward Br_2 (via number of additions of Br).

Besides MS, other analytical methods, such as nuclear magnetic resonance (NMR) spectroscopy and electron paramagnetic resonance (EPR) spectroscopy, have been used to interpret the speciation of crude oil fractions.[32–39] Typically, NMR spectra of crude oil fractions contain significant line broadening from aggregation and stabilized free radicals that hinder data interpretations.[20] In addition, the asphaltene fraction may contain paramagnetic metals, which can cause further line broadening.[3] EPR spectroscopy has previously been employed in studying these unpaired electrons in crude oil[21–23] but has not been used to compare the influence of metal ion content on crude oil NMR spectra.

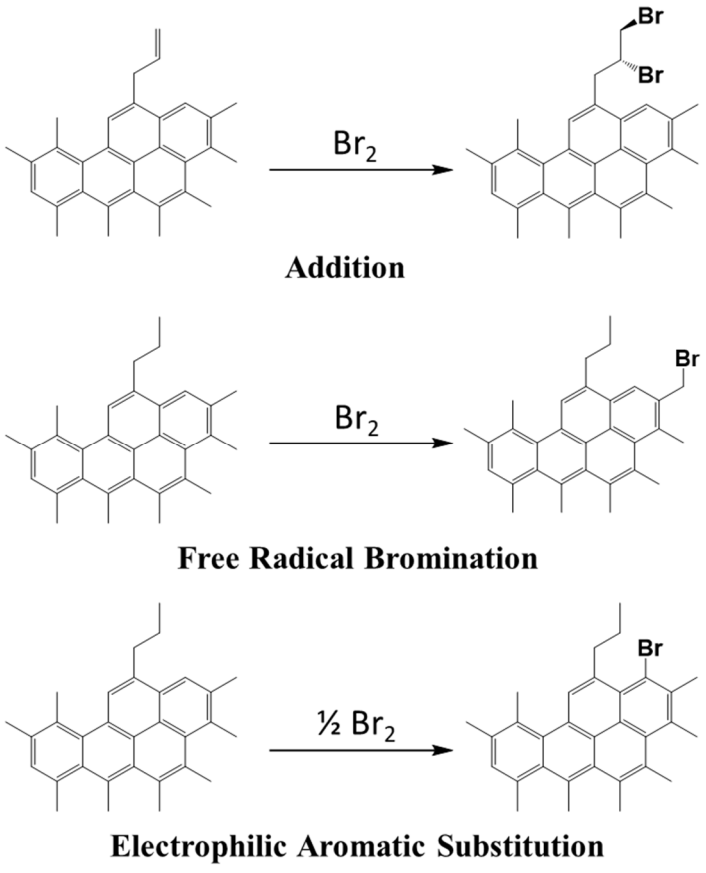

Scheme 4.1

Herein, we report results from KMD analysis of the crude oil product mixtures following bromination of the heptane and asphaltene fractions of West Texas crude oil. Additional details on chemical speciation are reported for $^{13}C/^{1}H$ NMR and EPR spectra of the crude oil fractions. We also demonstrate that a simple column purification dramatically reduces the paramagnetic content of the asphaltene fraction and enables NMR spectral analysis to provide characterization and quantification of a range of chemical functional groups within an asphaltene sample.

Experimental Section

All reagents and solvents were purchased from Sigma-Aldrich Chemical Co. (St. Louis, MO, U.S.A.). Unless otherwise noted, chemicals were used without further purification. Light crude oil (West Texas blended oil that is paraffin-based) samples from Texas Crude (Midland, TX, U.S.A.) were purchased for complex mixture analysis.

Asphaltene and n-heptane fractions of the crude oil were prepared following the IP 143/01 method.[24] Briefly, crude oil was mixed with n-heptane at a volume by volume ratio of 1:30 oil:n-heptane. The mixture was refluxed for 60 minutes at 150 °C and then sealed and allowed to cool for 90 min in the dark to avoid photo-reactivity. Once cooled, the mixture was filtered through a Büchner funnel. The material that remained on the filter was washed with 70 °C n-heptane. The filtrate (hereafter referred to as then-heptane fraction) was collected and stored at 0 °C. Toluene at 70 °C was then used to dissolve the asphaltenes collected on the filter frit into a clean flask (hereafter referred to as the asphaltene fraction). An aliquot was taken of each asphaltene and n-heptane fraction and evaporated to yield concentrations of 70 mg mL^{-1} of asphaltenes in toluene and 250 mg $mL^{-1}$of solid in then-heptane fraction. A sample from each fraction was diluted with

toluene to 0.25 mg mL^{-1} and brominated (under dark conditions in glass amber vials that had been wrapped with aluminum foil to prevent any free radical bromination) with 5 μL of elemental bromine (with an approximate mole ratio of 1:200 asphaltene/Br_2, with the rough assumption of 500 g $mol^{-1}$for an average asphaltene molecular weight). The resulting mixtures were analyzed by Orbitrap MS after 30 min of reaction time.

Additionally, a silica gel gravity column separated asphaltene solution was generated by passing 10 mg of dried asphaltene sample through a 1" diameter and 3". long glass column packed with 3 g of silica gel [using 0.06−0.20 mm outer diameter (OD) silica beads]. The column was packed by making a toluene and silica gel slurry and quickly adding the resulting slurry to the column [using∼2:1 (v/v) ratio of toluene/silica]. The resulting silica gel column was washed with 50 mL of high-performance liquid chromatography (HPLC)-grade toluene. After loading 1.0 mL of asphaltene solution (at 10 g L^{-1} dissolved toluene), three sequential eluents were used to purify the asphaltenes: (a) 50 mL of toluene, (b) 50 mL of methanol, and (c) 50 mL chloroform. The flow rate for the column was roughly 1 drop (∼0.05 mL) per 2 s. All resulting solutions were combined, and the solvents were removed via rotovap at∼25°C. The resulting solid was put under vacuum (∼5.0×10^{-3} torr) for 24 h to ensure complete solvent removal, yielding∼9.0 mg of silica-column-treated asphaltenes.

Sample Preparation for inductively Coupled Plasma Mass Spectrometry (ICP-MS) Analysis

For ICP−MS analysis, pre- and post-column samples were prepared from non-brominated asphaltene solutions using an "emulsion breaking" method adapted from Cassella et al.[25] In brief, 1 mg of asphaltenes (for both the pre- and post-column ICP−MS

samples) was dissolved in 10 mL of toluene. A total of 2 mL of an acidic Triton-X114 solution was added to 1 mg of both asphaltenes in 10 mL of toluene solution, vigorously shaken for 30 min, and then placed on a roller mixer for 60 min. No true emulsion formed in either solution (because the toluene and aqueous fractions were observed to separate after ~1 min of no mixing). The two mixtures were centrifuged at 10,000 rpm for 10 min. The acidic, aqueous subnatant of each solution was carefully removed via pipet and analyzed without dilution using ICP−MS (details discussed below).

Instrumentation

For KMD plots, MS measurements in positive-ion mode were carried out using an Orbitrap Discovery mass spectrometer equipped with an atmospheric pressure photo ionization (APPI) source (ThermoFisher Scientific, Waltham, MA, U.S.A.). Sample solutions were infused at a rate of 5 μL min^{-1} with nitrogen as the sheath gas. The optimized APPI conditions were as follows: ion spray voltage, 5 V; capillary temperature, 275°C; and tube lens voltage, 110 V. For metal analysis, an Agilent Technologies (Santa Clara, CA, U.S.A.) 7900 ICP−MS was used in positive-ion mode and a flow of 9.5 L min^{-1} Ar gas. The radio frequency (RF) power was set to 1550W, and the nebulizer pump was set to 0.10 rotations per second (rps). An internal standard solution of ^{7}Li, ^{89}Y, and ^{205}Tl was carried concurrently to the samples (with one of the nebulizer pump lines). Analogous to other experiments reported here, method blanks were used in between the pre- and post-column samples to avoid carry over.

^{1}H, distortionless enhancement by polarization transfer (DEPT) ^{13}C, and ^{13}C NMR spectra were recorded on an Ascend 600 MHz NMR spectrophotometer (Bruker, Billerica, MA, U.S.A.) at 298 K and referenced to chloroform (7.26 ppm for ^{1}H and

77.23 ppm for ^{13}C). The spectral widths for the ^{1}H and ^{13}C NMR spectra analyses were ~20.03 and ~240.05 ppm, respectively. The averaged number of scans for proton and carbon NMR spectra were 32 (Figure 3) and 10,000 (Figure 4), respectively. The excitation pulse widths for the ^{1}H and ^{13}C NMR spectra were 12 and 10 μs, respectively.

EPR spectra were recorded on an EMX Plus spectrometer (Bruker, Billerica, MA, U.S.A.). The center field was 3200 G with a sweep width of 6000 G and sweep time of 60 s for 20 averaged scans. The microwave frequency was 9.85 GHz.

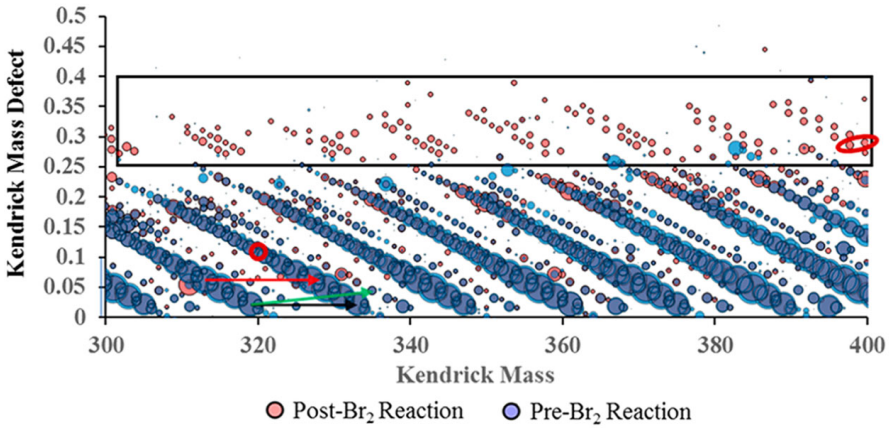

Figure 4.1. KMD plot of the unreacted (blue) and brominated (red) *n*-heptane fraction from 300 to 400 KM units. Doublet peaks associated with Br-R species, as described in the text, are highlighted in the inset black box. The two points circled in red highlight a representative bromination event. The red, green, and black arrows point to observed KM and KMD shifts with the substitution of H for NH, O, and CH_2, respectively.

Results and Discussion

CH_2-based KMD plots were generated by redefining the masses of the observed analytes in the original mass spectrum from C to CH_2 given by equation 4.1; these Kendrick mass (KM) values were used to form the x axis of the KMD plot.[17] KMD (the difference between nominal mass and KM) is plotted as a function of the KM. Sizes of the points in the KMD plot of Figure 1 are correlated to relative abundances of peaks.

$$Equation\ 4.1\ Kendrick\ mass = (observed\ mass)\ x \frac{nominal\ mass\ of\ CH_2}{Exact\ mass\ of\ CH_2}$$

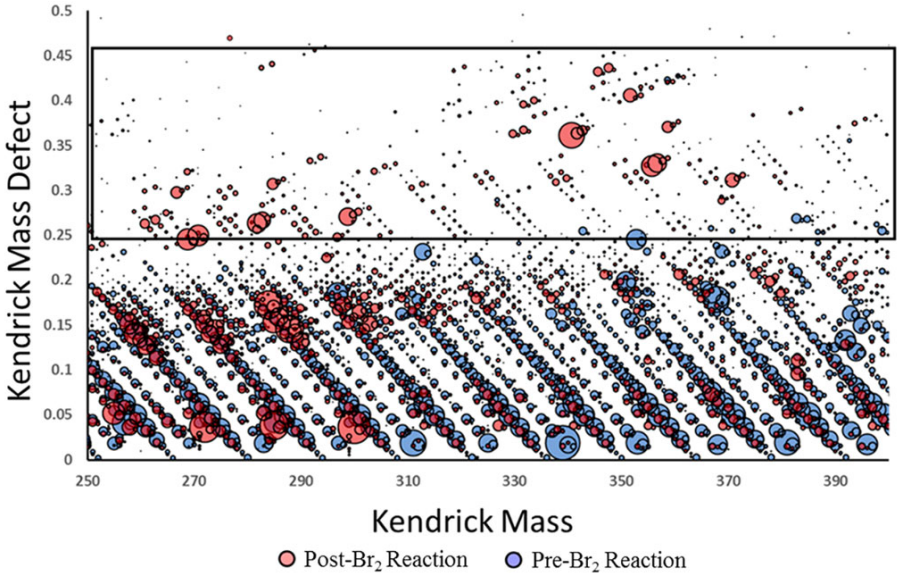

Figure 4.2. KMD plot of the unreacted (blue) and brominated (red) asphaltene fraction from 250 to 400 KM units. Doublet peaks associated with Br-R, as described in the text, are located in the boxed region.

Scheme 4.2

The KMD plots of the pre-bromination (blue) and post bromination (red) n-heptane fractions generated from two separate mass spectra are overlaid in Figure 4.1. For clarity, only the zoomed-in area between 300 and 400 KM units is shown. The full KMD plot of each sample is included in the Supporting Information as well as a similar "zoomed-in" crude oil figure (Appendix C1-4). Each diagonal line defines various polyaromatic hydrocarbons with decreasing saturation, with the lower abundance chains containing various hetero-substitutions. Brominated species (Br−R) are identifiable by

apparent “doublet” peaks as a result of the near equal natural abundance of ^{79}Br and ^{81}Br isotopes with double and triple brominations seen as “triplets” and “quartets”, respectively. The two points circled in red are a representation of a bromination showing the change in mass and mass defect from a specific point. The red, green, and black arrows show the shift in KM units from NH, O, and CH_2 replacing H, respectively. In the n-heptane fraction, only single brominations (highlighted by the black box) are observed.

Smaller aromatic species are less likely to undergo substitution reactions, which agrees with previous studies that indicate that the aromatic species in the n-heptane fraction are smaller than that of asphaltenes.[26,27] Bromine substitution does not occur until ~0.11 mass deficiency (corresponding to a loss of ~16 protons from a pure CH_2 chain). This is due to Br_2 substitution occurrence only on larger aromatic systems (in the absence of a catalyst or UV light). In addition, the majority of brominations in the n-heptane fraction occur from non-heterosubstituted species.

Pre- and post-bromination KMD analysis was also performed on the asphaltene fraction in Figure 4.2. The asphaltene fraction (relative to n-heptane fraction) undergoes more extensive brominations. The Br−R species in the asphaltene fraction displayed mostly single and some double substitutions (no asphaltene species was observed to brominate more than 3 times). Substitution occurs at the same mass deficiency (~0.11) as the n-heptane fraction. The majority of brominations come from non-heterosubstituted polyaromatics, but some arise from heterosubstituted species. The lack of substitution from hetero-substituted asphaltenes is presumed to be due to the electron-withdrawing nature of heteroatom-containing functional groups.

To better understand the extent of asphaltene bromination, benzo[a]pyrene (BP, 252.31 g mol^{-1}) was added as an internal standard to the asphaltene samples and its brominations were compared to other asphaltenes. Although BP has 12 potential bromination sites, based on the interpretation of the KMD plots (Appendix C5 of the Supporting Information), only first, second, and third brominations were observed; this level of bromination for BP (up to three, as shown in Scheme 4.2, in any position) is higher than the number of brominations observed for other asphaltenes in the asphaltene fraction (especially for asphaltenes of similar masses). In a separate MS experiment, it was confirmed that BP did not react with asphaltene and remained intact within the asphaltene mixture. The lack of triple brominations of the asphaltenes may be attributed to a deactivation of the ring system, recruitment into larger aggregates, steric hindrance, or general lack of aromatic protons. Two other possible explanations for the lack of triple brominations of the asphaltenes are a lack of available bromine atoms for substitution and slow Br_2 EAS reaction kinetics. However, the ~200:1 mol ratio of Br_2/asphaltenes (discussed in the Experimental Section) means that there should be enough Br atoms to substitute more than three aromatic protons on each asphaltene. Additionally, BP brominated multiple times (i.e., up to 3 times) given the same reaction time and conditions (i.e., 30 min with Br_2 in dark conditions, with a toluene solvent, present in a solution of other asphaltenes) as the asphaltene fraction. Therefore, it appears (although it is not certain) that the substitution is not kinetically limited.

NMR spectroscopic analysis was performed to verify the specific reason that higher numbers of brominations were not observed (because NMR spectroscopy might provide evidence for steric hindrance, lack of available aromatic protons, etc.).

Additionally, to better understand the structural makeup of asphaltenes and characterize their functional groups, the NMR spectra of fractionated crude oil samples (i.e., toluene/asphaltene and n-heptane/non-asphaltene fractions) were compared. The initial intent was to investigate the relative abundances of aromatic protons present in the asphaltene by obtaining ratios of aromatic to non-aromatic protons, a rough measure of alkyl versus aromatic content.[28–30] However, as previously reported,[28,29] because of the significant line broadening observed in ^{1}H NMR spectra of asphaltenes (presumably because of potential aggregation and/or the presence of paramagnetic organic radicals and transition metal ions in crude oil samples), NMR spectra provide limited information for complete structural characterization.

It is well documented that asphaltenes contain a variety of organic radicals and paramagnetic metal ions, such as V, Ni, and Fe species.[3,21–23] As seen in Figure 3, EPR spectra of the asphaltene fraction shows a sharp absorbance at g = 2.00 (where g is the "g tensor" of EPR spectra),[31] attributable to organic radicals, and a broader signal at g = 2.29, attributable to paramagnetic metal ions, similar to previous characterizations of asphaltene.[23,32,33]

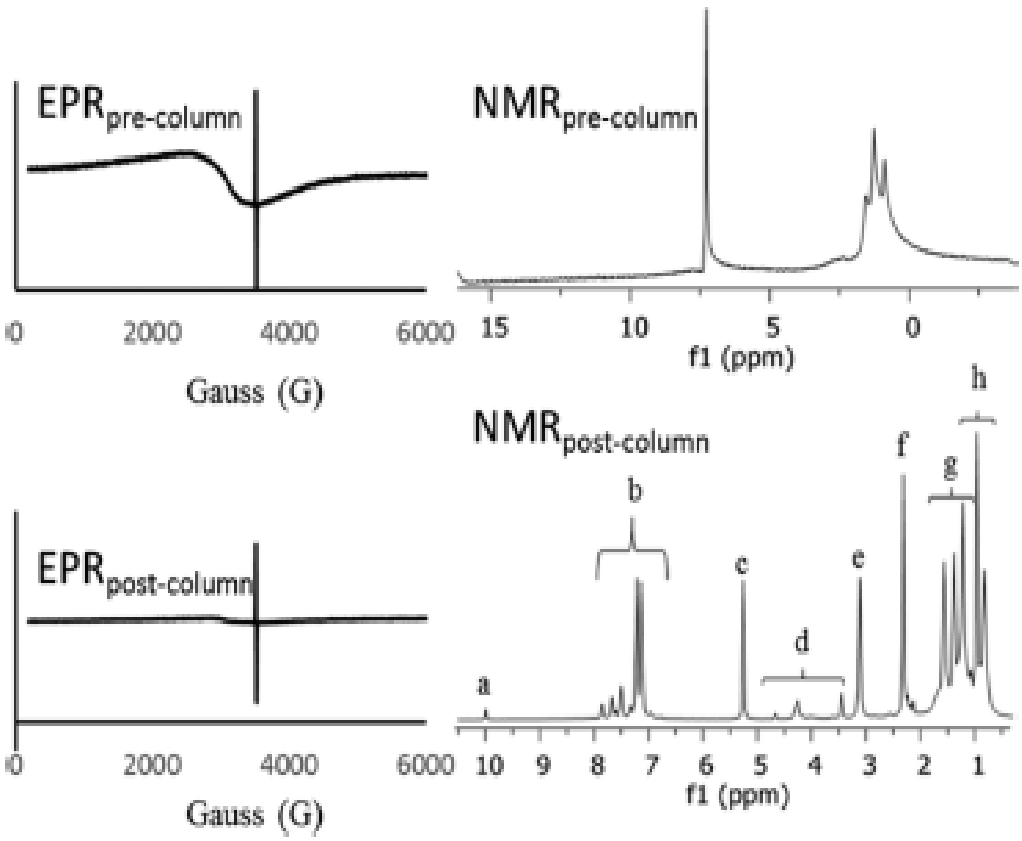

Figure 4.3. (Left) EPR spectra and (right) ^{1}H NMR spectra of (top) pre-column cleanup and (bottom) post-column cleanup asphaltenes in a 10mg mL^{-1} $CDCl_3$ solution. Labels in lower right ^{1}H NMR spectrum show assignments of peaks to (a) aldehyde or carboxylic acid, (b) aromatic (also solvent $CDCl_3$), (c) phenolic, (d) OH/NH, (e) amine-substituted CH_2 and CH_3, (f) carbonyl- and benzyl-substituted CH_3, (g) alkyl-branched CH_2 and CH, and (h) terminal CH_3 protons.

To remove the paramagnetic metal ion species detected by EPR spectroscopy, a short column purification on silica gel was performed that resulted in dramatically improved ^{1}H NMR spectral resolution, as seen in Figure 4.3. This sample cleanup resulted in a loss of ~10% of asphaltene mass (from 10.0 mg of precolumn to 9.0 mg of recovered post-column). ICP−MS analysis was performed on the asphaltene fractions pre- and post-column and showed a 95% reduction in all paramagnetic signals studied, including a 98% reduction of Fe, the most abundant paramagnetic species. Thus, the 10%

loss in mass is attributed primarily to paramagnetic and other metal-ion containing species. For further information, including results from ICP−MS analyses of the pre- and post-column asphaltenes, the reader is referred to Appendix C6 of the Supporting Information. To determine if sample complexity was retained post-column, mass spectra were reacquired for the post- column fraction and did not show any loss in complexity (see Appendix C7 and C8 for Supporting Information).

The post-column ^{1}H NMR spectra showed a dramatic increase in resolution that allows for the identification of a variety of functional groups present in the asphaltene mixture. The relatively narrow line widths of the NMR spectra of cleaned samples are likely due to the loss of paramagnetic species and reduced aggregation (with the loss of only ∼10% mass based on the weighing of samples before and after the column cleanup procedure).

As assigned in Figure 4.3 (post-column NMR spectrum), a small peak near 10 ppm (labeled as “a”) indicates the presence of aldehydes or carboxylic acids. Well-defined aromatic peaks (labeled as “b”) are observed between 7 and 8 ppm; the lack of peaks between 8 and 9 ppm in Figure 4.3 suggests that few N-substituted pyridine-like heterocycles are present. This is not surprising because the studied asphaltene species between 8 and 9 ppm would most likely be bound to metals and, thus, lost in the column (contributing to the observed 10% mass loss after the cleanup). The peak at ∼5.3 ppm (labeled as “c”) is indicative of phenolic alcohols. This region is also attributable to unconjugated double bonds, but the absence of Br_2 addition in mass spectra (i.e., addition of two bromines across a double bond) discounts this possibility. Non-aromatic NH and OH peaks between 3 and 5 ppm (labeled as “d”) are in much lower abundance but

observed. NR_2 (where R is any alkane) protons are also present (labeled "e"). A high abundance of carbonyl and benzylic protons are present (labeled as "f"), indicating that there are likely many alkyl groups attached to the aromatic core. Lastly, the branching CH and CH_2 species (labeled as "g") and terminal CH_3 protons are observed between 0 and 2 ppm (labeled as "h"). Most of these protons are branching, instead of the terminal CH_3, meaning that the aromatic cores within asphaltenes are highly substituted. Using peak integration of the assignments above yields estimates of proton content percentages provided in Table 1; aliphatic $-CH_{1/2/3}$ peaks make up the majority of all observed ^1H signals, at ~65%. The quantification of aromatic protons, ~10%, is complicated by subtraction of the solvent $CDCl_3$ peak but in good agreement with previous estimates.[34–38] The lack of aromatic protons coupled with the extensive branching found in the NMR spectra analysis correlates well with our MS results and KMD tagging studies. The lack of multiple brominations is likely caused by the steric hindrance of the branched alkanes or deactivation of the aromatic core by electron-withdrawing functional groups.

Table 4.1. Relative speciation of protons by NMR spectra peak integration

peak assignment	percentage
-C(O)H	0.21
Ar-H	10.24
Ar-OH	3.02
-OH and $-NH_x$	4.13
N-$CH_{2/3}$	7.47
C(O)$CH_{2/3}$ and Ar-CH_3	9.84
-CH_2 and -CH	40.97
-CH_3	24.12

[a]As per refs 36-42. [b]By integration of the assigned area under assigned ^1H NMR spectrum peaks, as a percentage of the total.

The ^{13}C NMR spectrum of the column-purified asphaltene sample is shown in Figure 4.4; this cleaned-up asphaltene also shows enhanced spectral resolution not attainable for unpurified samples. As above, downfield peaks between 160 and 200 ppm can be attributed to the presence of aldehyde, carboxylic acid, and ester carbons (labeled

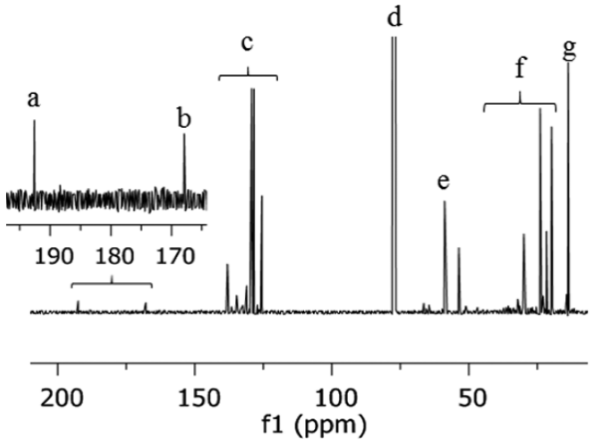

Figure 4.4. ^{13}C NMR spectrum of the column-purified asphaltene sample. Labels show assignments of peaks to (a) aldehyde or carboxylic acid, (b) ester, (c) aromatic, (d) solvent ($CDCl_3$), (e) N- or O-substituted, (f) branched CH_2 and CH, and (g) terminal CH_3 carbons.

as "a" and "b" in Figure 4.4). Similar to the ^{1}H spectrum shown in Figure 4.3, the aromatic species are not as deshielded as possible (labeled as "c"); this suggests a lack of heteroatom substitutions within the aromatic cores. Various other non-aromatic carbons attached to amine or ether functional groups above 50 ppm are also observed in ^{13}C NMR spectra (including the peak labeled as "e" in Figure 4.4), consistent with the NR_2 species seen in the ^{1}H NMR spectra of Figure 4.3. Similar to ^{1}H NMR spectra, more branching carbons, region "f" in Figure 4.4, are observed than terminal CH_3 carbons, region "g". In addition, DEPT-135 carbon experiments were performed (Appendix C9-12), and results agree with MS and ^{1}H and ^{13}C NMR spectroscopic data. These DEPT−NMR spectra

assist in identifying many quaternary carbons (carbons with no protons attached) in the alkane region (labeled as "f" in Figure 4.4), from 15 to 60 ppm (e.g., Figure 4.4 and Appendix C10 of the Supporting Information), suggesting extensive alkyl branching. Only a few such peaks are apparent in the aromatic region ("c" in Figure 4.4); as a result of poor spin−lattice relaxation of these absorbances, we cannot assign all quaternary carbon functional groups in the mixture (Appendix C7−10 of the Supporting Information).[39−44] It is interesting to note that the crude oil and its n-heptane fraction are more similar than its asphaltene fraction (see ^{1}H NMR spectra in Appendix C13 and Appendix C14 of the Supporting Information); this is expected for light crude oils (such as Texas Crude) that do not contain high weight-percent asphaltene fractions.

The lack of both aromatic protons (confirmed by NMR spectroscopy) and multiple brominations (confirmed by MS results) from the analyzed asphaltenes did not follow the conventional model used for asphaltenes.[45] Hence, our MS, Br_2 tagging, and NMR spectra results of cleaned asphaltene samples suggest that a more appropriate model asphaltene structure should contain more substituted aromatic positions and increased branching, as shown in the model structure presented in Figure 4.5.

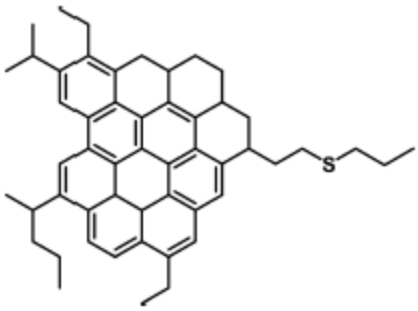

Figure 4.5. New proposed model structure of asphaltenes with more steric hindrance and fewer EAS sites.

Conclusion

A combination of bromine tagging, spectrometric and spectroscopic analyses, and sample purifications were used to investigate the functional group speciation of asphaltene, and n-heptane fractions derived from Texas Crude oil. KMD plots of the direct-infusion Orbitrap data help to visualize the differences in reactivity between asphaltenes and crude oil; both MS tagging and NMR spectral data suggest that aromatic protons are not freely available for electrophilic aromatic substitution. The observed reactivity patterns do not match current models of asphaltenes that show freely available aromatic protons. In other words, structures containing available aromatic protons would be expected to undergo multiple electrophilic aromatic substitutions, but our Br-tagging experiments do not support this view.

Additionally, it was shown that simple silica gel column purification removes a majority of paramagnetic species in asphaltene. Post-column NMR spectroscopy allowed for the identification and relative quantification of many distinct chemical functionalities never previously characterized in asphaltenes. The diminished line broadening after removal of metal ion contaminants makes paramagnetism the more likely cause of the decreased resolution of NMR spectra and not just the difficulty of asphaltene molecules tumbling. Moreover, our combined MS and NMR spectroscopy analyses suggest greater steric hindrance around aromatic protons in asphaltenes than previously proposed. Our preliminary NMR spectra simulations suggest that the NMR spectrum for proposed asphaltene model structure, shown in Figure 4.5, better resembles the experimentally observed NMR spectra of asphaltene samples than previous models. However, because asphaltene samples contain hundreds of structures that contribute to the observed NMR

spectra appearances, more detailed comparisons between one- and two-dimensional studies will be needed for potential deconvolution of NMR signals. We predict that the ability to probe functional group details of macromolecules present in complex mixtures, such as crude oil samples and biological fluids, will address existing limitations with complex sample analyses and benefit multiple areas of science.

References

1. Chaisoontornyotin, W.; Haji-Akbari, N.; Fogler, H. S.; Hoepfner, M. P. Combined Asphaltene Aggregation and Deposition Investigation. *Energy Fuels* **2016**, 30 (3), 1979−1986.

2. Mullins, O. C.; Sabbah, H.; Eyssautier, J.; Pomerantz, A. E.; Barré, L.; Andrews, A. B.; Ruiz-Morales, Y.; Mostowfi, F.; McFarlane, R.; Goual, L.; Lepkowicz, R.; Cooper, T.; Orbulescu, J.; Leblanc, R. M.; Edwards, J.; Zare, R. N. Advances in Asphaltene Science and the Yen−Mullins Model. *Energy Fuels* **2012**, 26 (7), 3986−4003.

3. Nelson, J.; Yamanaka, M.; Lopez-Linares, F.; Poirier, L.; Rogel, E. Characterization of Dissolved Metals and Metallic Nanoparticles in Asphaltene Solutions by Single-Particle Inductively Coupled Plasma Mass Spectrometry. *Energy Fuels* **2017**, 31 (11), 11971−11976.

4. Gonzalez, D. L.; Ting, P. D.; Hirasaki, G. J.; Chapman, W. G. Prediction of Asphaltene Instability under Gas Injection with the PCSAFT Equation of State. *Energy Fuels* **2005**, 19 (4), 1230−1234.

5. Vargas, F. M.; Creek, J. L.; Chapman, W. G. On the Development of an Asphaltene Deposition Simulator. *Energy Fuels* **2010**, 24 (4), 2294−2299.

6. Creek, J. L. Freedom of Action in the State of Asphaltenes: Escape from Conventional Wisdom. *Energy Fuels* **2005**, 19 (4), 1212− 1224.

7. Sirota, E. B. Physical Structure of Asphaltenes. *Energy Fuels* **2005**, 19 (4), 290−1296.

8. Choi, S.; Pyeon, W.; Kim, J.-D.; Nho, N.-s. Simple Functionalization of Asphaltene and Its Application for Efficient Asphaltene Removal. *Energy Fuels* **2016**, 30 (9), 991−7000.

9. Ovalles, C.; Rogel, E.; Lopez, J.; Pradhan, A.; Moir, M. Predicting Reactivity of Feedstocks to Resid Hydroprocessing Using Asphaltene Characteristics. *Energy Fuels* **2013**, 27 (11), 6552−6559.

10. Wang, T.; Jupiter, D.; Devkota, L.; Chambliss, C. K.; Pinney, K.; Solouki, T. Identification of Sulfur Compounds in Petroleum Samples Using Derivatization with Mass Deficent Reagents. Proceedings of the 61st Annual American Society for Mass Spectrometry Conference; Minneapolis, MN, June 9−13, **2013**.

11. Wang, X.; Liu, R.-F.; Cork, J.; Gu, Y.; Upham, D. C.; Laycock, B.; McFarland, E. W. Investigation of the Bromination/Dehydrobromination of Long Chain Alkanes. *Ind. Eng. Chem. Res.* **2017**, 56 (34), 9411−9418.

12. Saikia, I.; Borah, A. J.; Phukan, P. Use of Bromine and Bromo- Organic Compounds in Organic Synthesis. *Chem. Rev.* **2016**, 116 (12), 6837−7042.

13. Corvari, L.; McKee, J. R.; Zanger, M. The synthesis of 2′-bromostyrene. *J. Chem. Educ*. **1991**, 68 (2), 161.

14. Stoermer, M.; Pinhey, J. 2(S,R),3(R,S)-2,3-Dibromo-3-methyl-5-phenyl-2-pentanoic Acid. *Molecules* **1998**, 3 (3), M55.

15. Cakmak, O.; Aydogan, L.; Berkil, K.; Gulcin, I.; Buyukgungor, O. Highly brominated anthracenes as precursors for the convenient synthesis of 2,9,10-trisubstituted anthracene derivatives. *Beilstein J. Org. Chem.* **2008**, 4, 50.

16. Hughey, C. A.; Hendrickson, C. L.; Rodgers, R. P.; Marshall, A. G.; Qian, K. Kendrick Mass Defect Spectrum: A Compact Visual Analysis for Ultrahigh-Resolution Broadband Mass Spectra. *Anal. Chem.* **2001**, 73 (19), 4676−4681.

17. Kendrick, E. A Mass Scale Based on CH2 = 14.0000 for High Resolution Mass Spectrometry of Organic Compounds. *Anal. Chem*. **1963**, 35 (13), 2146−2154.

18. Mullins, O. C.; Seifert, D. J.; Zuo, J. Y.; Zeybek, M. Clusters of Asphaltene Nanoaggregates Observed in Oilfield Reservoirs. *Energy Fuels* **2013**, 27 (4), 1752−1761.

19. Klein, G. C.; Kim, S.; Rodgers, R. P.; Marshall, A. G.; Yen, A.; Asomaning, S. Mass Spectral Analysis of Asphaltenes. I. Compositional Differences between Pressure-Drop and Solvent-Drop Asphaltenes Determined by Electrospray Ionization Fourier Transform Ion Cyclotron Resonance Mass Spectrometry. *Energy Fuels* **2006**, 20 (5), 1965−1972.

20. Lisitza, N. V.; Freed, D. E.; Sen, P. N.; Song, Y.-Q. Study of Asphaltene Nanoaggregation by Nuclear Magnetic Resonance (NMR). *Energy Fuels* **2009**, 23 (3), 1189−1193.

21. Yu, C.; Zhang, L.; Guo, X.; Xu, Z.; Sun, X.; Xu, C.; Zhao, S. Association Model for Nickel and Vanadium with Asphaltene during Solvent Deasphalting. *Energy Fuels* **2015**, 29 (3), 1534−1542.

22. Kurian, V.; Gupta, R. Distribution of Vanadium, Nickel, and Other Trace Metals in Soot and Char from Asphaltene Pyrolysis and Gasification. *Energy Fuels* **2016**, 30 (3), 1605−1615.

23. Di Mauro, E.; Guedes, C. L. B.; Nascimento, O. R. Multifrequency (X-band to W-band) CW EPR of the organic free radical in petroleum asphaltene. *Appl. Magn. Reson*. **2005**, 29 (4), 569.

24. ASTM International. ASTM D6560-17, Standard Test Method for Determination of Asphaltenes (Heptane Insolubles) in Crude Petroleum and Petroleum Products; ASTM International: West Conshohocken, PA, **2017**.

25. Cassella, R. J.; Brum, D. M.; Robaina, N. F.; Rocha, A. A.; Lima, C. F. Extraction induced by emulsion breaking for metals determination in diesel oil by ICP-MS. *J. Anal. At. Spectrom*. **2012**, 27 (2), 364−370.

26. Voronetskaya, N. G.; Pevneva, G. S.; Golovko, A. K. Composition of naphthene hydrocarbons in crude oils from deposits of different ages. *Pet. Chem*. **2014**, 54 (3), 165−170.

27. Cui, T.-B.; Luo, T.-L.; Zhang, C.; Mao, Z.-B.; Liu, G.-J. Measurement and Correlation for Solubilities of Naphthalene in Acetone, Toluene, Xylene, Ethanol, Heptane, and 1-Butanol. *J. Chem. Eng. Data* **2009**, 54 (3), 1065−1068.

28. AlHumaidan, F. S.; Hauser, A.; Rana, M. S.; Lababidi, H. M. S. NMR Characterization of Asphaltene Derived from Residual Oils and Their Thermal Decomposition. *Energy & Fuels* **2017**, 31 (4), 3812− 3820.

29. Betancourt Cardozo, F.; Avella Moreno, E.; Trujillo, C. A. Structural Characterization of Unfractionated Asphalts by ^{1}H NMR and ^{13}C NMR. *Energy Fuels* **2016**, 30 (4), 2729−2740.

30. Pekerar, S.; Lehmann, T.; Méndez, B.; Acevedo, S. Mobility of Asphaltene Samples Studied by ^{13}C NMR Spectroscopy. *Energy Fuels* **1999**, 13 (2), 305−308.

31. Schreckenbach, G.; Ziegler, T. Calculation of the G-Tensor of Electron Paramagnetic Resonance Spectroscopy Using Gauge-Including Atomic Orbitals and Density Functional Theory. *J. Phys. Chem. A* **1997**, 101 (18), 3388−3399.

32. Benamsili, L.; Korb, J.-P.; Hamon, G.; Louis-Joseph, A.; Bouyssiere, B.; Zhou, H.; Bryant, R. G. Multi-dimensional Nuclear Magnetic Resonance Characterizations of Dynamics and Saturationsof Brine/Crude Oil/Mud Filtrate Mixtures Confined in Rocks: The Role of Asphaltene. *Energy Fuels* **2014**, 28 (3), 1629−1640.

33. Kiruri, L. W.; Dellinger, B.; Lomnicki, S. Tar Balls from Deep Water Horizon Oil Spill: Environmentally Persistent Free Radicals (EPFR) Formation During Crude Weathering. *Environ. Sci. Technol.* **2013**, 47 (9), 4220−4226.

34. Netzel, D. A.; McKay, D. R.; Heppner, R. A.; Guffey, F. D.; Cooke, S. D.; Varie, D. L.; Linn, D. E. ^{1}H- and ^{13}C-NMR studies on naphtha and light distillate saturate hydrocarbon fractions obtained from in-situ shale oil. *Fuel* **1981**, 60 (4), 307−320.

35. Seshadri, K. S.; Albaugh, E. W.; Bacha, J. D. Characterization of needle coke feedstocks by magnetic resonance spectroscopy. *Fuel* **1982**, 61 (4), 336−340.

36. Suzuki, T.; Itoh, M.; Takegami, Y.; Watanabe, Y. Chemical structure of tar-sand bitumens by ^{13}C and ^{1}H NMR spectroscopic methods. *Fuel* **1982**, 61 (5), 402−410.

37. Hasan, M. U.; Ali, M. F.; Bukhari, A. Structural characterization of Saudi Arabian heavy crude oil by NMR spectroscopy. *Fuel* **1983**, 62 (5), 518−523.

38. Silverstein, R. M.; Webster, F. X.; Kiemle, D. J. Spectrometric Identification of Organic Compounds, 7th ed.; Wiley: Hoboken, NJ, **2005**; pp 127−204.

39. Poveda, J.-C.; Molina, D.-R.; Pantoja-Agreda, E.-F. ^{1}H- and ^{13}C-NMR Structural Characterization of Asphaltenes from Vacuum Residua Modified by Thermal Cracking. CT&F, Cienc., *Tecnol. Futuro* **2014**, 5, 49−60.

40. Gillet, S.; Rubini, P.; Delpuech, J.-J.; Escalier, J.-C.; Valentin, P. Quantitative carbon-13 and proton nuclear magnetic resonance spectroscopy of crude oil and petroleum products. 1. Some rules for obtaining a set of reliable structural parameters. *Fuel* **1981**, 60 (3), 221−225.

41. Gillet, S.; Rubini, P.; Delpuech, J.-J.; Escalier, J.-C.; Valentin, P. Quantitative carbon-13 and proton nuclear magnetic resonance spectroscopy of crude oil and petroleum products. 2. Average structure parameters of representative samples. *Fuel* **1981**, 60 (3), 226−230.

42. Dickinson, E. M. Structural comparison of petroleum fractions using proton and ^{13}C NMR spectroscopy. *Fuel* **1980**, 59 (5), 290−294.

43. O'Donnell, D. J.; Sigle, S. O.; Berlin, K. D.; Sturm, G. P.; Vogh, J. W. Characterization of high-boiling petroleum distillate fractions by proton and ^{13}C nuclear magnetic resonance spectrometry. *Fuel* **1980**, 59 (3), 166−174.

44. Silverstein, R. M.; Webster, F. X.; Kiemle, D. J. Spectrometric Identification of Organic Compounds, 7th ed.; Wiley: Hoboken, NJ, **2005**; pp 205−224.

45. Sedghi, M.; Goual, L.; Welch, W.; Kubelka, J. Effect of Asphaltene Structure on Association and Aggregation Using Molecular Dynamics. *J. Phys. Chem. B* **2013**, 117 (18), 5765−5776.

CHAPTER FIVE

Generation and Reactivity of Unusual S-oxidation Products

Oxidation of thiomaltol and selenomaltol

The biological function and mechanism of action for endogenously generated H_2S is uncertain.[1-2] Some reports implicate the oxidized forms of H_2S being responsible for its biological functions.[3-4] To that end our lab has begun studying sulfur oxoacid generation from H_2S and characterizing the S(0) and S(II) intermediates.[5-6] As part of this effort, we are developing small molecules that release oxidized sulfur compounds to study the effect sulfur oxoacids may have in cells. One of these molecules is the oxidation product of thiomaltol ((3-hydroxy-2-methylpyrylium-4-yl)sulfenate) or Htma-O.

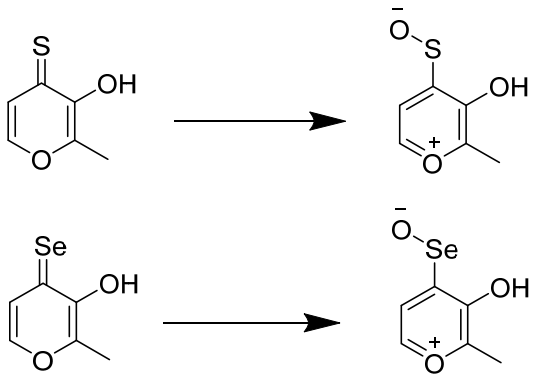

Scheme 5.1

To generate Htma-O, a variety of oxidants (peroxide, tert-butyl hydrogen peroxide, and urea hydrogen peroxide) were used to try and generate thiomaltol and selenomaltol oxide, as shown in Scheme 5.1 above; similar reaction conditions were previously used to generate S-oxides of dithiocarbamates and their metal complexes,[7-9] as

well as previous investigations of metal complexes of thiomaltol and related chelates.[10-11] However, the S-oxides are difficult to purify as they decompose on silica and alumina columns, and are not isolatable by extraction into polar aprotic solvents. To remedy this, the oxidation reactions were performed using colder conditions and lower oxidant ratios that selectively produce the mono-oxide. In a typical procedure, a 200 mg sample of Htma was added to ethanol, and 30% hydrogen peroxide was added in a 2:1 molar ratio. This solution was placed in a -80 °C freezer for 1 hour, and the solvent was removed by lyophilization. These conditions generate a mixture of Htma and Htma-O, and a simple hexane or chloroform wash removed the excess Htma from the product. The Htma-O product was characterized by mass spectrometry and NMR spectroscopy, in yields of ~60 mg (27%) using this synthesis.

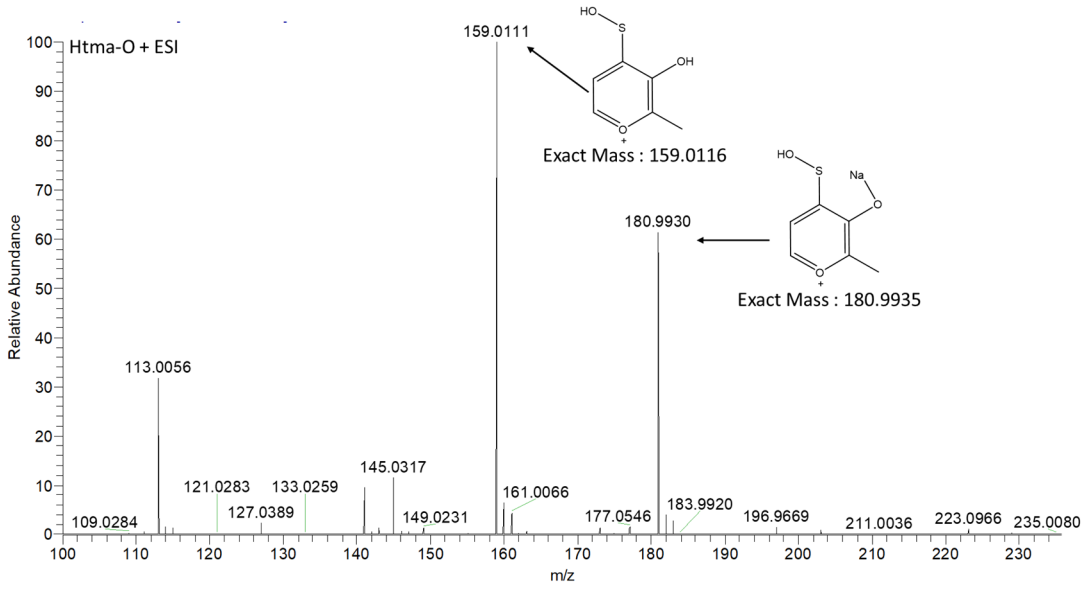

Figure 5.1. Mass spectrum of Htma-O in positive ion mode.

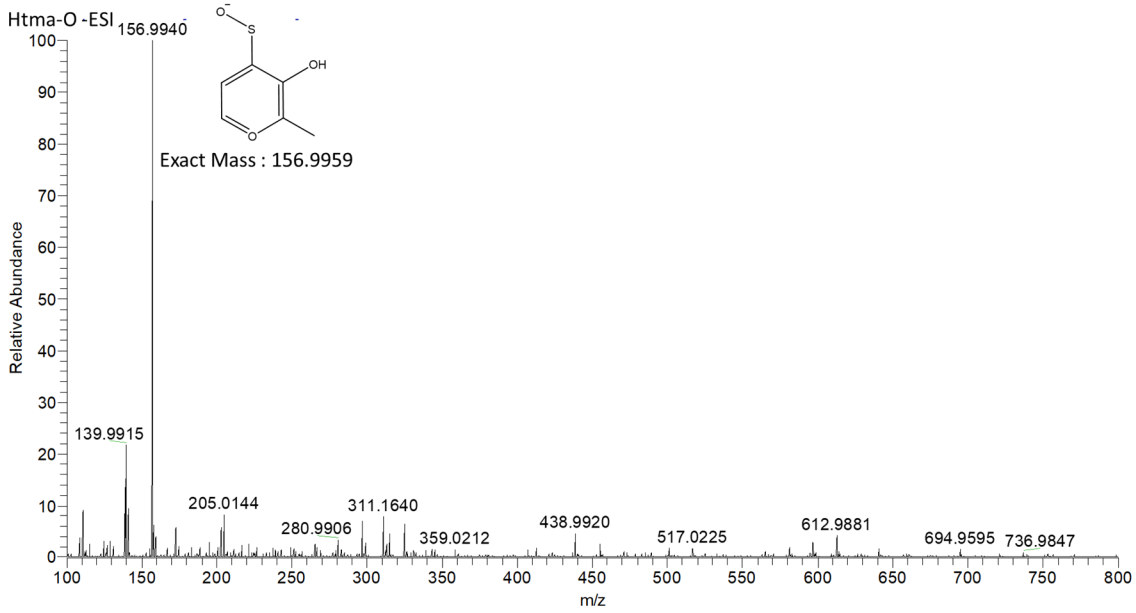

Figure 5.2. Mass spectrum of Htma-O in negative ion mode.

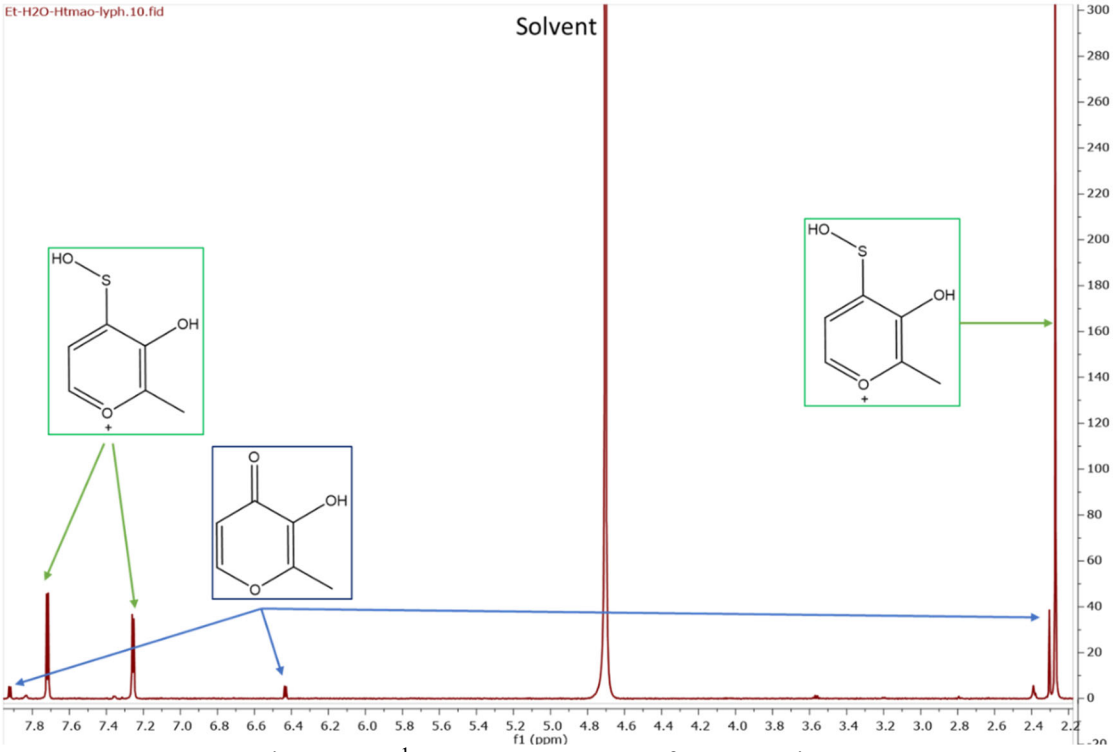

Figure 5.3. ^{1}H NMR spectrum of Htma-O in D_2O.

A similar route was used to make crude samples of thiomaltol-dioxide, Htma-O_2, and selenomaltol-oxide, Hsma-O, both of which were never cleanly isolated. The selenium oxide Hsma-O was generated in similar yields, but its purification was not pursued. The dioxide Htma-O_2 was found to be hydroscopic and decomposed rapidly in the presence of water.

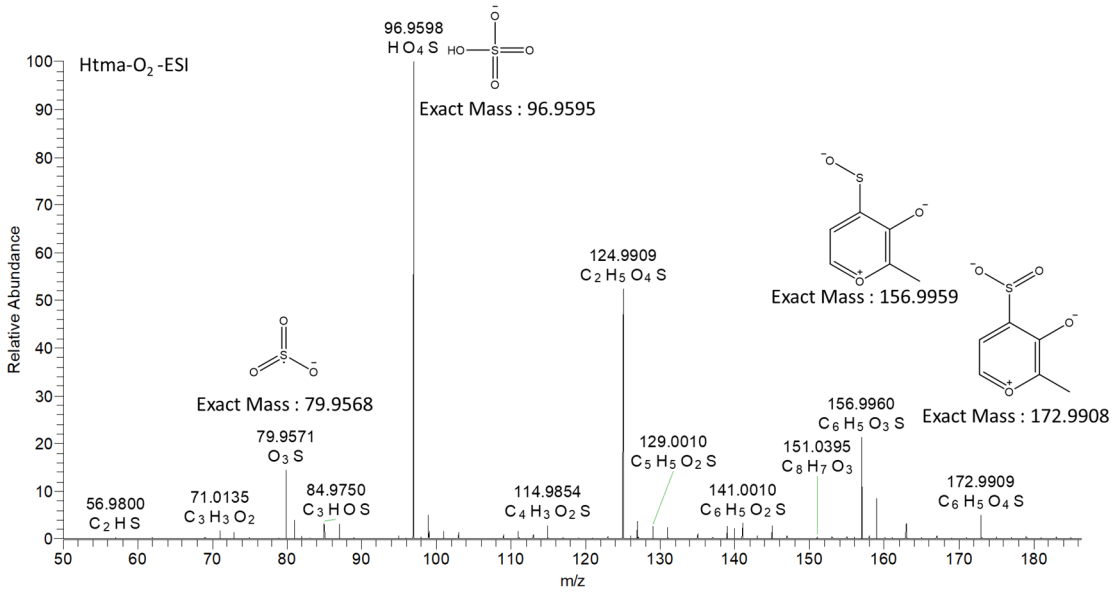

Figure 5.4. Htma-O_2 mass spectrum in negative ion mode.

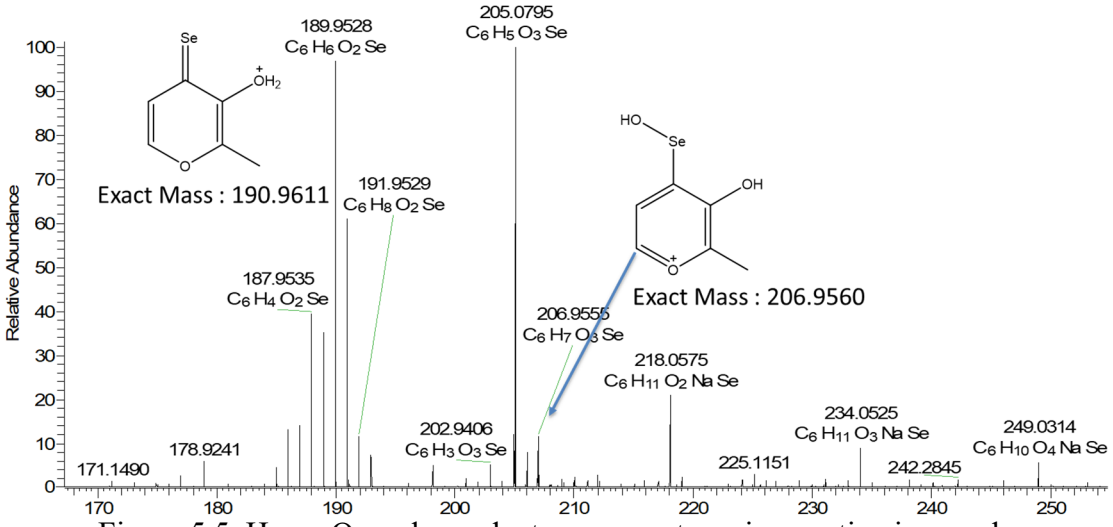

Figure 5.5. Hsma-O crude product mass spectrum in negative ion mode.

Synthesis of Htma-O ((3-hydroxy-2-methylpyrylium-4-yl)sulfenate).

Htma-O was prepared by dissolving 200 mg of Htma in 30mL of ethanol. A 30% peroxide solution was added to the mixture dropwise in a 2:1 molar ratio (2.39 mL), and the solution began turning from yellow to orange. The mixture was then placed in a -80 °C freezer and allowed to cool for 1 hour. Once cool, the solution was lyophilized to remove the solvent, leaving behind a yellow/orange mixture of thiomaltol and Htma-O. The product was washed twice with 30 mL of chloroform, and once with 30 mL of hexane, and allowed to dry under vacuum. The resulting orange product was hydroscopic and stored under nitrogen. Yield 27% (60 mg) ESI MS: m/z(pos.) 159.0111 (M + H) (calculated: 159.0116). ^{1}H NMR (600 MHz, $CDCl_3$): δ 7.68 (d, 1H), 7.26 (d, 1H), 2.30 (s, 3H).

Synthesis of Htma-O_2 (3-hydroxy-2-methylpyrylium-4-sulfinate).

Htma-O_2 was prepared by dissolving 200 mg of Htma in 30 mL of ethanol. A 30% peroxide solution was added to the mixture dropwise in a 1:2 molar ratio (9.58 mL), and the solution began turning from yellow to orange. The mixture was then placed in a -80 °C freezer and allowed to cool for 1 hour. Once cool, the solution was lyophilized to remove the solvent, leaving behind an orange product that was a mixture of Htma-O and Htma-O_2. The product mixture was washed twice with 30 mL of chloroform, and once with 30 mL of hexane, and allowed to dry under vacuum. The resulting orange product was much more hydroscopic than Htma-O, and quickly decomposed in the presence of water. It was stored under nitrogen in a similar fashion to Htma-O. The yield is not definitive but estimated as ~80% Htma-O_2 (194 mg). ESI MS: m/z (neg.) 172.9909 (M –

H) (calculated: 172.9908). An NMR spectrum is not shown, as the product decomposed quickly and the exact peaks for Htma-O_2 could not be determined.

Synthesis of Hsma-O ((3-hydroxy-2-methylpyrylium-4-yl)selanate).

Hsma-O was prepared in an identical fashion to Htma-O, however its product was not fully purified (washed with hexanes) as shown by the mixture of Hsma and Hsma-O in the mass spectrum (Figure 5.5). ESI MS: m/z (pos.) 206.9555 (M + H) (calculated: 206.9560).

Metalation of Htma-O

The coordination chemistry of the new sulfenate ligands is potentially of interest in their bioactivity. As initial tests, Htma-O was reacted with $Cu(acetate)_2$ or $Zn(acetate)_2$ in a ratio of 2:1. No Cu(tma-O) or Zn(tma-O) chelates were observed by mass spectrometry, only the parent $M(tma)_2$ complexes were seen as the dominant product in the figures below. It is possible that the formation of the complex caused the loss of oxygen from the ligand, but the nature of this loss is unknown.

Reaction of $Cu(ac)_2$ with Htma-O.

A sample of 15 mg of Htma-O was dissolved in 5 mL of ethanol. An 8.6 mg sample of copper acetate was then dissolved in 2 mL of DI water The Htma-O was added to the copper solution dropwise up to a 2:1 molar ratio. The resulting brown product was characterized by mass spectrometry and the dominant product was $Cu(tma)_2$. ESI MS: m/z(pos.) 367.9210 (M + Na) (calculated: 367.9214).

Reaction of $Zn(ac)_2$ with Htma-O.

A sample of 20 mg of Htma-O was dissolved in 5 mL of ethanol. An 11.6 mg sample of anhydrous zinc acetate was then dissolved in 2 mL of DI water The Htma-O was added to the zinc solution dropwise up to a 2:1 molar ratio. The resulting yellow product was characterized by mass spectrometry and the dominant product was $Zn(tma)_2$. ESI MS: m/z(pos.) 368.9210 (M + Na) (calculated: 368.9210).

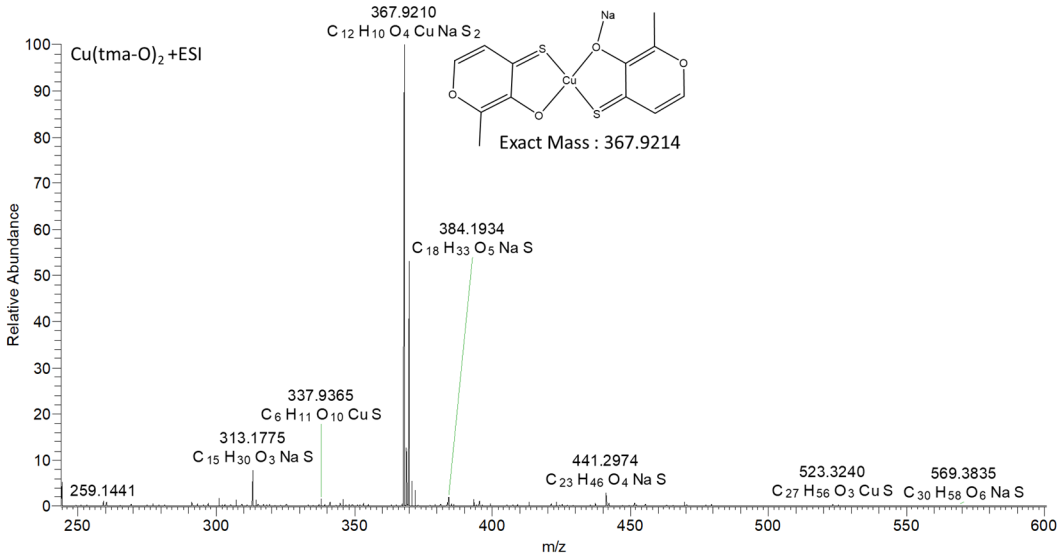

Figure 5.6. Mass spectrum (+ESI) of Cu^{2+} reacting with Htma-O.

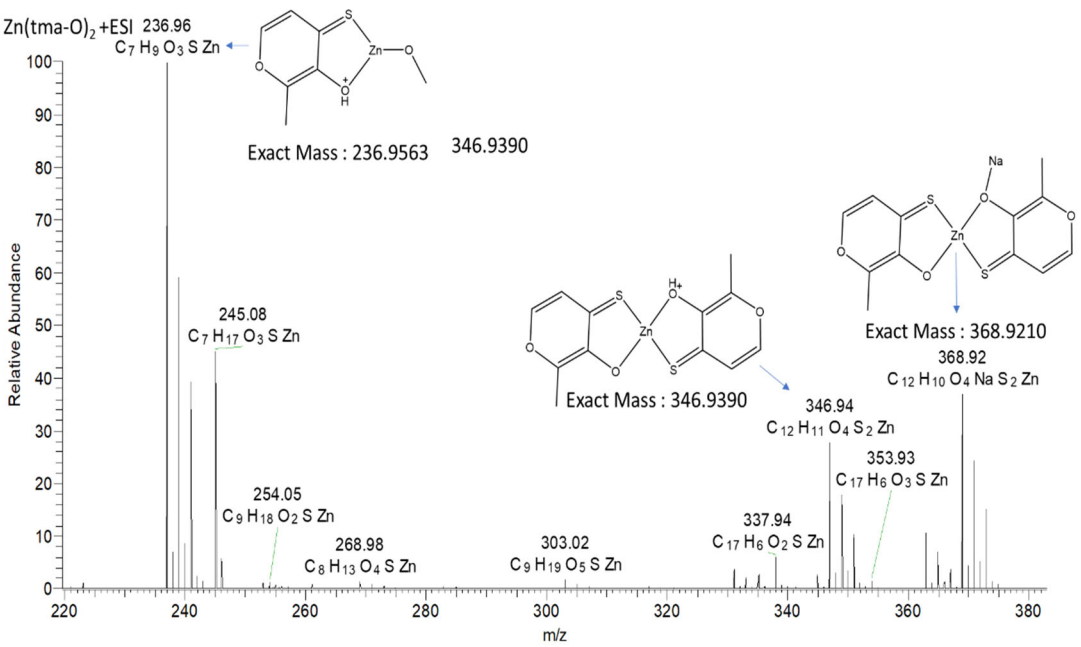

Figure 5.7. Mass spectrum of (+ESI) of Zn^{2+} reacting with Htma-O.

Other Alkyl Substitutions of thiomaltol

In Chapter Three, thiomaltol (3-hydroxy-2-methyl-4H-pyran-4-thione) was reacted with methyl iodide to make the product (mtp)I (3-hydroxy-2-methyl-4-(methylthio)pyrylium). Other syntheses were attempted to discern the scope of electrophiles that would generate pyrylium products, as shown in Scheme 5.2 below.

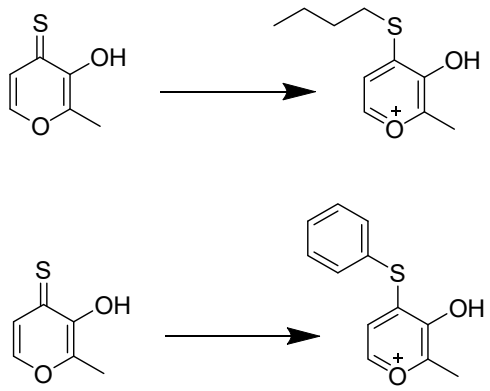

Scheme 5.2

The iodobutane (4-(butylthio)-3-hydroxy-2-methylpyrylium or (btp)I product was successfully synthesized and characterized using mass spectrometry. The iodobutane did not react to form the product, likely because it is a weaker electrophile. A crude NMR spectrum of the btp product can also be found below, but a clean NMR spectrum would require a chloroform wash.

Synthesis of 4-(butylthio)-3-hydroxy-2-methylpyrylium (btp)I.

The novel compound btp ($C_{10}H_{15}O_2S$) was prepared by dissolving 100 mg of Htma in 10 mL of dry acetonitrile. Butyl iodide was then added in a 1:5 stoichiometric ratio, and the yellow thiomaltol butyl iodide solution was reacted in a microwave at 65 °C for 30 minutes, and the solvent removed by evaporation. The resulting crude red product was characterized by mass spectrometry and NMR spectroscopy, although only the vinylic protons were assigned. ESI MS: m/z(pos.) 199.0787 (M +) (Calculated: 199.0792). ^{1}H NMR (600 MHz, $CDCl_3$): δ 7.68 (d, 1H), δ 7.38 (d, 1H), 6.98.

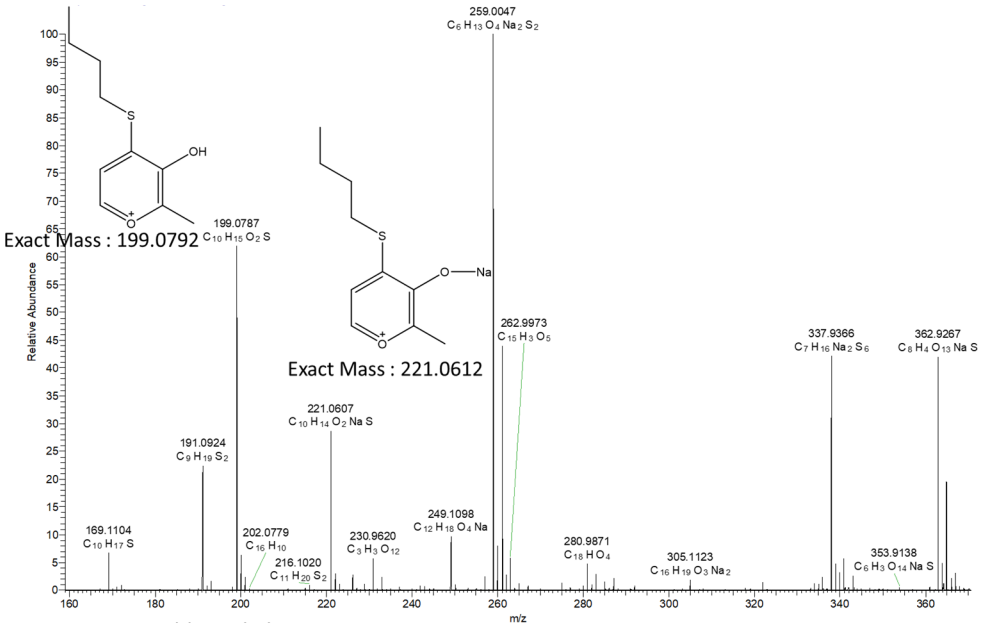

Figure 5.8. Butylthiomaltol mass spectrum in positive ion mode.

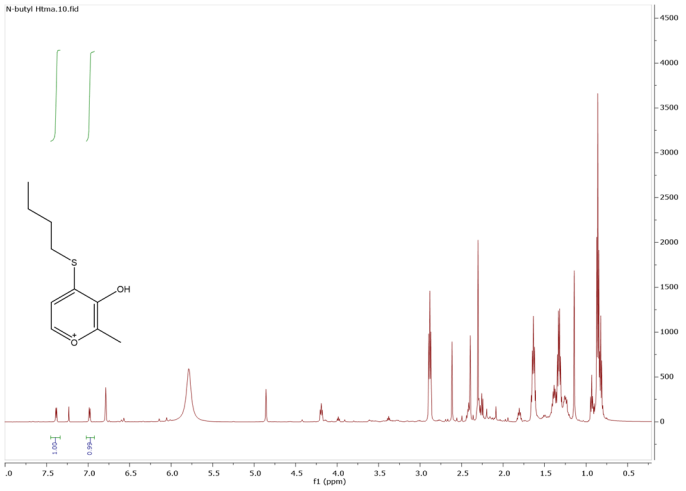

Figure 5.9. ^{1}H NMR spectrum of butylated Htma, btp.

Selenomaltol Radicals Characterization

In chapter three, the oxidation products of selenomaltol and thiomaltol complexes were described and attributed to the sulfur/selenium cation radicals. To isolate and study these radicals, a variety of chemical oxidations (cerium (IV) ammonium nitrate, cerium (IV) ammonium sulfate, $NOBF_4$ and NO_2BF_4) were attempted in dichloromethane as depicted in Scheme 5.3.

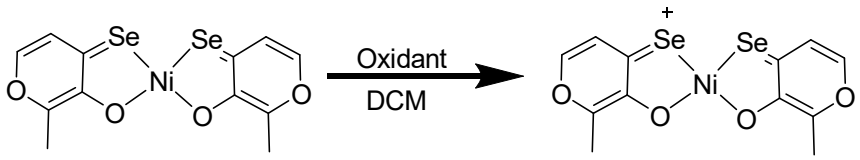

Scheme 5.3

The diamagnetic nickel complex was chosen because when oxidized it would have an EPR signal, but the unreacted complex would not interfere with the signal, as would be the case with the Cu and Fe complexes. The oxidant that gave the strongest signal was ammonium cerium (IV) sulfate, and the resulting EPR spectra can be seen in Figure 5.10. Additionally, the same product was shown to have formed during ionization

using mass spectrometry. The solvent used was aprotic (CH_2Cl_2) using an ESI source, which would only show the product peaks for cations in solution when in positive ion ESI mode, shown in Figure 5.11.

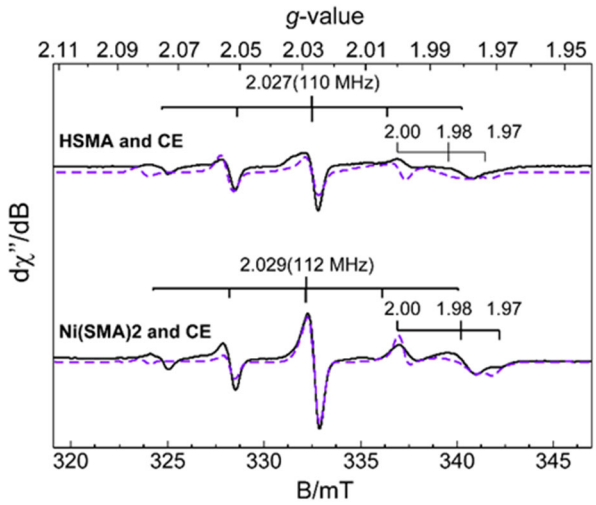

Figure 5.10. EPR spectra of oxidized $Ni(sma)_2$ (bottom) and Hsma (top), with the experimental data given as a dashed line.

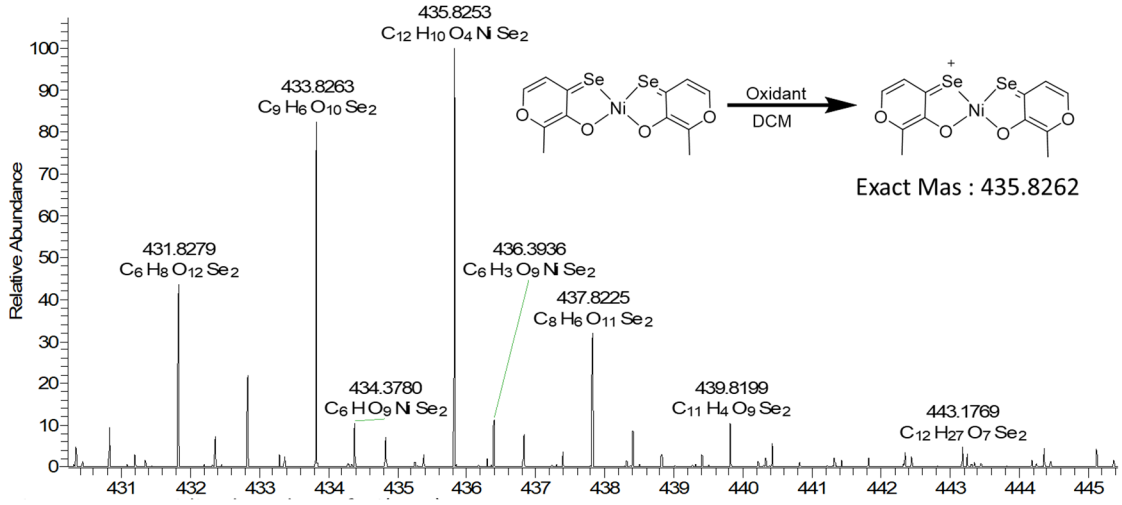

Figure 5.11. Mass spectrum of oxidized product of $Ni(sma)_2$ from reaction with cerium ammonium sulfate, in positive ion mode.

Both spectra in Figure 5.10 were modeled with equal contributions from an alkyl radical (located on the selenoketone) and an anisotropic selenium cation radical. While a good first approximation, the g value for the selenium radical is higher than expected, ~2.03 vs the expected 1.98.[15] In addition, the splitting between peaks in these spectra is also larger than expected (40 G). Last, the free ligand appears to have more of the radical localized on the Se.

Synthesis of [BITT](BF$_4$)$_2$

In addition to Htma-O, our lab has been interested in the product of disulfiram oxidation, N,N'-(1,2,4,5-tetrathiane-3,6-diylidene)bis(N-ethylethanaminium) (or BITT^{2+}) as a potential sulfur oxoacid generator. Several previous syntheses for these complexes have been published,[12-14] but many have problematic toxic counterions such as Cu(Cl)$_2^-$ or I_3^- and are therefore less suitable for use in biological experiments. Initial attempts used $AgBF_4$ as an oxidant with the hope of producing a less toxic BITT salt for use in cell culture. After analysis of the product the molecule made was not BITT, but instead a Ag-BITT adduct, with the overall synthesis shown below in Scheme 5.4. We have characterized this molecule by mass spectrometry and NMR spectroscopy but have not obtained a crystal structure; further studies are underway.

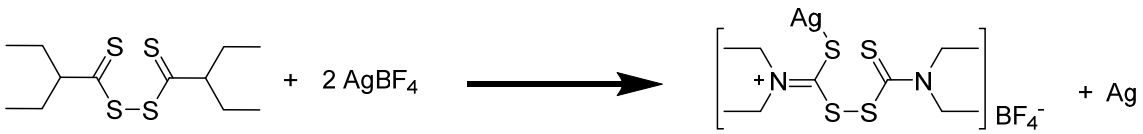

Scheme 5.4

Synthesis of Ag-BITT(BF_4) ($AgC_{10}N_2H_{20}S_4)BF_4$)

The new derivative was prepared by dissolving 100 mg of disulfiram in 20 mL of CH_2Cl_2. A 132 mg sample of $AgBF_4$ was then added in a 1:2 molar ratio; the solution went from a clear to yellow immediately and a yellow product precipitated. The solid was washed twice with 30 mL of chloroform, and once with 30 mL of hexane, and allowed to dry under vacuum. The resulting yellow product was hydroscopic and stored under nitrogen, but eventually turned brown over 24 hours. We believe this product is a BITT-Ag adduct which decomposes in the presence of water. ESI MS: m/z (pos.) 148.0248 (Split M + radical) (Calculated: 148.0255), 402.9554 (M + Ag) (Calculated: 402.9560). ^{1}H NMR (600 MHz, $CDCl_3$): δ 4.15 (q, 1H), 4.01 (q, 1H), 1.46 (t, 1H), 1.37 (t, 1H).

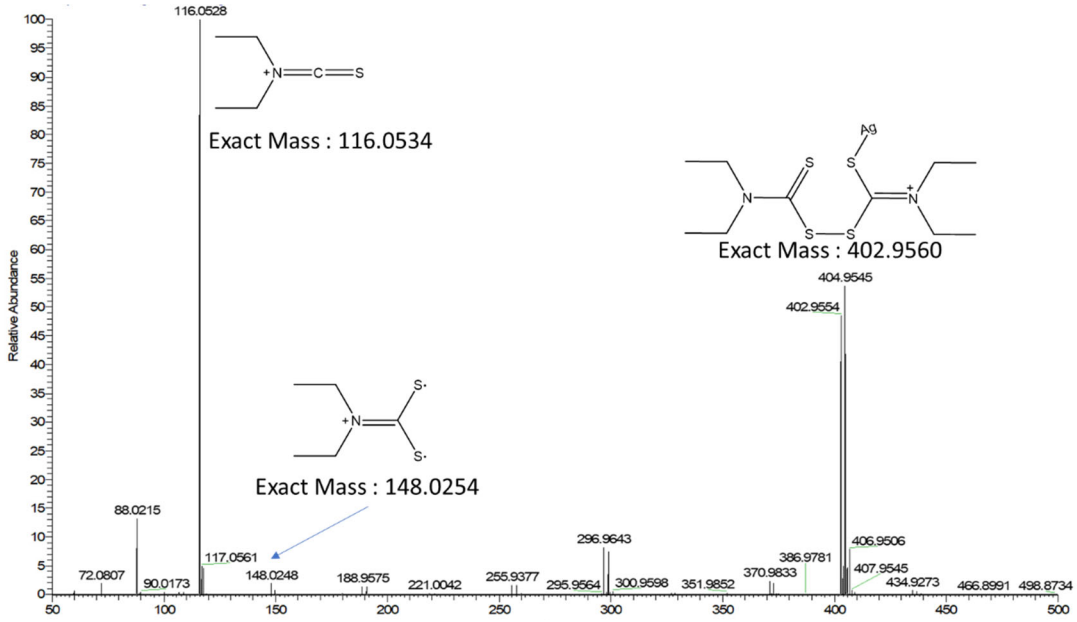

Figure 5.12. Mass spectrum of Ag-BITT(BF_4) adduct made by oxidation of DSF with $AgBF_4$

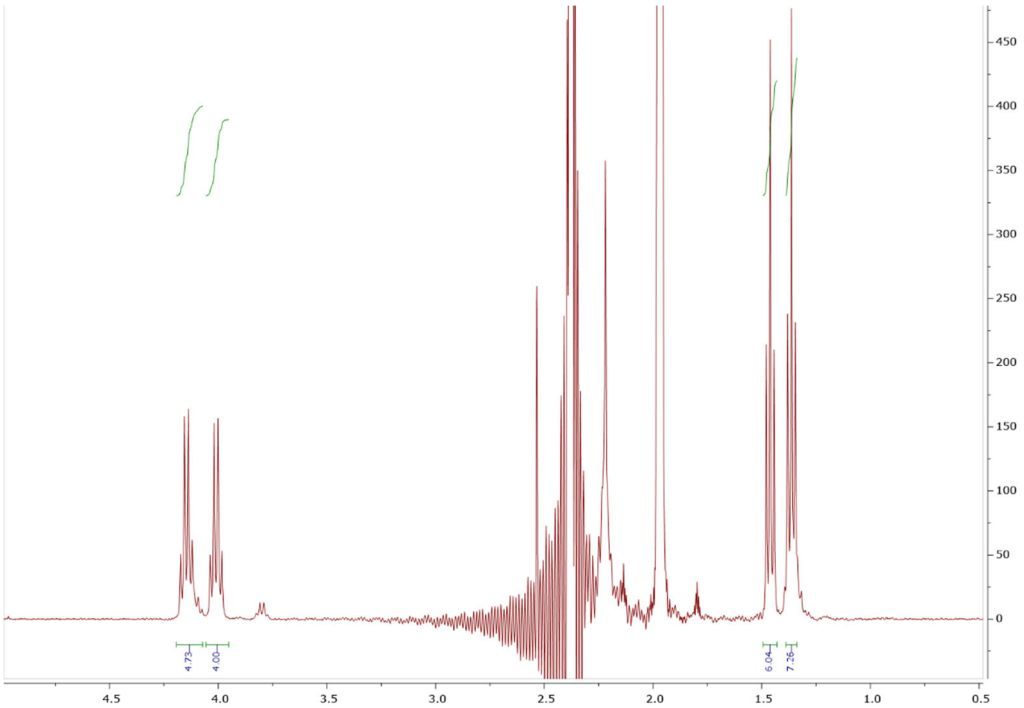

Figure 5.13. ^{1}H NMR spectrum of crude Ag-BITT(BF_4) in CH_3CN.

Experimental

Microwave syntheses were carried out in an discover SP microwave system. NMR spectra were recorded on a 600 Hz NMR spectrometer. For MS measurements an orbitrap discovery mass spectrometer equipped with an electrospray ionization (ESI) source was used. Sample solutions were infused at a rate of 5 μL min^{-1} with nitrogen as the sheath gas. The optimized ESI conditions were as follows: ion spray voltage, 5 V; capillary temperature, 250 °C; and tube lens voltage, 70 V.

References

1. Szabõ, C., Hydrogen sulphide and its therapeutic potential. *Nature Reviews Drug Discovery* **2007**, 6 (11), 917-935.

2. Wang, R., Physiological implications of hydrogen sulfide: A whiff exploration that blossomed. *Physiological Reviews* **2012**, 92 (2), 791-896.

3. Ida, T.; Sawa, T.; Ihara, H.; Tsuchiya, Y.; Watanabe, Y.; Kumagai, Y.; Suematsu, M.; Motohashi, H.; Fujii, S.; Matsunaga, T.; Yamamoto, M.; Ono, K.; Devarie-Baez, N. O.; Xian, M.; Fukuto, J. M.; Akaike, T., Reactive cysteine persulfides and S-polythiolation regulate oxidative stress and redox signaling. *Proceedings of the National Academy of Sciences of the United States of America* **2014**, 111 (21), 7606-7611.

4. Ono, K.; Akaike, T.; Sawa, T.; Kumagai, Y.; Wink, D. A.; Tantillo, D. J.; Hobbs, A. J.; Nagy, P.; Xian, M.; Lin, J.; Fukuto, J. M., Redox chemistry and chemical biology of H_2S, hydropersulfides, and derived species: Implications of their possible biological activity and utility. *Free Radical Biology and Medicine* **2014**, 77, 82-94.

5. Kumar, M. R.; Farmer, P. J., Chemical trapping and characterization of small oxoacids of sulfur (SOS) generated in aqueous oxidations of H_2S. *Redox Biology* **2018**, 14, 485-491.

6. Kumar, M. R.; Farmer, P. J., Trapping Reactions of the Sulfenyl and Sulfinyl Tautomers of Sulfenic Acids. *ACS Chemical Biology* **2017**, 12 (2), 474-478.

7. Ng, S.; Ziller, J. W.; Farmer, P. J., Multiple Pathways for the Oxygenation of a Ruthenium(II) Dithiocarbamate Complex: S-Oxygenation and S-Extrusion. *Inorganic Chemistry* **2004**, 43 (26), 8301-8309.

8. Brayton, D. F.; Tanabe, K.; Khiterer, M.; Kolahi, K.; Ziller, J.; Greaves, J.; Farmer, P. J., Oxygenation of Zinc Dialkyldithiocarbamate Complexes: Isolation, Characterization, and Reactivity of the Stoichiometric Oxygenates. *Inorganic Chemistry* **2006**, 45 (15), 6064-6072.

9. Ng, S.; Walker, M. B.; Farmer, P. J., Photo- and thermal-induced linkage isomerizations in a peroxydithiocarbamate–Ru complex. *Inorganica Chimica Acta* **2009**, 362 (11), 4013-4016.

10. Backlund, M.; Ziller, J.; Farmer, P. J., Unexpected C−H Activation of Ru(II)−Dithiomaltol Complexes upon Oxidation. *Inorganic Chemistry* **2008**, 47 (7), 2864-2870.

11. Bruner, B.; Walker, M. B.; Ghimire, M. M.; Zhang, D.; Selke, M.; Klausmeyer, K. K.; Omary, M. A.; Farmer, P. J., Ligand-based photooxidations of dithiomaltolato complexes of Ru(ii) and Zn(ii): photolytic CH activation and evidence of singlet oxygen generation and quenching. *Dalton Transactions* **2014**, 43 (30), 11548-11556.

12. Chen, I.; Das, T. P., Molecular Orbital Theory of Sulfur and Selenium Radicals. *The Journal of Chemical Physics* **1966**, 45 (10), 3526-3535.

13. Cen, D.; Brayton, D.; Shahandeh, B.; Meyskens, F. L.; Farmer, P. J., Disulfiram Facilitates Intracellular Cu Uptake and Induces Apoptosis in Human Melanoma Cells. *Journal of Medicinal Chemistry* **2004**, 47 (27), 6914-6920.

14. Ainscough, E. W.; Brodie, A. M., Sulphur-ligand–metal complexes. Part 7. The interaction of some diphosphine dichalcogenides and tetra-alkylthiuram disulphides with halogens and some first-row transition-metal salts. Journal of the Chemical Society, *Dalton Transactions* **1977**, (6), 565-570.

15. Willemse, J.; Steggerda, J. J., Oxidation of dithiocarbamate ligands to positive ions. *Journal of the Chemical Society D: Chemical Communications* **1969**, (19), 1123-1124.

APPENDICES

APPENDIX A

Supplemental Data for Chapter Two

Table 1A: Crystallographic data for $Fe(sma)_3$, $Ni(sma)_2$, $Zn(sma)_2$, and Hsma

	Fe(sma)3	Ni(sma)2	$Cu(sma)_2$	$Zn(Sma)_2$	Hsma
Molecular formula	$C_{18}H_{15}O_6Se_3Fe$	$C_{12}H_{12}NiO_5Se_2$	$C_{12}H_{10}CuO_4Se_2$	$C_{12}H_{10}ZnO_4Se_2$	$C_6H_6O_2Se$
Formula weight	620.03	452.85	439.66	441.49	189.07
T/K	150(2)	150(2)	150(2)	150(2)	150(2)
crystal system	Trigonal	Monoclinic	Monoclinic	Monoclinic	Monoclinic
space group	R3c	P21/c	P21/c	P21/c	P21/c
a, Å	14.8261(12)	8.2986(6)	7.4765(3)	7.6565(3)	5.4980(2)
b, Å	14.8261(12)	24.7783(14)	13.1079(5)	23.8778(11)	8.8047(5)
c, Å	16.0571(13)	6.9641(5)	6.9501(2)	7.4531(3)	13.7294(7)
α, °	90	90	90	90	90
β, °	90	101.042(3)	100.9898(13)	91.8542(16)	100.429(2)
γ, °	120	90	90	90	90
$V/Å^3$	3056.7(6)	1405.48	668.63(4)	1361.87(10)	653.64(6)
Z	6	4	2	4	4
Density (Mg/M^3)	2.021	2.14	2.184	2.153	1.921
Crystal size, mm	.198x.184x.125	.136x.089x.020	.242x.113x.083	.404x.141x.101	.293 x.14 x.116
Reflections collected	10165	15045	6801	14978	5861
Independent refelctions	1651	3482	1663	3370	1618
R(int)	0.0426	0.0946	0.0212	0.0316	0.0281
Data/Restraints/Param	1651/1/86	3482/0/189	1663/0/89	3370/0/174	1618/0/87
GOF on F2	1.129	1.028	1.144	1.067	1.054
R1 wR2 [1>2s(I)]	0.0185, 0.0404	0.0399, 0.0552	0.0199, 0.0489	0.0222, 0.0477	0.0228, 0.0527
R1, wR2 [all data]	0.0195, 0.0406	0.0802, 0.0628	0.0218, 0.0499	0.0282, 0.0502	0.026, 0.0544
largest peak/hole difference, A^{-3}	.594 and -.190	.848 and -.742	.600 and -.237	.486 and -.344	.477 and -.388

Table 2A: Select metal bond angles

Compound	O1-M-O2	Se1-M-Se2	Se1-M-O1	Se2-M-O2	Se1-M-O2	Se2-M-O1
$Zn(sma)_2$	120.00(6)	125.612(13)	89.89(4)	90.30(4)	116.58(5)	117.58(5)
$Cu(sma)_2$	180	180	88.74(4)	88.74(4)	91.26(4)	91.26(4)
$Ni(sma)_2$	85.81(11)	93.86(2)	90.44(8)	89.92(8)	176.10(8)	175.53(8)
$Fe(sma)_3$	91.42(9)	84.18(2)	80.51(6)	80.51(6)	107.21(6)	159.76(6)

Table 3A: Select metal ligand bond lengths

Compound	M-Se1	M-Se2	M-O1	M-O2
1 - Zn	2.2791(6)	2.2799(6)	1.879(3)	1.878(2)
2 - Cu	2.4002(2)	2.4002(2)	1.9108(13)	1.9108(13)
3 - Ni	2.2791(6)	2.2799(6)	1.879(3)	1.878(2)
4 - Fe	2.6114(6)	2.66146(6)	1.991(2)	1.991(2)

New synthesis of Htma

Analogous microwave method to that used for selenomaltol synthesis was used to generate thiomaltol. A 1:0.3 stoichiometric ratio of samples of maltol to Lawessons reagent were placed in anhydrous 1,4-dioxane in a 35 mL microwave reaction vessel. The resulting slurry was heated to 125 °C for 30 minutes in a microwave reactor. Water was added to the resulting black/orange mixture and the product was extracted with hexanes and subsequently evaporated to give a bright yellow powder. Purity was assessed by NMR spectroscopy and mass spectrometry.

Synthesis of $Cu(tma)_2$

A sample of Htma was dissolved in ethanol. $Cu(OAc)_2$ was dissolved in water and stirred under nitrogen. The thiomaltol mixture was added drop wise to the copper solution to form a brown/green precipitate. The resulting mixture was filtered and washed with 5mL of hexanes twice and 5 mL of DI water and then left under vacuum to dry overnight

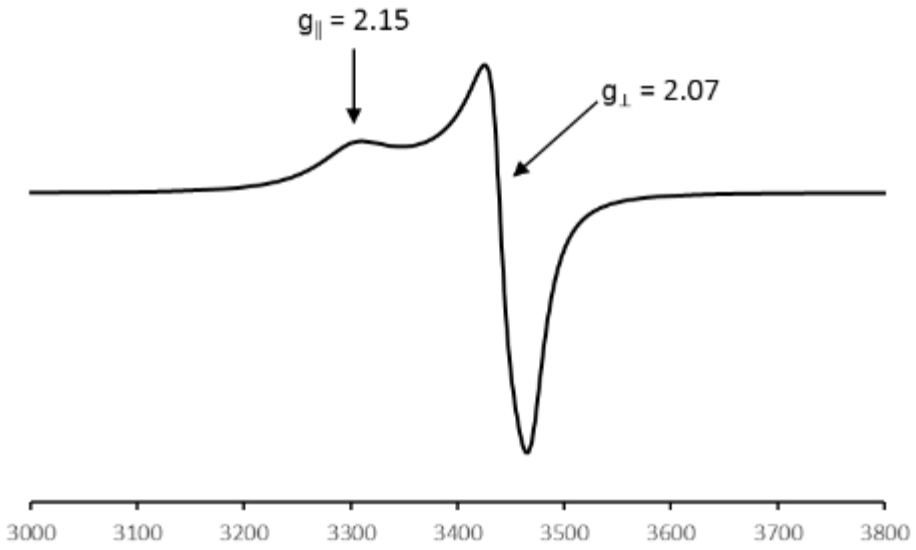

Figure 1A: A crystalline powder sample of Cu(tma) was placed in an EPR tube and spectrum were collected at room temperature. Conditions: microwave frequency 9.85 GHz, microwave power 2.00 mW, modulation amplitude 4.00 G, time constant 0.01 ms, sweep width 2000 G, sweep time 20.0ms.

APPENDIX B

Table 1B: Crystallographic data for (mtp)I and (msp)I

	(mtp)I	(msp)I
emperical formula	C8 H10 Cl3 I O2 S	C8 H10 Cl3 I O2 Se
temp, K	150(2)	150(2)
crystal system	Triclinic	Orthorhobic
space group	P-1	Pnma
a, Å	6.9124(5)	17.0322(6)
b, Å	10.0230(7)	7.0741(2)
c, Å	10.2975(7)	11.419(4)
α, °	73.673(2)	90
β, °	82.577(2)	90
γ, °	87.403(2)	90
vol, Å	678.90(8)	1375.86(8)
zed	2	4
density (Mg/M^3)	1.974	2.174
crystal size, mm^3	0.331 x 0.072 x 0.045	0.216 x 0.078 x 0.051
reflections collected	14526	14207
Independent reflections	3379 [R(int) = 0.0505]	1851 [R(int) = 0.0334]
data/restraints/params	3379/0/142	1851/2/101
GOF on F^2	1.063	1.379
R1	0.039	0.018
wR2	0.1034	0.0372
R(F) all data	0.0451	0.0238
Rw(F)(all data)	0.1073	0.0391
largest peak/hole difference, e $Å^{-3}$	2.343 and -1.349	0.734 and -0.299

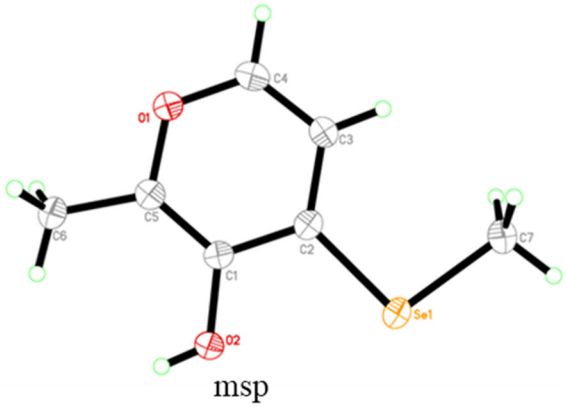

Figure 1B. Crystal Structure of (msp)I

The crystal structure of (msp)I is similar to that of (mtp)I, which more uniform bond lengths and an elongated C-Se bond.

APPENDIX C

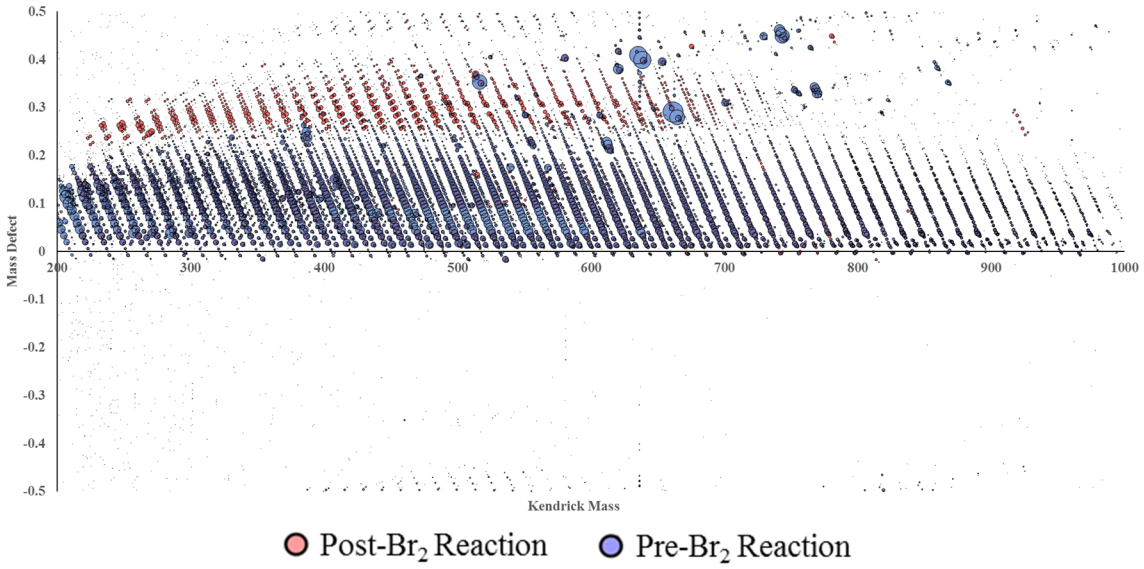

Figure 1C: KMD plot of pre- (blue) and post- (red) brominated crude oil (from Texas Crude) between 200-1000 KMU.

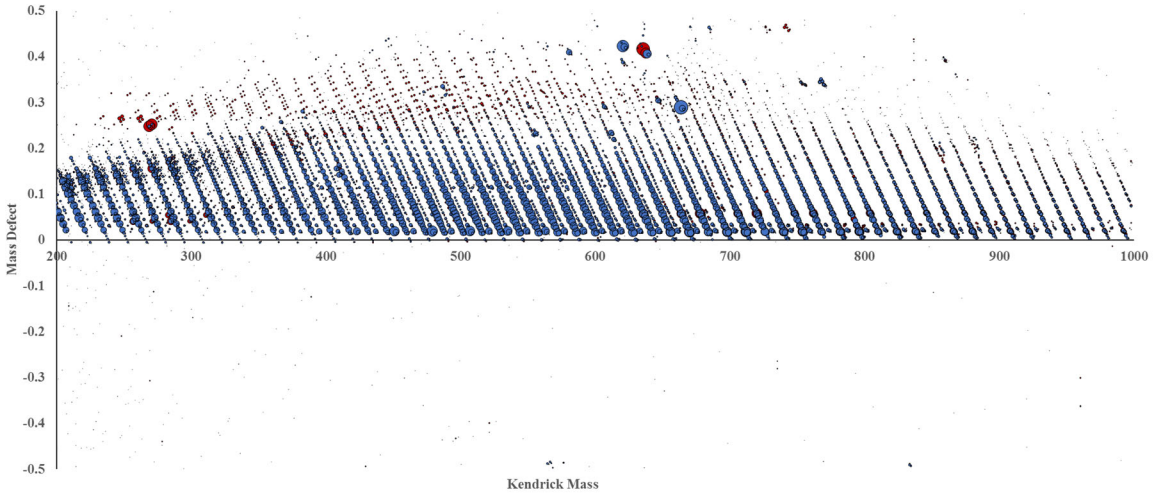

Figure 2C: KMD plot of pre- (blue) and post- (red) brominated n-heptane fraction (from Texas Crude) between 200-1000 KMU.

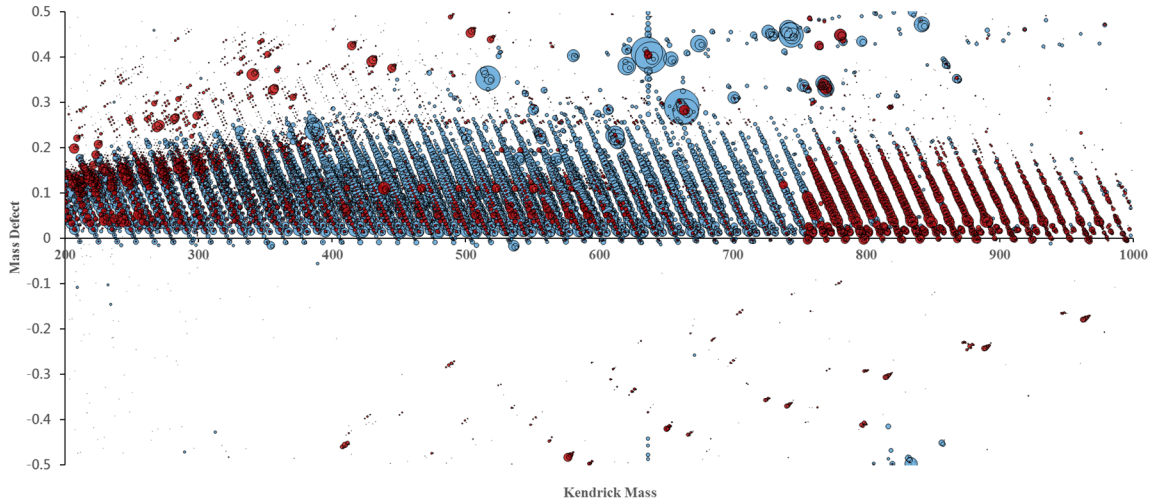

Figure 3C: KMD plot of pre- (blue) and post- (red) brominated asphaltene fraction (from Texas Crude) between 200-1000 KMU.

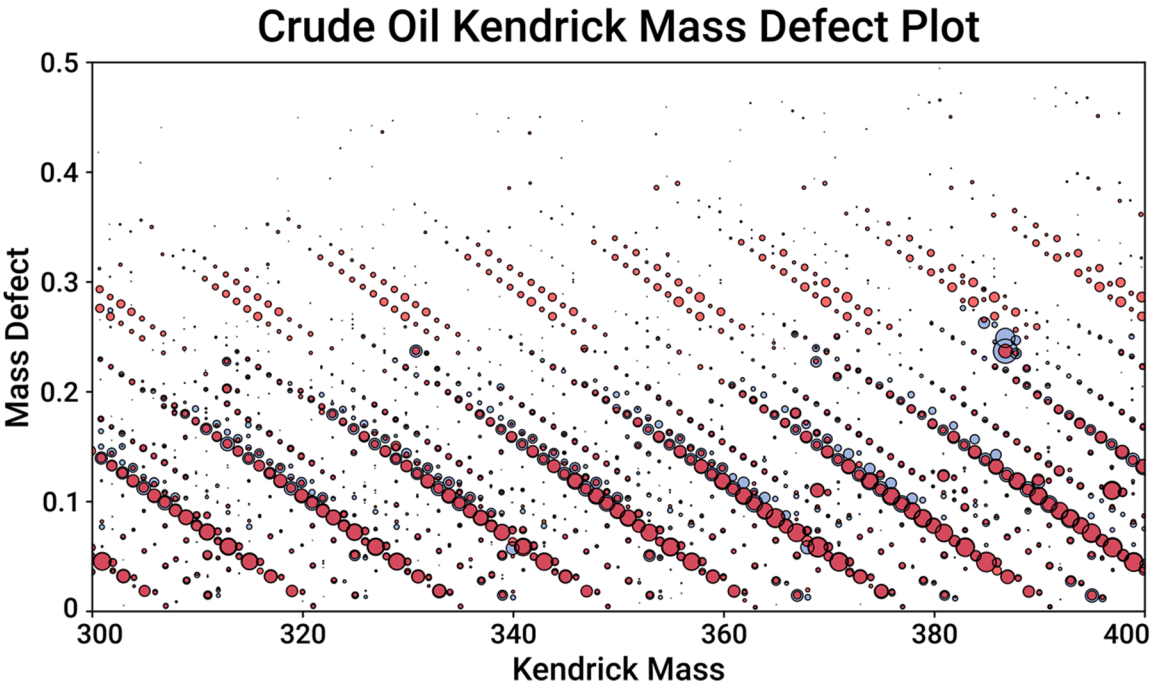

Figure 4C: KMD plot of the unreacted (blue) and brominated (red) crude oil fraction from 300 to 400 Kendrick mass units.

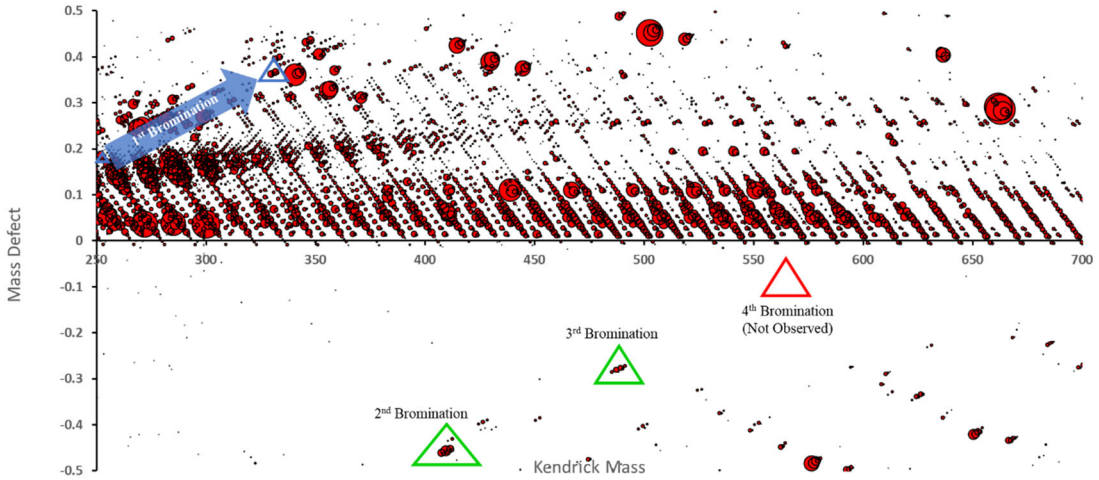

Figure 5C: KMD of benzo-[a]-pyrene (exact mass of 252.0939 Da) spiked asphaltene. Bromination profile of benzo-a-pyrene (KM_{CH2} = 251.8124), including its first bromination (as indicated in blue triangles), can be tracked. The second (Kendrick mass of 407.4594, MD = -0.4594) and third (KM_{CH2} = 485.2830, MD = -0.2830) brominations (indicated in green triangles) are also observed; however, the potential forth bromination corresponding to KM = 563.1065 (MD = -0.1065) is not observed (as indicated within the red triangle).

Table 1C: ICP-MS of relevant elements in asphaltene. Highlighted are the paramagnetic which show a ~95% reduction by weight in material after the column.

Elemental Metal	Blank (counts)	Wash (counts)	Pre-Column (counts)	Post-Column (counts)	Pre-Column (wt. %)	Post-Colum (wt. %)	Reduction (%)
Mg	1.8	N/D	1600	470	0.32	0.09	71
Al	47	N/D	8700	970	1.74	0.19	89
Ca	N/D	N/D	11000	2500	2.20	0.50	77
Ti	N/D	N/D	560	13	0.11	0.00	98
V	N/D	0.043	19	2.7	0.00	0.00	86
Cr	0.94	N/D	32	2.4	0.01	0.00	93
Mn	0.25	0.083	300	3.9	0.06	0.00	99
Fe	4.0	0.97	8000	134	1.60	0.03	98
Co	N/D	0.031	1.9	0.44	0.00	0.00	77
Ni	0.15	0.15	35	175	0.01	0.04	-400
Cu	0.27	0.143	86	132	0.02	0.03	-53
Zn	4.1	2.0	1000	874	0.20	0.17	13
Br	13	N/D	2600	113	0.52	0.02	96
Mo	N/D	0.044	10	1.3	0.00	0.00	87
I	3.9	4.5	5200	30	1.04	0.01	99

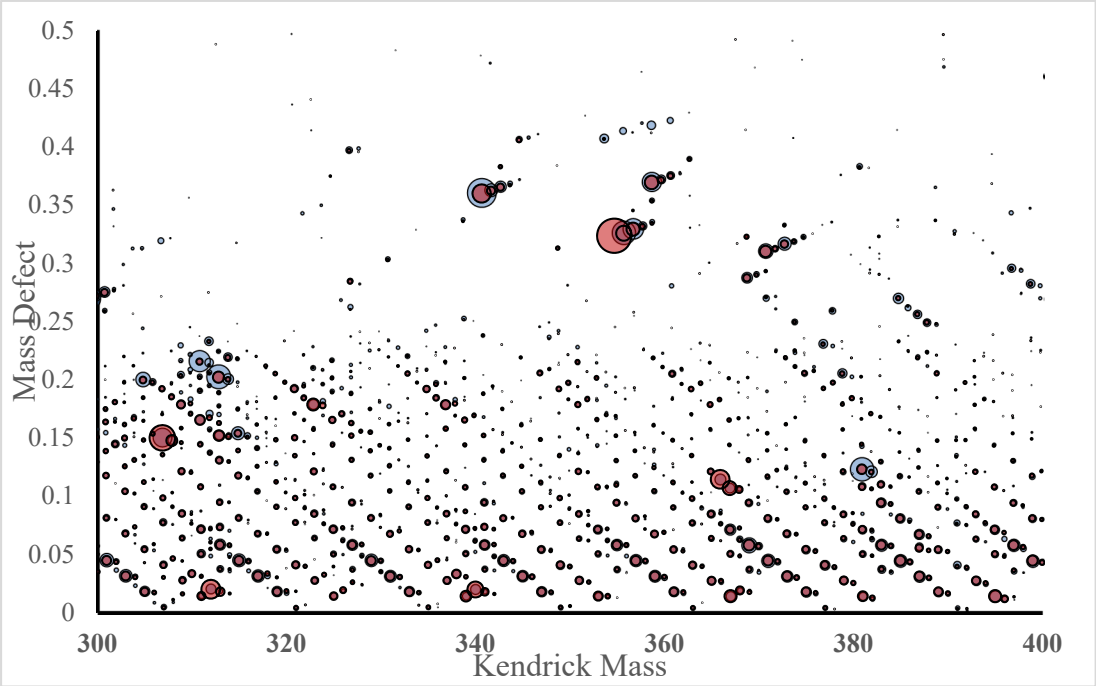

Figure 6C: KMD of pre- (blue) and post-(red) column asphaltenes.

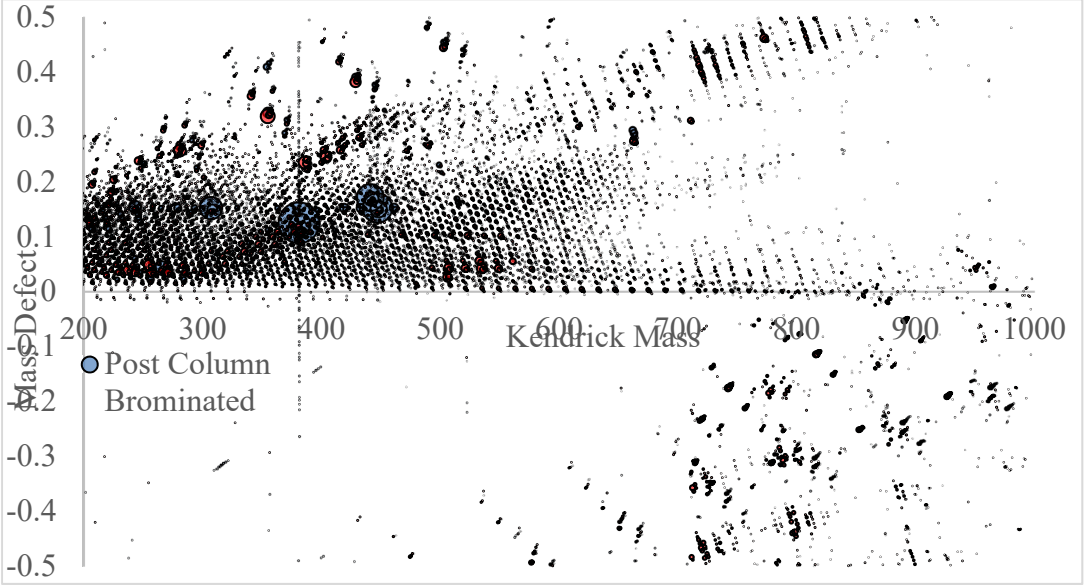

Figure 7C: KMD of pre- (blue) and post-(red) brominated column purified asphaltenes.

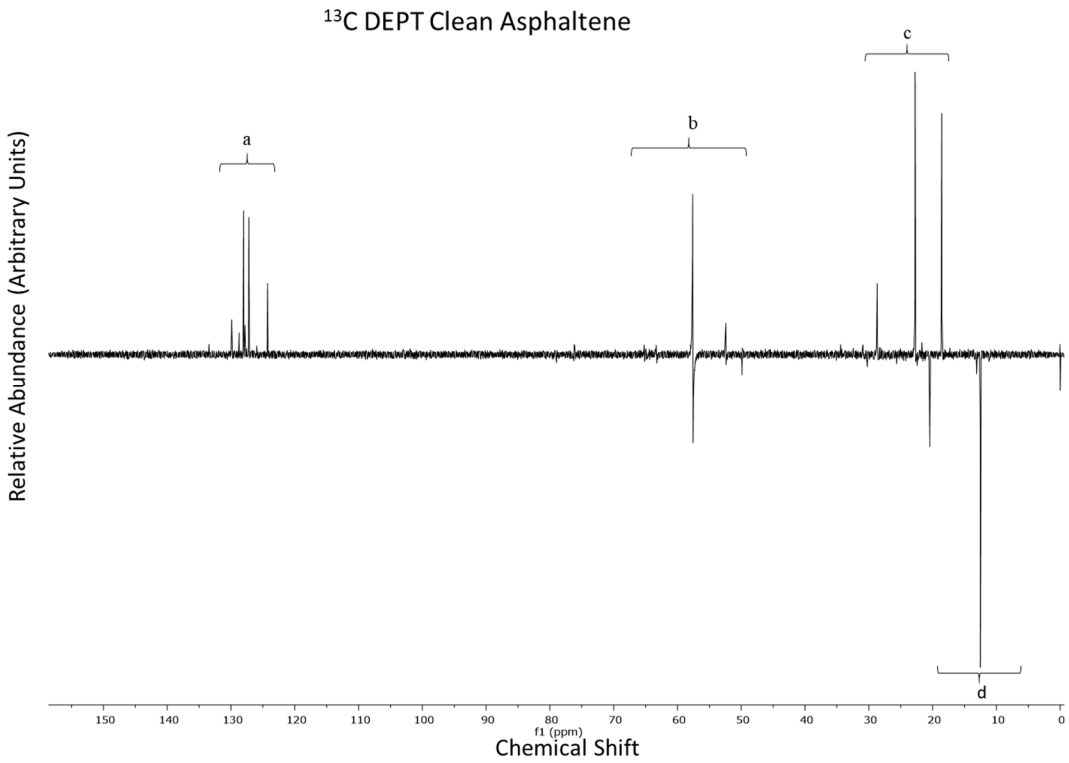

Figure 8C: DEPT 135 ^{13}C NMR spectrum of the columned asphaltene sample. Signals for quaternary carbon will not be observed in DEPT 135 ^{13}C NMR spectrum; however, signals for all other carbon functional groups can be detected and are assigned as: a) aromatic protons, b) N- Or O- substituted carbons such as alcohols or amines, c) CH (down) and CH_2 (up) carbon chains, d) terminal CH_3.

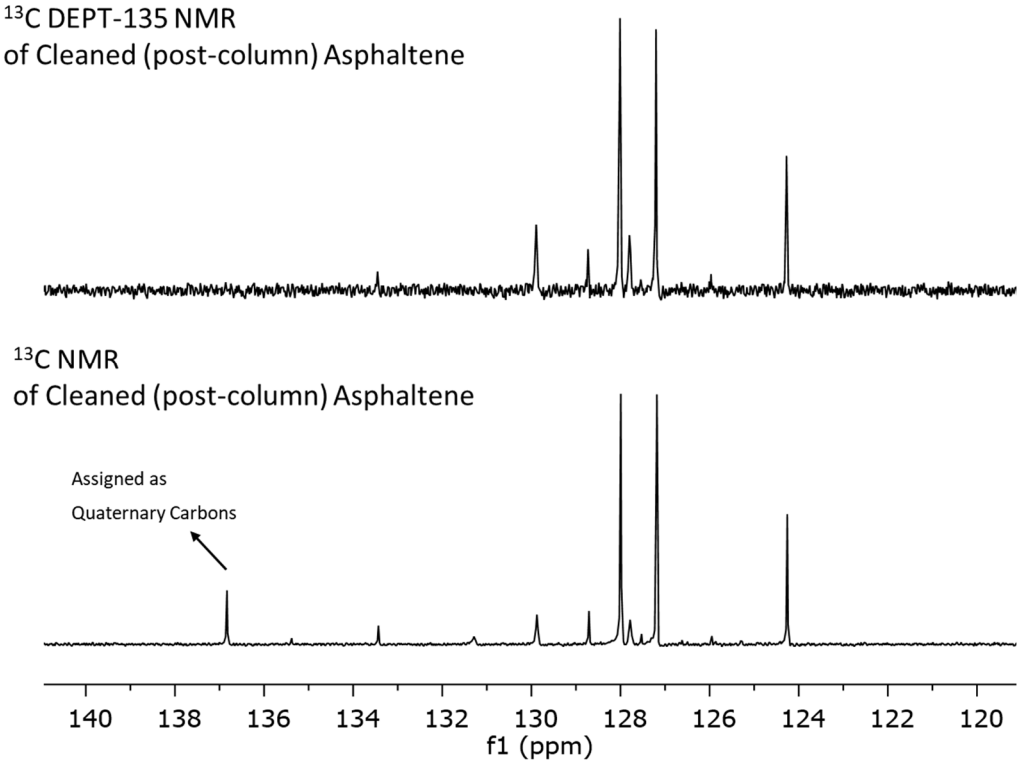

Figure 9C: Zoomed regions from 115 ppm to 145 ppm of ^{13}C NMR and DEPT-135 ^{13}C spectra. Comparison between the two spectra allows for confident assignment of quaternary carbons; for instance, R-**C**-CH type quaternary carbons (boldface) at ~ 137 ppm cannot be detected by DEPT-135 ^{13}C (spectrum shown at the top) but can be observed in conventional ^{13}C NMR (bottom spectrum) .

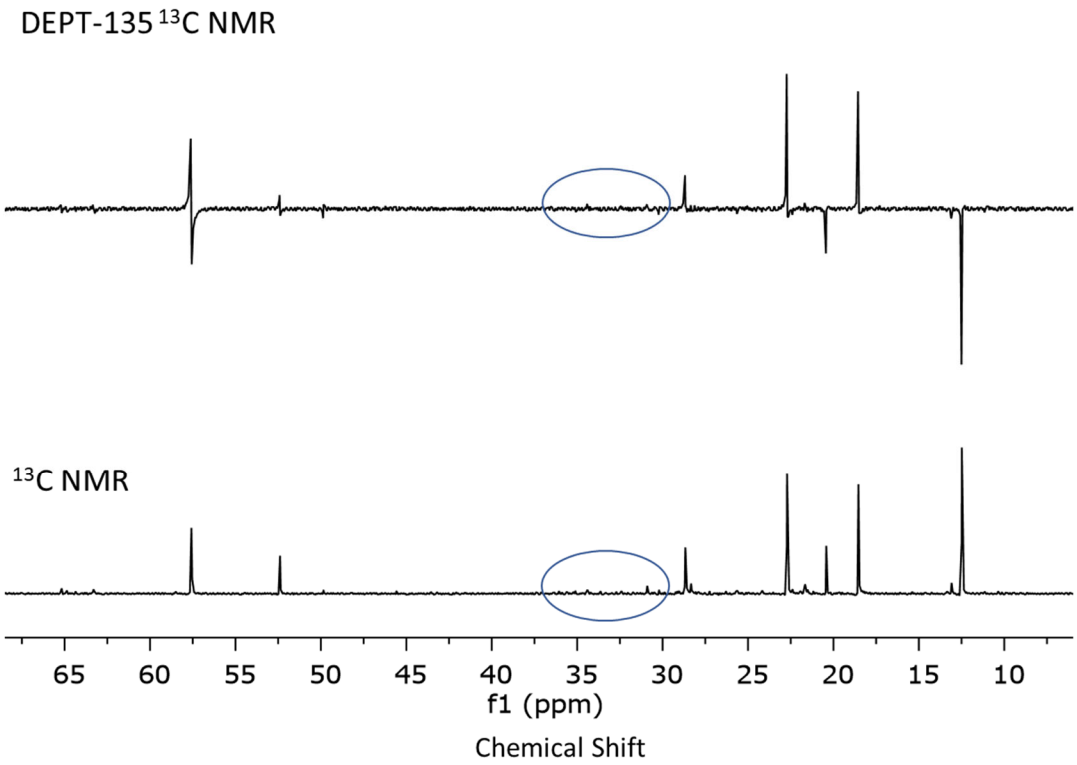

Figure 10C: Zoomed regions from 115 ppm to 145 ppm of ^{13}C NMR and DEPT-135 ^{13}C spectra. Comparison between the two spectra allows for confident assignment of quaternary carbons; for instance, R-**C**-CH type quaternary carbons (boldface) at ~ 137 ppm cannot be detected by DEPT-135 ^{13}C (spectrum shown at the top) but can be observed in conventional ^{13}C NMR (bottom spectrum) .

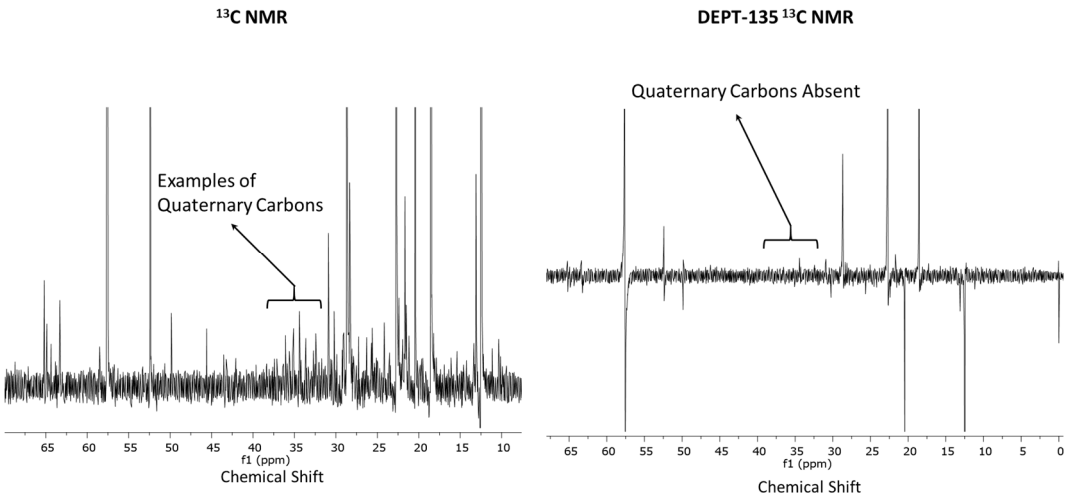

Figure 11C: Expanded regions of S9 ^{13}C NMR and DEPT-135 ^{13}C NMR spectra . Very low intensity peaks in ~32-38 ppm region indicative of quaternary carbon examples are observed in ^{13}C NMR spectrum.

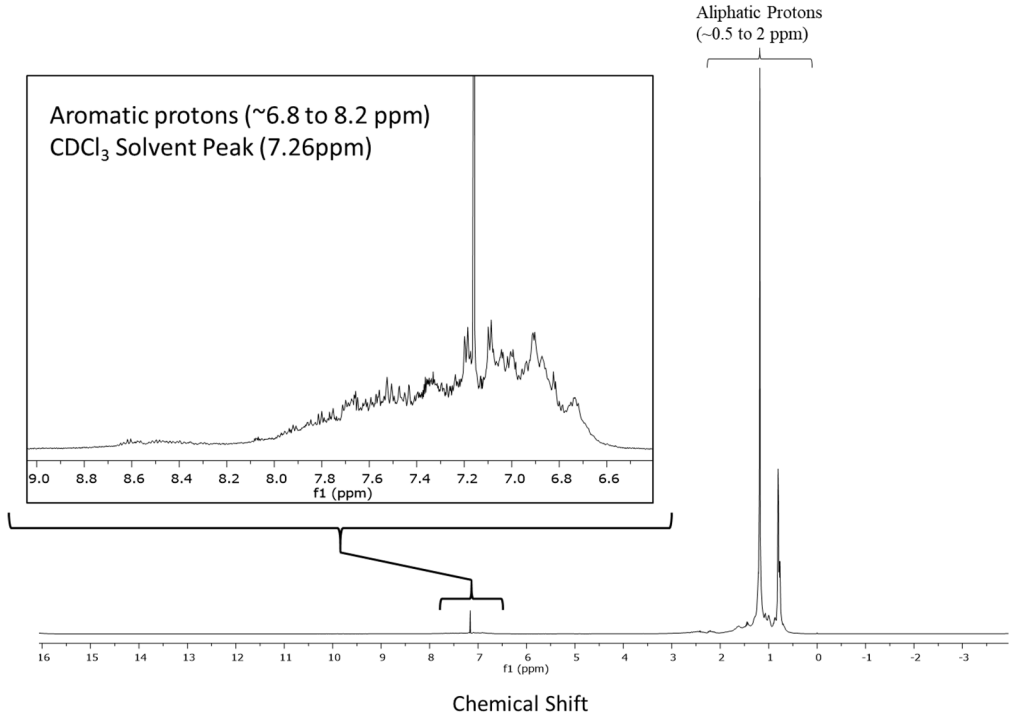

Figure 12C: ^{1}H NMR spectrum of the N-heptane fraction. Inset: zoomed in area from 6.5 – 9.1 ppm shows the region where NMR spectrum signal for the solvent peak and aromatic protons are present.

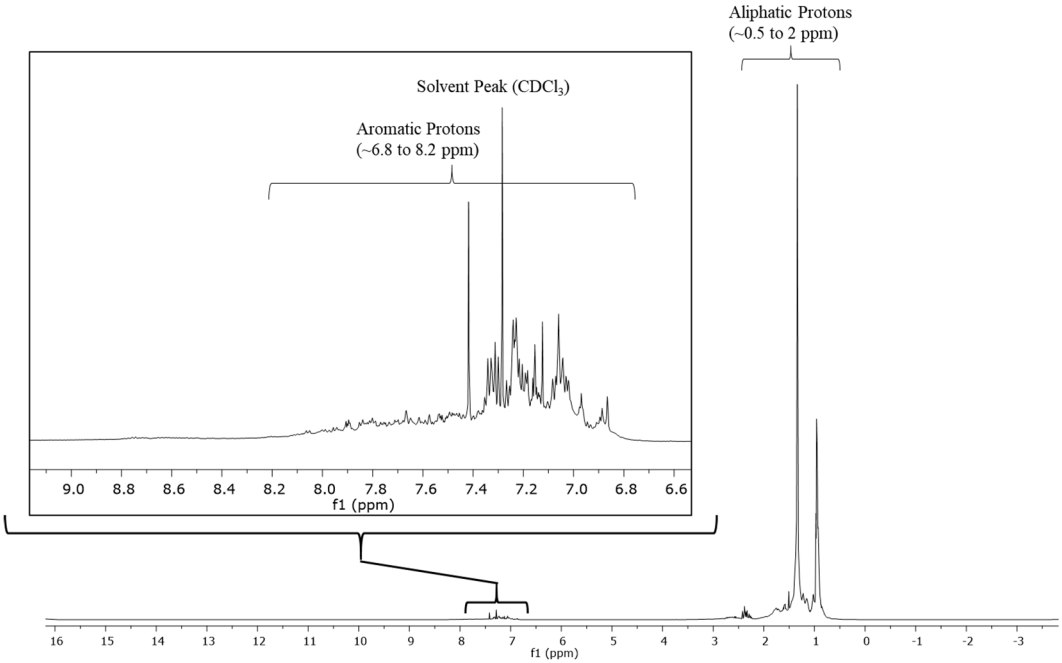

Figure 13C: ^{1}H NMR spectrum of crude oil. Inset: zoomed in area from 6.5 to 9.1 ppm shows the region where NMR spectrum signals for the solvent peak and aromatic protons are present.

BIBLIOGRAPHY

A. M. Bond and R. L. Martin, Coord. Chem. Rev., 1984, 54, 23–98.

AlHumaidan, F. S., Hauser, A., Rana, M. S., & Lababidi, H. M. S. (2017). NMR Characterization of Asphaltene Derived from Residual Oils and Their Thermal Decomposition. Energy & Fuels, 31(4), 3812-3820. doi:10.1021/acs.energyfuels.6b03433

AlHumaidan, F. S.; Hauser, A.; Rana, M. S.; Lababidi, H. M. S. NMR Characterization of Asphaltene Derived from Residual Oils and Their Thermal Decomposition. Energy Fuels 2017, 31 (4), 3812− 3820.

AlHumaidan, F. S.; Hauser, A.; Rana, M. S.; Lababidi, H. M. S., NMR Characterization of Asphaltene Derived from Residual Oils and Their Thermal Decomposition. Energy & Fuels 2017, 31 (4), 3812-3820.

Artok, L., Su, Y., Hirose, Y., Hosokawa, M., Murata, S., & Nomura, M. (1999). Structure and Reactivity of Petroleum-Derived Asphaltene. Energy & Fuels, 13(2), 287-296. doi:10.1021/ef980216a

Artok, L.; Su, Y.; Hirose, Y.; Hosokawa, M.; Murata, S.; Nomura, M., Structure and Reactivity of Petroleum-Derived Asphaltene. Energy & Fuels 1999, 13 (2), 287-296.

ASTM International. ASTM D6560-17, Standard Test Method for Determination of Asphaltenes (Heptane Insolubles) in Crude Petroleum and Petroleum Products; ASTM International: West Conshohocken, PA, 2017.

B. Bruner, M. B. Walker, M. M. Ghimire, D. Zhang, M. Selke, K. K. Klausmeyer, M. A. Omary and P. J. Farmer, Dalton Trans., 2014, 43, 11548–11556.

B. D. Liboiron, K. H. Thompson, G. R. Hanson, E. Lam, N. Aebischer and C. Orvig, J. Am. Chem. Soc., 2005, 127, 5104–5115.

B. L. Ellis, A. K. Duhme, R. C. Hider, M. B. Hossain, S. Rizvi and D. van der Helm, J. Med. Chem., 1996, 39, 3659–3670.

Backlund, M., Ziller, J., & Farmer, P. J. (2008). Unexpected C−H Activation of Ru(II)−Dithiomaltol Complexes upon Oxidation. Inorganic Chemistry, 47(7), 2864-2870. doi:10.1021/ic7021962

Backlund, M.; Ziller, J.; Farmer, P. J., Unexpected C−H Activation of Ru(II)−Dithiomaltol Complexes upon Oxidation. Inorganic Chemistry 2008, 47 (7), 2864-2870.

Balaban, A. T. (2010). CHAPTER 3 - Monocyclic Hetarenes with π-Electron Aromatic Sextet. In A. R. Katritzky (Ed.), Advances in Heterocyclic Chemistry (Vol. 99, pp. 61-105): Academic Press.

Benamsili, L.; Korb, J.-P.; Hamon, G.; Louis-Joseph, A.; Bouyssiere, B.; Zhou, H.; Bryant, R. G. Multi-dimensional Nuclear Magnetic Resonance Characterizations of Dynamics and Saturationsof Brine/Crude Oil/Mud Filtrate Mixtures Confined in Rocks: The Role of Asphaltene. Energy Fuels 2014, 28 (3), 1629−1640.

Betancourt Cardozo, F.; Avella Moreno, E.; Trujillo, C. A. Structural Characterization of Unfractionated Asphalts by ^{1}H NMR and ^{13}C NMR. Energy Fuels 2016, 30 (4), 2729−2740.

Brayton, D., Jacobsen, F. E., Cohen, S. M., & Farmer, P. J. (2006). A novel heterocyclic atom exchange reaction with Lawesson's reagent: a one-pot synthesis of dithiomaltol. Chemical Communications(2), 206-208. doi:10.1039/B511966A

Brayton, D.; Jacobsen, F. E.; Cohen, S. M.; Farmer, P. J., A novel heterocyclic atom exchange reaction with Lawesson's reagent: a one-pot synthesis of dithiomaltol. Chemical Communications 2006, (2), 206-208.

Bruner, B., Walker, M. B., Ghimire, M. M., Zhang, D., Selke, M., Klausmeyer, K. K., . . . Farmer, P. J. (2014). Ligand-based photooxidations of dithiomaltolato complexes of Ru(ii) and Zn(ii): photolytic CH activation and evidence of singlet oxygen generation and quenching. Dalton Transactions, 43(30), 11548-11556. doi:10.1039/C4DT00961D

Bruner, B.; Walker, M. B.; Ghimire, M. M.; Zhang, D.; Selke, M.; Klausmeyer, K. K.; Omary, M. A.; Farmer, P. J., Ligand-based photooxidations of dithiomaltolato complexes of Ru(ii) and Zn(ii): photolytic CH activation and evidence of singlet oxygen generation and quenching. Dalton Transactions 2014, 43 (30), 11548-11556.

Cakmak, O.; Aydogan, L.; Berkil, K.; Gulcin, I.; Buyukgungor, O. Highly brominated anthracenes as precursors for the convenient synthesis of 2,9,10-trisubstituted anthracene derivatives. Beilstein J. Org. Chem. 2008, 4, 50.

Cassella, R. J.; Brum, D. M.; Robaina, N. F.; Rocha, A. A.; Lima, C. F. Extraction induced by emulsion breaking for metals determination in diesel oil by ICP-MS. J. Anal. At. Spectrom. 2012, 27 (2), 364−370.

Chaisoontornyotin, W., Haji-Akbari, N., Fogler, H. S., & Hoepfner, M. P. (2016). Combined Asphaltene Aggregation and Deposition Investigation. Energy & Fuels, 30(3), 1979-1986. doi:10.1021/acs.energyfuels.5b02427

Chaisoontornyotin, W.; Haji-Akbari, N.; Fogler, H. S.; Hoepfner, M. P., Combined Asphaltene Aggregation and Deposition Investigation. Energy & Fuels 2016, 30 (3), 1979-1986.

Chaisoontornyotin, W.; Haji-Akbari, N.; Fogler, H. S.; Hoepfner, M. P. Combined Asphaltene Aggregation and Deposition Investigation. Energy Fuels 2016, 30 (3), 1979−1986.

Choi, S.; Pyeon, W.; Kim, J.-D.; Nho, N.-s. Simple Functionalization of Asphaltene and Its Application for Efficient Asphaltene Removal. Energy Fuels 2016, 30 (9), 991−7000.

Corvari, L.; McKee, J. R.; Zanger, M. The synthesis of 2′-bromostyrene. J. Chem. Educ. 1991, 68 (2), 161.

Creek, J. L. Freedom of Action in the State of Asphaltenes: Escape from Conventional Wisdom. Energy Fuels 2005, 19 (4), 1212− 1224.

Cui, T.-B.; Luo, T.-L.; Zhang, C.; Mao, Z.-B.; Liu, G.-J. Measurement and Correlation for Solubilities of Naphthalene in Acetone, Toluene, Xylene, Ethanol, Heptane, and 1-Butanol. J. Chem. Eng. Data 2009, 54 (3), 1065−1068.

D. Brayton, F. E. Jacobsen, S. M. Cohen and P. J. Farmer, Chem. Commun., 2006, 206–208, DOI: 10.1039/B511966A.

D. P. Martin, P. G. Blachly, A. R. Marts, T. M. Woodruff, C. A. F. de Oliveira, J. A. McCammon, D. L. Tierney and S. M. Cohen, J. Am. Chem. Soc., 2014, 136, 5400–5406.

Di Mauro, E., Guedes, C. L. B., & Nascimento, O. R. (2005). Multifrequency (X-band to W-band) CW EPR of the organic free radical in petroleum asphaltene. Applied Magnetic Resonance, 29(4), 569. doi:10.1007/bf03166333

Di Mauro, E.; Guedes, C. L. B.; Nascimento, O. R. Multifrequency (X-band to W-band) CW EPR of the organic free radical in petroleum asphaltene. Appl. Magn. Reson. 2005, 29 (4), 569.

Di Mauro, E.; Guedes, C. L. B.; Nascimento, O. R., Multifrequency (X-band to W-band) CW EPR of the organic free radical in petroleum asphaltene. Applied Magnetic Resonance 2005, 29 (4), 569.

Dickinson, E. M. Structural comparison of petroleum fractions using proton and ^{13}C NMR spectroscopy. Fuel 1980, 59 (5), 290−294.

E. Orlowska, A. Roller, M. Pignitter, F. Jirsa, R. Krachler, W. Kandioller and B. K. Keppler, Sci. Total Environ., 2017, 577, 94–104.

E. R. Cullen, F. S. Guziec, C. J. Murphy, T. C. Wong and K. K. Andersen, J. Am. Chem. Soc., 1981, 103, 7055–7057.

Farmer, P. J. (2013). Cu-based drugs in combination therapy for melanoma. Abstracts of Papers, 245th ACS National Meeting & Exposition, New Orleans, LA, United States, April 7-11, 2013, INOR-1149.

Farmer, P. J., Cu-based drugs in combination therapy for melanoma. Abstracts of Papers, 245th ACS National Meeting & Exposition, New Orleans, LA, United States, April 7-11, 2013 2013, INOR-1149.

Gagliardi, L. G., Castells, C. B., Ràfols, C., Rosés, M., & Bosch, E. (2007). Static Dielectric Constants of Acetonitrile/Water Mixtures at Different Temperatures and Debye−Hückel A and a0B Parameters for Activity Coefficients. Journal of Chemical & Engineering Data, 52(3), 1103-1107. doi:10.1021/je700055p

Gillet, S.; Rubini, P.; Delpuech, J.-J.; Escalier, J.-C.; Valentin, P. Quantitative carbon-13 and proton nuclear magnetic resonance spectroscopy of crude oil and petroleum products. 1. Some rules for obtaining a set of reliable structural parameters. Fuel 1981, 60 (3), 221−225.

Gillet, S.; Rubini, P.; Delpuech, J.-J.; Escalier, J.-C.; Valentin, P. Quantitative carbon-13 and proton nuclear magnetic resonance spectroscopy of crude oil and petroleum products. 2. Average structure parameters of representative samples. Fuel 1981, 60 (3), 226−230.

Gonzalez, D. L.; Ting, P. D.; Hirasaki, G. J.; Chapman, W. G. Prediction of Asphaltene Instability under Gas Injection with the PCSAFT Equation of State. Energy Fuels 2005, 19 (4), 1230−1234.

H. J. Reich and R. J. Hondal, ACS Chem. Biol., 2016, 11, 821–841.

H. Luo, S. J. Rettig and C. Orvig, Inorg. Chem., 1993, 32, 4491–4497.

Hasan, M. U.; Ali, M. F.; Bukhari, A. Structural characterization of Saudi Arabian heavy crude oil by NMR spectroscopy. Fuel 1983, 62 (5), 518−523.

Helsel, M. E., White, E. J., Razvi, S. Z. A., Alies, B., & Franz, K. J. (2017). Chemical and functional properties of metal chelators that mobilize copper to elicit fungal killing of Cryptococcus neoformans. Metallomics, 9(1), 69-81. doi:10.1039/C6MT00172F

Helsel, M. E.; White, E. J.; Razvi, S. Z. A.; Alies, B.; Franz, K. J., Chemical and functional properties of metal chelators that mobilize copper to elicit fungal killing of Cryptococcus neoformans. Metallomics 2017, 9 (1), 69-81.

HIDER, R. C., & ZHOU, T. (2005). The Design of Orally Active Iron Chelators. Annals of the New York Academy of Sciences, 1054(1), 141-154. doi:10.1196/annals.1345.017

Hider, R. C.; Zhou, T., The Design of Orally Active Iron Chelators. Annals of the New York Academy of Sciences 2005, 1054 (1), 141-154.

Hughey, C. A.; Hendrickson, C. L.; Rodgers, R. P.; Marshall, A. G.; Qian, K. Kendrick Mass Defect Spectrum: A Compact Visual Analysis for Ultrahigh-Resolution Broadband Mass Spectra. Anal. Chem. 2001, 73 (19), 4676−4681.

J. A. Jacobsen, J. L. Fullagar, M. T. Miller and S. M. Cohen, J. Med. Chem., 2011, 54, 591–602.

J. A. Lewis and S. M. Cohen, Inorg. Chem., 2004, 43, 6534–6536.

J. A. Lewis, B. L. Tran, D. T. Puerta, E. M. Rumberger, D. N. Hendrickson and S. M. Cohen, Dalton Trans., 2005, 2588–2596, DOI: 10.1039/B505034K.

J. A. Lewis, D. T. Puerta and S. M. Cohen, Inorg. Chem., 2003, 42, 7455–7459.

J. C. Slater, J. Chem. Phys., 1964, 41, 3199–3204.

J. P. Barbier, A. El Biyyadh, C. Kappenstein, N. D. Mabiala and R. P. Hugel, Inorg. Chem., 1985, 24, 3615–3620.

K. H. Thompson, C. A. Barta and C. Orvig, Chem. Soc. Rev., 2006, 35, 545–556.

Kahn, V. (1995). Multiple Effects of Maltol and Kojic Acid on Enzymatic Browning. In Enzymatic Browning and Its Prevention (Vol. 600, pp. 277-294): American Chemical Society.

Kahn, V., Multiple Effects of Maltol and Kojic Acid on Enzymatic Browning. In Enzymatic Browning and Its Prevention, American Chemical Society: 1995; Vol. 600, pp 277-294.

Kendrick, E. A Mass Scale Based on CH2 = 14.0000 for High Resolution Mass Spectrometry of Organic Compounds. Anal. Chem. 1963, 35 (13), 2146−2154.

Kiruri, L. W.; Dellinger, B.; Lomnicki, S. Tar Balls from Deep Water Horizon Oil Spill: Environmentally Persistent Free Radicals (EPFR) Formation During Crude Weathering. Environ. Sci. Technol. 2013, 47 (9), 4220−4226.

Klein, G. C.; Kim, S.; Rodgers, R. P.; Marshall, A. G.; Yen, A.; Asomaning, S. Mass Spectral Analysis of Asphaltenes. I. Compositional Differences between Pressure-Drop and Solvent-Drop Asphaltenes Determined by Electrospray Ionization Fourier Transform Ion Cyclotron Resonance Mass Spectrometry. Energy Fuels 2006, 20 (5), 1965−1972.

Kurian, V., & Gupta, R. (2016). Distribution of Vanadium, Nickel, and Other Trace Metals in Soot and Char from Asphaltene Pyrolysis and Gasification. Energy & Fuels, 30(3), 1605-1615. doi:10.1021/acs.energyfuels.5b02296

Kurian, V.; Gupta, R. Distribution of Vanadium, Nickel, and Other Trace Metals in Soot and Char from Asphaltene Pyrolysis and Gasification. Energy Fuels 2016, 30 (3), 1605−1615.

Kurian, V.; Gupta, R., Distribution of Vanadium, Nickel, and Other Trace Metals in Soot and Char from Asphaltene Pyrolysis and Gasification. Energy & Fuels 2016, 30 (3), 1605-1615.

Lewis, J. A., & Cohen, S. M. (2004). Addressing Lead Toxicity: Complexation of Lead(II) with Thiopyrone and Hydroxypyridinethione O,S Mixed Chelators. Inorganic Chemistry, 43(21), 6534-6536. doi:10.1021/ic0493696

Lewis, J. A.; Cohen, S. M., Addressing Lead Toxicity: Complexation of Lead(II) with Thiopyrone and Hydroxypyridinethione O,S Mixed Chelators. Inorganic Chemistry 2004, 43 (21), 6534-6536.

Liboiron, B. D., Thompson, K. H., Hanson, G. R., Lam, E., Aebischer, N., & Orvig, C. (2005). New Insights into the Interactions of Serum Proteins with Bis(maltolato)oxovanadium(IV): Transport and Biotransformation of Insulin-Enhancing Vanadium Pharmaceuticals. Journal of the American Chemical Society, 127(14), 5104-5115. doi:10.1021/ja043944n

Liboiron, B. D.; Thompson, K. H.; Hanson, G. R.; Lam, E.; Aebischer, N.; Orvig, C., New Insights into the Interactions of Serum Proteins with Bis(maltolato)oxovanadium(IV): Transport and Biotransformation of Insulin-Enhancing Vanadium Pharmaceuticals. Journal of the American Chemical Society 2005, 127 (14), 5104-5115.

Lisitza, N. V., Freed, D. E., Sen, P. N., & Song, Y.-Q. (2009). Study of Asphaltene Nanoaggregation by Nuclear Magnetic Resonance (NMR). Energy & Fuels, 23(3), 1189-1193. doi:10.1021/ef800631a

Lisitza, N. V.; Freed, D. E.; Sen, P. N.; Song, Y.-Q. Study of Asphaltene Nanoaggregation by Nuclear Magnetic Resonance (NMR). Energy Fuels 2009, 23 (3), 1189−1193.

Lisitza, N. V.; Freed, D. E.; Sen, P. N.; Song, Y.-Q., Study of Asphaltene Nanoaggregation by Nuclear Magnetic Resonance (NMR). Energy & Fuels 2009, 23 (3), 1189-1193.

Liu, Z. D., & Hider, R. C. (2002). Design of clinically useful iron(III)-selective chelators. Medicinal Research Reviews, 22(1), 26-64. doi:10.1002/med.1027

Liu, Z. D.; Hider, R. C., Design of clinically useful iron(III)-selective chelators. Medicinal Research Reviews 2002, 22 (1), 26-64.

M. Backlund, J. Ziller and P. J. Farmer, Inorg. Chem., 2008, 47, 2864–2870.

M. C. Barret, M. F. Mahon, K. C. Molloy, J. W. Steed and P. Wright, Inorg. Chem., 2001, 40, 4384–4388.

M. E. Helsel, E. J. White, S. Z. A. Razvi, B. Alies and K. J. Franz, Metallomics, 2017, 9, 69–81.

M. J. Frisch, G. W. Trucks, H. B. Schlegel, G. E. Scuseria, M. A. Robb, J. R. Cheeseman, G. Scalmani, V. Barone, B. Mennucci, G. A. Petersson, H. Nakatsuji, M. Caricato, X. Li, H. P. Hratchian, A. F. Izmaylov, J. Bloino, G. Zheng, J. L. Sonnenberg, M. Hada, M. Ehara, K. Toyota, R. Fukuda, J. Hasegawa, M. Ishida, T. Nakajima, Y. Honda, O. Kitao, H. Nakai, T. Vreven, J. A. Montgomery, Jr., J. E. Peralta, F. Ogliaro, M. Bearpark, J. J. Heyd, E. Brothers, K. N. Kudin, V. N. Staroverov, R. Kobayashi, J. Normand, K. Raghavachari, A. Rendell, J. C. Burant, S. S. Iyengar, J. Tomasi, M. Cossi, N. Rega, J. M. Millam, M. Klene, J. E. Knox, J. B. Cross, V. Bakken, C. Adamo, J. Jaramillo, R. Gomperts, R. E. Stratmann, O. Yazyev, A. J. Austin, R. Cammi, C. Pomelli, J. W. Ochterski, R. L. Martin, K. Morokuma, V. G. Zakrzewski, G. A. Voth, P. Salvador, J. J. Dannenberg, S. Dapprich, A. D. Daniels, Ö. Farkas, J. B. Foresman, J. V. Ortiz, J. Cioslowski and D. J. Fox, Gaussian 09, Gaussian, Inc., Wallingford CT, 2009.

M. Melchior, K. H. Thompson, J. M. Jong, S. J. Rettig, E. Shuter, V. G. Yuen, Y. Zhou, J. H. McNeill and C. Orvig, Inorg. Chem., 1999, 38, 2288–2293.

Ma, Y., Luo, W., Quinn, P. J., Liu, Z., & Hider, R. C. (2004). Design, Synthesis, Physicochemical Properties, and Evaluation of Novel Iron Chelators with Fluorescent Sensors. Journal of Medicinal Chemistry, 47(25), 6349-6362. doi:10.1021/jm049751s

Mascareñas, J. L., Pérez, I., Rumbo, A., & Castedo, L. (1997). A New [5+2] Annulation Method for the Synthesis of 8-Oxabicyclo[3.2.1]octanes from Pyrones. Synlett, 1(01), 81-82. doi:10.1055/s-1997-698

Mascareñas, J. L.; Pérez, I.; Rumbo, A.; Castedo, L., A New [5+2] Annulation Method for the Synthesis of 8-Oxabicyclo[3.2.1]octanes from Pyrones. Synlett 1997, 1 (01), 81-82.

Melchior, M., Thompson, K. H., Jong, J. M., Rettig, S. J., Shuter, E., Yuen, V. G., . . . Orvig, C. (1999). Vanadium Complexes as Insulin Mimetic Agents: Coordination Chemistry and in Vivo Studies of Oxovanadium(IV) and Dioxovanadate(V) Complexes Formed from Naturally Occurring Chelating Oxazolinate, Thiazolinate, or Picolinate Units. Inorganic Chemistry, 38(10), 2288-2293. doi:10.1021/ic981231y

Melchior, M.; Thompson, K. H.; Jong, J. M.; Rettig, S. J.; Shuter, E.; Yuen, V. G.; Zhou, Y.; McNeill, J. H.; Orvig, C., Vanadium Complexes as Insulin Mimetic Agents: Coordination Chemistry and in Vivo Studies of Oxovanadium(IV) and Dioxovanadate(V) Complexes Formed from Naturally Occurring Chelating Oxazolinate, Thiazolinate, or Picolinate Units. Inorganic Chemistry 1999, 38 (10), 2288-2293.

Morris, J. A., Khettry, A., & Seitz, E. W. (1979). Antimicrobial activity of aroma chemicals and essential oils. Journal of the American Oil Chemists' Society, 56(5), 595-603. doi:10.1007/bf02660245

Mullins, O. C., Sabbah, H., Eyssautier, J., Pomerantz, A. E., Barré, L., Andrews, A. B., . . . Zare, R. N. (2012). Advances in Asphaltene Science and the Yen–Mullins Model. Energy & Fuels, 26(7), 3986-4003. doi:10.1021/ef300185p

Mullins, O. C.; Sabbah, H.; Eyssautier, J.; Pomerantz, A. E.; Barré, L.; Andrews, A. B.; Ruiz-Morales, Y.; Mostowfi, F.; McFarlane, R.; Goual, L.; Lepkowicz, R.; Cooper, T.; Orbulescu, J.; Leblanc, R. M.; Edwards, J.; Zare, R. N., Advances in Asphaltene Science and the Yen–Mullins Model. Energy & Fuels 2012, 26 (7), 3986-4003.

Mullins, O. C.; Sabbah, H.; Eyssautier, J.; Pomerantz, A. E.; Barré, L.; Andrews, A. B.; Ruiz-Morales, Y.; Mostowfi, F.; McFarlane, R.; Goual, L.; Lepkowicz, R.; Cooper, T.; Orbulescu, J.; Leblanc, R. M.; Edwards, J.; Zare, R. N. Advances in Asphaltene Science and the Yen−Mullins Model. Energy Fuels 2012, 26 (7), 3986−4003.

Mullins, O. C.; Seifert, D. J.; Zuo, J. Y.; Zeybek, M. Clusters of Asphaltene Nanoaggregates Observed in Oilfield Reservoirs. Energy Fuels 2013, 27 (4), 1752−1761.

Nelson, J., Yamanaka, M., Lopez-Linares, F., Poirier, L., & Rogel, E. (2017). Characterization of Dissolved Metals and Metallic Nanoparticles in Asphaltene Solutions by Single-Particle Inductively Coupled Plasma Mass Spectrometry. Energy & Fuels. doi:10.1021/acs.energyfuels.7b02380

Nelson, J.; Yamanaka, M.; Lopez-Linares, F.; Poirier, L.; Rogel, E., Characterization of Dissolved Metals and Metallic Nanoparticles in Asphaltene Solutions by Single-Particle Inductively Coupled Plasma Mass Spectrometry. Energy & Fuels 2017.

Nelson, J.; Yamanaka, M.; Lopez-Linares, F.; Poirier, L.; Rogel, E. Characterization of Dissolved Metals and Metallic Nanoparticles in Asphaltene Solutions by Single-Particle Inductively Coupled Plasma Mass Spectrometry. Energy Fuels 2017, 31 (11), 11971−11976.

Netzel, D. A.; McKay, D. R.; Heppner, R. A.; Guffey, F. D.; Cooke, S. D.; Varie, D. L.; Linn, D. E. ^{1}H- and ^{13}C-NMR studies on naphtha and light distillate saturate hydrocarbon fractions obtained from in-situ shale oil. Fuel 1981, 60 (4), 307−320.

O'Donnell, D. J.; Sigle, S. O.; Berlin, K. D.; Sturm, G. P.; Vogh, J. W. Characterization of high-boiling petroleum distillate fractions by proton and ^{13}C nuclear magnetic resonance spectrometry. Fuel 1980, 59 (3), 166−174.

Ovalles, C.; Rogel, E.; Lopez, J.; Pradhan, A.; Moir, M. Predicting Reactivity of Feedstocks to Resid Hydroprocessing Using Asphaltene Characteristics. Energy Fuels 2013, 27 (11), 6552−6559.

Pekerar, S.; Lehmann, T.; Méndez, B.; Acevedo, S. Mobility of Asphaltene Samples Studied by ^{13}C NMR Spectroscopy. Energy Fuels 1999, 13 (2), 305−308.

Platzer, S., Sap, O., Leyma, R., Wallner, G., Jirsa, F., Kandioller, W., . . . Keppler, B. K. (2015). Extraction of natural radionuclides from aqueous solutions by novel maltolate-based task-specific ionic liquids. Journal of radioanalytical and nuclear chemistry, 303(3), 2483-2488. doi:10.1007/s10967-014-3782-x

Platzer, S.; Sap, O.; Leyma, R.; Wallner, G.; Jirsa, F.; Kandioller, W.; Krachler, R.; Keppler, B. K., Extraction of natural radionuclides from aqueous solutions by novel maltolate-based task-specific ionic liquids. J Radioanal Nucl Chem 2015, 303 (3), 2483-2488.

Poveda, J.-C.; Molina, D.-R.; Pantoja-Agreda, E.-F. ^{1}H- and ^{13}C-NMR Structural Characterization of Asphaltenes from Vacuum Residua Modified by Thermal Cracking. CT&F, Cienc., Tecnol. Futuro 2014, 5, 49−60.

R. D. Shannon, Acta Crystallogr., Sect. A: Cryst. Phys., Diffr.,Theor. Gen. Crystallogr., 1976, 32, 751–767.

S. J. Lord, N. A. Epstein, R. L. Paddock, C. M. Vogels, T. L. Hennigar, M. J. Zaworotko, N. J. Taylor, W. R. Driedzic, T. L. Broderick and S. A. Westcott, Can. J. Chem., 1999, 77, 1249–1261.

S. R. Schlesinger, B. Bruner, P. J. Farmer and S.-K. Kim, J. Enzyme Inhib. Med. Chem., 2013, 28, 137–142.

Saikia, I.; Borah, A. J.; Phukan, P. Use of Bromine and Bromo- Organic Compounds in Organic Synthesis. Chem. Rev. 2016, 116 (12), 6837−7042.

Schreckenbach, G.; Ziegler, T. Calculation of the G-Tensor of Electron Paramagnetic Resonance Spectroscopy Using Gauge-Including Atomic Orbitals and Density Functional Theory. J. Phys. Chem. A 1997, 101 (18), 3388−3399.

Schulze, M., Lechner, M. P., Stryker, J. M., & Tykwinski, R. R. (2015). Aggregation of asphaltene model compounds using a porphyrin tethered to a carboxylic acid. Organic & Biomolecular Chemistry, 13(25), 6984-6991. doi:10.1039/C5OB00836K

Schulze, M.; Lechner, M. P.; Stryker, J. M.; Tykwinski, R. R., Aggregation of asphaltene model compounds using a porphyrin tethered to a carboxylic acid. Organic & Biomolecular Chemistry 2015, 13 (25), 6984-6991.

Sedghi, M.; Goual, L.; Welch, W.; Kubelka, J. Effect of Asphaltene Structure on Association and Aggregation Using Molecular Dynamics. J. Phys. Chem. B 2013, 117 (18), 5765−5776.

Seshadri, K. S.; Albaugh, E. W.; Bacha, J. D. Characterization of needle coke feedstocks by magnetic resonance spectroscopy. Fuel 1982, 61 (4), 336−340.

Silverstein, R. M.; Webster, F. X.; Kiemle, D. J. Spectrometric Identification of Organic Compounds, 7th ed.; Wiley: Hoboken, NJ, 2005; pp 127−204.

Silverstein, R. M.; Webster, F. X.; Kiemle, D. J. Spectrometric Identification of Organic Compounds, 7th ed.; Wiley: Hoboken, NJ, 2005; pp 205−224.

Sirota, E. B. Physical Structure of Asphaltenes. Energy Fuels 2005, 19 (4), 290−1296.

Spiegel, M. T., Hoogerbrugge, A., Truksa, S., Smith, A. G., Shuford, K. L., Klausmeyer, K. K., & Farmer, P. J. (2018). Synthesis of first row transition metal selenomaltol complexes. Dalton Transactions, 47(27), 9030-9037. doi:10.1039/C8DT01170B

Stoermer, M.; Pinhey, J. 2(S,R),3(R,S)-2,3-Dibromo-3-methyl-5-phenyl-2-pentanoic Acid. Molecules 1998, 3 (3), M55.

Suzuki, T.; Itoh, M.; Takegami, Y.; Watanabe, Y. Chemical structure of tar-sand bitumens by ^{13}C and ^{1}H NMR spectroscopic methods. Fuel 1982, 61 (5), 402−410.

T. M. Krygowski, H. Szatylowicz, O. A. Stasyuk, J. Dominikowska and M. Palusiak, Chem. Rev., 2014, 114, 6383–6422.

T. W. Keal and D. J. Tozer, Mol. Phys., 2005, 103, 1007–1011.

Thompson, K. H., Barta, C. A., & Orvig, C. (2006). Metal complexes of maltol and close analogues in medicinal inorganic chemistry. Chemical Society Reviews, 35(6), 545-556. doi:10.1039/B416256K

Thompson, K. H., Lichter, J., LeBel, C., Scaife, M. C., McNeill, J. H., & Orvig, C. (2009). Vanadium treatment of type 2 diabetes: A view to the future. Journal of Inorganic Biochemistry, 103(4), 554-558. doi:https://doi.org/10.1016/j.jinorgbio.2008.12.003

Thompson, K. H.; Barta, C. A.; Orvig, C., Metal complexes of maltol and close analogues in medicinal inorganic chemistry. Chemical Society Reviews 2006, 35 (6), 545-556.

V. Kahn, in Enzymatic Browning and Its Prevention, American Chemical Society, 1995, ch. 22, vol. 600, pp. 277–294.

Vargas, F. M.; Creek, J. L.; Chapman, W. G. On the Development of an Asphaltene Deposition Simulator. Energy Fuels 2010, 24 (4), 2294−2299.

Voronetskaya, N. G.; Pevneva, G. S.; Golovko, A. K. Composition of naphthene hydrocarbons in crude oils from deposits of different ages. Pet. Chem. 2014, 54 (3), 165−170.

W. Tejchman, E. Żesławska, K. Zborowski, W. Nitek and M. Żylewski, ARKIVOC, 2015, 216–230, DOI: 10.3998/ark.5550190.p009.262.

W. Tejchman, K. Zborowski, W. Lasocha and L. M. Proniewicz, Heterocycles, 2008, 75, 1931–1942.

W. Tejchman, L. M. Proniewicz and K. K. Zborowski, J. Phys. Org. Chem., 2015, 28, 536–541.

Wang, T.; Jupiter, D.; Devkota, L.; Chambliss, C. K.; Pinney, K.; Solouki, T. Identification of Sulfur Compounds in Petroleum Samples Using Derivatization with Mass Deficent Reagents. Proceedings of the 61st Annual American Society for Mass Spectrometry Conference; Minneapolis, MN, June 9−13, 2013.

Wang, X.; Liu, R.-F.; Cork, J.; Gu, Y.; Upham, D. C.; Laycock, B.; McFarland, E. W. Investigation of the Bromination/Dehydrobromination of Long Chain Alkanes. Ind. Eng. Chem. Res. 2017, 56 (34), 9411−9418.

Ylijoki, K. E. O., & Stryker, J. M. (2013). [5 + 2] Cycloaddition Reactions in Organic and Natural Product Synthesis. Chemical Reviews, 113(3), 2244-2266. doi:10.1021/cr300087g

Yu, C.; Zhang, L.; Guo, X.; Xu, Z.; Sun, X.; Xu, C.; Zhao, S. Association Model for Nickel and Vanadium with Asphaltene during Solvent Deasphalting. Energy Fuels 2015, 29 (3), 1534−1542.

Z. Chen, C. S. Wannere, C. Corminboeuf, R. Puchta and P. v. R. Schleyer, Chem. Rev., 2005, 105, 3842–3888.

Zborowski, K. K., Solà, M., Poater, J., & Proniewicz, L. M. (2011). Theoretical studies on aromaticity of selected hydroxypyrones. Part 3#. Chelatoaromaticity phenomenon in metalcomplexes of hydroxypyrones. Journal of Physical Organic Chemistry, 24(6), 499-506. doi:10.1002/poc.1794

Zborowski, K. K.; Solà, M.; Poater, J.; Proniewicz, L. M., Theoretical studies on aromaticity of selected hydroxypyrones. Part 3#. Chelatoaromaticity phenomenon in metalcomplexes of hydroxypyrones. Journal of Physical Organic Chemistry 2011, 24 (6), 499-506.

Zborowski, K., & Proniewicz, L. M. (2008). Theoretical studies on aromaticity of selected hydroxypyrones and their cations and anions. Part 2. Electron delocalization in the OCCO group. Journal of Physical Organic Chemistry, 21(3), 207-214. doi:10.1002/poc.1294

Zborowski, K., Grybos, R., & Proniewicz, L. M. (2005). Theoretical studies on the aromaticity of selected hydroxypyrones and their cations and anions. Part 1—Aromaticity of heterocyclic pyran rings. Journal of Physical Organic Chemistry, 18(3), 250-254. doi:10.1002/poc.844

Zborowski, K.; Grybos, R.; Proniewicz, L. M., Theoretical studies on the aromaticity of selected hydroxypyrones and their cations and anions. Part 1—Aromaticity of heterocyclic pyran rings. Journal of Physical Organic Chemistry 2005, 18 (3), 250-254.

Zborowski, K.; Proniewicz, L. M., Theoretical studies on aromaticity of selected hydroxypyrones and their cations and anions. Part 2. Electron delocalization in the OCCO group. Journal of Physical Organic Chemistry 2008, 21 (3), 207-214.